

Functional characterisation of a novel heterozygous mutation in the transcriptional activation domain of the human *FOXN1* gene

IOANNA A. ROTA
Green Templeton College
University of Oxford

Doctor of Philosophy
October 2019

To Ale and Matteo

ACKNOWLEDGEMENTS

First and foremost, I would like to thank my supervisor, Prof Georg Holländer, for his guidance and support. The time spent working in his lab has undoubtedly shaped my scientific and personal development in many ways. I would also like to acknowledge the time he spent reading every single word of this thesis and providing very constructive feedback.

I would also like to thank my co-supervisor Prof Katja Simon, for her mentorship during this time. On multiple occasions I relied on her advice to combine motherhood and research.

Thanks to all current and previous members of the Developmental Immunology lab for the friendly and supportive working environment. In particular I would like to acknowledge those who actively contributed to this project: Adam Handel, Stefano Maio, Mary Deadman, Eleni Adamopoulou, Fatima Dhalla, Wei Wu and Annina Grädel. Bergithe Oftedal for her helpful advices, Emma Haberman, Adli Ali and Stanley Cheuk for their help with FACs. Special thanks to Annina Grädel and Hector Barbosa for their invaluable help in the lab over the last two years.

Equally, I would like to thank our collaborators Erdinc Sezgin, Philip Hublitz, Yale Michaels, Joseph Newman, Tudor Fulga, Philip Charles, Alistair Pagnamenta and Carme Camps, from the University of Oxford and Athina Soragia Gkazi from UCL, for their contribution to this project.

The feedback I received from Prof Thomas Milne and Prof Irene Roberts, the members of my thesis committee, during the early stages of my thesis has been extremely helpful.

Undoubtedly, the WIMM is an excellent place for research and I am immensely grateful to all those who kindly shared their knowledge, their reagents and their advice. Thanks to Laura Santana Gonzalez for her coding skills, Philip Hublitz for generously sharing his knowledge on CRISPR and his plasmids, Martyna Lukoseviciute for her advices on ChIP and many more, Erdinc Sezgin for bringing colourful microscopy images to this thesis, Athina Cavounidis for her help with English spelling, Mafalda Santos for her useful advice and Matteo Morotti for his skills in H&E.

The completion of my thesis wouldn't have been possible without all those friends who were there to share a break over a cup of coffee, a bar of swiss chocolate or a Turkish kebab. All of you have been a source of inspiration. In particular, Annina Grädel, Martyna Lukoseviciute, Laura Santana Gonzalez, Athina Cavounidis, Lilliana Barbieri, Eleni Adamopoulou, Agapi Loulourga, Anna Papanikou, Erdinc Sezgin, Hector Barbosa, Gennaro Prota, Quentin Ferry, David Saliba, Stefano Maio.

I would like to acknowledge Eleni Adamopoulou for the precious time she dedicated on reading a part of the thesis and for her extremely helpful corrections. Stefano Rota, Matteo Morotti, Bergithe Oftedal and Annina Grädel read parts of the thesis and gave helpful feedback.

I can’t fully express all my gratitude to all those who helped us when Ale was born. In particular, our parents Alekos Rotas and Voula Vazaiou, Erminia Pozzi and Giancarlo Morotti for their dedication to Ale and our new family. Furthermore, all our friends with their frequent visits, their supplies on food and their moral encouragement.

My biggest gratitude goes to my parents Voula Vazaiou and Aleko Rota for their unconditional support and trust in me since very early on. All the skills and values I gained next to them have been essential for this journey. I would also like to thank my brother Reno Rota for always inspiring me in his own unique way.

Ale’s birth has been the driving force to complete this project. I appreciate his patience and understanding for the time I had to spent working and for being an easy sleeper.

Last and not least, I am deeply grateful to my partner Matteo Morotti. Thank you for being inspiring, understanding, supportive, patient, funny and overall a great company throughout this adventure.

ABSTRACT

The competence of the human body to fight infections relies on lymphocytes, which differentiate in the thymus, a primary organ of the immune system. There, thymic epithelial cells (TECs) have a unique role to instruct developing T lymphocytes to discriminate self-proteins from foreign pathogens and react only against the latter. The development, function and maintenance of TECs are primarily dependent on the transcription factor FOXN1, which acts as a master regulator of the thymus organogenesis and maintenance. Its loss of function results in athymia followed by severe immunodeficiency and is the molecular cause of the "nude" phenotype in humans and mice. Despite its crucial role in thymic development, very little is known about the molecular mechanism of its function.

We have recently identified 3 individuals that presented, from as early as a few months of life, with significant lymphopenia, reduced frequency of naïve T cells, absent T cell receptor excision circles (TRECs) and a lack of radiographic signs of thymus tissue. Surprisingly, these individuals were otherwise clinically healthy. Each was heterozygous for a deletion in the genomic sequence encoding the C-terminus of FOXN1 thus causing a frameshift and consequently a premature stop at amino acid 550, leading to a significantly shortened protein (designated *Δ550*).

Using both *in-vitro* and *in-vivo* models that mimicked the heterozygous patients we explored how a co-expression of the wild-type and mutant FOXN1 proteins compromise thymus development and function. Using RNA-seq coupled with ChIP-Seq we explored differences in gene expression regulated by the two proteins. We also employed mass-spectrometry proteomics analysis followed by CRISPR arrayed screening, to reveal, to our best of knowledge for the first time, the molecular interactome of FOXN1 and how the *Δ550* mutation may interfere with the binding of these interaction partners. With advanced microscopy we showed that FOXN1 participates in the formation of nuclear bodies, essential for its activity as a transcriptional regulator. Finally, we studied the impact of the *Δ550* mutation on TEC differentiation and function in a mouse model heterozygous for a mutation equivalent to that of human *Δ550*. Taken together our studies elucidate aspects of the molecular mechanism by which FOXN1 operates and provide a molecular understanding on how heterozygous *FOXN1* mutations can lead to pathologies.

TABLE OF CONTENTS

List of figures 13

List of tables 16

List of abbreviations 17

CHAPTER 1: INTRODUCTION 21

Preface 22

1.1 The immune system 23

1.2 The thymus as a primary site for T-cell development 23

1.3 Generation of a TCR with unique antigen specificity 28

1.4 Severe combined immunodeficiencies 28

1.5 The Forkhead box protein N1 (FOXN1) 30

1.6 Absence of FOXN1 results in the “nude” phenotype 31

1.7 FOXN1 is a member of the forkhead family of transcription factors 34

1.8 The role of FOXN1 in thymus organogenesis and development 35

1.9 The role of FOXN1 in thymus maintenance and involution 38

1.10 FOXN1 is a master transcriptional regulator in TECs 40

1.11 *Foxn1’s* regulation in TECs 41

1.12 Efforts to correct thymic epithelial cell defects through the manipulation of FOXN1 44

1.13 Outstanding questions in FOXN1 biology 48

1.14 Hypothesis and aims 49

CHAPTER 2: CLINICAL AND IMMUNOLOGIC PHENOTYPE OF A PATIENT WITH A NOVEL MUTATION IN THE *FOXN1* GENE 51

2.2 Introduction and aims 52

2.2 Materials and methods 53

2.2.1 Whole genome sequencing analysis pipeline 53

2.2.2 MiSeq sequencing to determine the length of the CDR3 region of TCR alpha- and beta-chains 54

2.3 Results 55

2.3.1 Clinical and immunologic phenotype in carriers of Δ550 FOXN1 mutation 55

2.3.2 CDR3 length distribution for Valpha (Vα) and Vbeta (Vβ) TCR chain is similar for T cells from the patient and a healthy control 60
2.3.3 TCR repertoire diversity is decreased in the patient 62
2.4 Discussion 63
CHAPTER 3 THE IMPACT OF THE *Δ550* FOXN1 MUTATION ON FOXN1 BIOLOGY 67
3.1 Introduction and Aims 68
3.2 Materials and Methods 69
3.2.1 Cell culture 69
3.2.2 Generation of C-terminally myc-tagged or FLAG-tagged wild type FOXN1 70
3.2.3 Site-directed mutagenesis for the generation of human and mouse FOXN1 variants 70
3.2.4 Transfection of human and mouse cell lines 71
3.2.5 RNA, cDNA synthesis and qRT-PCR 71
3.2.6 Immunohistochemistry 72
3.2.7 Protein preparations and Western blot 73
3.2.8 Luciferase reporter assay 74
3.2.9 RNA-sequencing of the human thymic epithelial 4D6 cell line transfected with either wild-type or *Δ550* mutant FOXN1 75
3.3 Results 76
3.3.1 The *Δ550* mutant allele encodes for a protein of reduced molecular weight compared to the WT protein 76
3.3.2 The *Δ550* mutant localises to the nucleus similar to the wild-type protein 78
3.3.3 The frameshift in the *Δ550* mutant disrupts the evolutionary conserved domain in the c-terminus of the FOXN1 protein 79
3.3.4 FOXN1's function is dose dependent 81
3.3.5 The *Δ550* FOXN1 exerts a dominant negative effect. 83
3.3.6 The *Δ550's* aberrant protein domain makes it a dominant negative mutant 85
3.3.7 The *Δ550* FOXN1 mutant impairs the transcriptionally activity of the WT FOXN1 88
3.3.8 Assessing the pathogenicity of different *FOXN1* variants found in two paediatric patients with immunodeficiency. 92
3.4 Discussion 97

CHAPTER 4 CHARACTERISATION OF THE FOXN1 INTERACTOME 101
4.1 Introduction and Aims 102
4.2 Materials and Methods 103
4.2.1 Generation of a C-terminally tagged *FOXN1* constructs 103
4.2.2 Immunoprecipitation of tagged *FOXN1* variants 104
4.2.3 Live cell imaging 104
4.2.4 Fluorescence recovery after photobleaching 105
4.2.5 Fluorescence correlation spectroscopy of wild type and *Δ550* FOXN1 105
4.2.6 Mass spectrometry proteomics analysis 106
4.2.7 Generation of the EYFP$^{\beta 5t}$FOXN1^{CMV} 4D6 reporter cell line 107
4.2.8 Cloning of sgRNAs in Cas9 expressing vector and transfection of 4D6 EYFP$^{\beta 5t}$FOXN1^{CMV} reporter cells. 110
4.3 Results
4.3.1 Wild-type FOXN1 forms multimers in vivo in 4D6 TEC cells 113
4.3.2 Live behavior of GFP tagged wild type FOXN1 114
4.3.3 Wild-type FOXN1 requires the specific environment of thymic epithelial to form multimers. 116
4.3.4 Wild-type FOXN1 does not form multimers in the presence of the *Δ550* mutant 117
4.3.5 Nuclear movement of Wild-type FOXN1 in the presence or absence of the *Δ550* FOXN1 120
4.3.6 Identification of putative FOXN1 partners by co-immunoprecipitation and mass spectrometry proteomics analysis 122
4.3.7 Validation of candidate FOXN1 interacting proteins using the EYFP$^{\beta 5t}$FOXN1^{CMV} reporter cell line 129
4.4 Discussion 134
CHAPTER 5: THE IMPACT OF THE *Δ550* FOXN1 MUTATION ON DNA BINDING 139
5.1 Introduction and Aims 140
5.2 Materials and Methods 141
5.2.1 Electrophoretic Mobility Shift Assay (EMSA) to assess the DNA binding affinity of purified wild type and mutant proteins. 141
5.2.2 Chromatin Immunoprecipitation (ChIP) followed by DNA-Sequencing 142

5.3 Results 145
5.3.1 Both the wild-type and the *Δ550* FOXN1 mutant bind DNA with comparable affinity 145
5.3.2 Qualitative differences in the DNA binding of WT and *Δ550* FOXN1 in 4D6 cells. 148
5.4 Discussion 153

CHAPTER 6 THE IMPACT OF THE Δ505 MUTATION ON TEC & T CELL DEVELOPMENT 157
6.1 Introduction-Aims 158
6.2 Materials and Methods 159
6.2.1 Mouse handling 159
6.2.2 Generation of FOXN1$^{WT/\Delta505}$ heterozygous mice using CRISPR/Cas9 159
6.2.3 Genotyping of FOXN1$^{WT/\Delta505}$ mice 160
6.2.4 Thymic epithelial cell isolation 163
6.2.5 Isolation of thymocytes 165
6.2.6 Antibody staining 166
6.2.7 FACS analysis and sorting 166
6.3 Results 168
6.3.1 The equivalent of the human *Δ550* mutation in the mouse Foxn1 gene 168
6.3.2 The impact of the *Δ505* mutation on TEC development 171
6.3.3 The impact of the *Δ505* mutation on thymocyte development 178
6.4 Discussion 182
CHAPTER 7 DISCUSSION 184
7.1 Summary-Proposed mechanism 186
7.2 Future work 192
7.3 Conclusion 196
REFERENCES 196

LIST OF FIGURES

Figure 1.1: Schematic representation of the thymus' cellular architecture and the journey of developing thymocytes through the thymic microenvironment. 27
Figure 1.2 Known NUDE mutations in the human FOXN1 gene 33
Figure 1.3: Distinct FOXN1 dosage requirements over different stages of TEC development 38
Figure 1.4 FOXN1 levels determine thymic involution and regeneration 46
Figure 2.1 Family pedigree of *Δ550 FOXN1* mutation 59
Figure 2.2: CDR3 length distribution for Vα and Vβ chain in the patient and an aged-matched healthy control. 61
Figure 3.1: Schematic representation of the luciferase reporter construct used for all reporter assays. 74
Figure 3.2 Transfection with the *Δ550*-FOXN1 results in higher FOXN1 relative mRNA expression levels compared to the WT FOXN1 76
Figure 3.3 *Δ550* FOXN1 protein expression levels are decreased compared to WT protein levels 77
Figure 3.4 *Δ550* FOXN1 localises to the nucleus similar to WT FOXN1 78
Figure 3.5 Amino acid sequence of the C-terminus domain conserved among species 80
Figure 3.6 Functionality of different FOXN1 mutants 82
Figure 3.7 *Δ550*-FOXN1 exerts a dominant negative effect on WT-FOXN1 84
Figure 3.8 Schematic representation of FOXN1 constructs differentially truncated at the C-terminus. 86
Figure 3.9 Dominant negative activity of different FOXN1 constructs. 87
Figure 3.10 Analysis of gene expression changes in the 4D6 cell line transfected with WT, *Δ550* or both 90
Figure 3.11 Schematic representation of FOXN1 variants found in two paediatric patients with athymia or thymic hypoplasia and immunodeficiency 94
Figure 3.12 Assessing the pathogenicity of the 325 FOXN1 variant found in a patient with athymia and immunodeficiency 95

Figure 3.13 Assessing the pathogenicity of 350 FOXN1 variant found in a patient with thymic hypoplasia and immunodeficiency. 96
Figure 4.1 Generation of the EYFP$^{\beta5t}$FOXN1^{CMV} reporter cell line 109
Figure 4.2 FACS gating strategy for the analysis of EYFP positive 4D6 EYFP$^{\beta5t}$FOXN1^{CMV} cells, after transfection with the Cas9-2A-mRuby2 vector. 112
Figure 4.3: WT FOXN1 forms homo-dimers or multimers. 113
Figure 4.4: WT-GFP forms higher ordered structures seen as bright spots in the nucleus of 4D6 TEC cells. 114
Figure 4.5: Dynamic turnover of WT -FOXN1 in nuclear bodies. 115
Figure 4.6: WT FOXN1 does not form homo-multimers in non-TEC cell lines HEK293 and HELA 117
Figure 4.7: WT FOXN1 does not form homo-multimers in the presence of *Δ550* FOXN1 118
Figure 4.8: *Δ550* mutant disrupts the formation of WT-FOXN1 nuclear bodies. 119
Figure 4.9 Diffusion coefficient of GFP-tagged WT-FOXN1 in the nucleus of 4D6 cells in the presence or absence of the *Δ550* mutant 121
Figure 4.10 Identification of FOXN1 binding partners using MS 124
Figure 4.11 Interaction network of FOXN1 associated proteins as identified by IP and MS. 126
Figure 4.12 Generation of a suitable reporter cell line and validation of candidate FOXN1 interacting partners 130
Figure 4.13 Verification of CBP and YBX1 as FOXN1 co-factors 133
Figure 5.1 EMSA analysis to assess the DNA binding ability of different FOXN1 constructs. 147
Figure 5.2 Qualitative differences in DNA binding between WT FOXN1 and *Δ550* mutant. 150
Figure 5.3 WT and Δ550 DNA binding and regulation of gene expression 152
Figure 6.1. Genotyping of FOXN1$^{WT/\Delta505}$ heterozygous mice 161
Figure 6.2 Gating strategy for the characterization of TEC subpopulations. 163
Figure 6.3 Gating strategy for the assessment of the different thymocyte developmental stages. 164
Figure 6.4 The molecular characteristics of the mouse *Δ505 FOXN1* mutant

(*mΔ505)* 168

Figure 6.5 Thymic phenotype of FOXN1$^{WT/\Delta505}$mice. 171

Figure 6.6 Partial differentiation block in mTEC maturation in FOXN1$^{WT/\Delta505}$mice 173

Figure 6.7 TRA expression by mTEC in FOXN1$^{WT/\Delta505}$ mice 176

Figure 6.8 Thymocyte differentiation in FOXN1$^{WT/\Delta505}$mice 179

Figure 6.9 Partial maturation block in SPCD8 thymocyte maturation in FOXN1$^{WT/\Delta505}$mice 180-181

Figure 7.1 A proposed mechanism for WT-FOXN1 function 189

Figure 7.2: A proposed mechanism for the function of the dominant negative *Δ550*-FOXN1 mutant 191

LIST OF TABLES

Table 2.1: Peripheral lymphocyte absolute counts and their percentages in the patient, her sister and father. 57

Table 2.2 The patient's peripheral lymphocyte frequencies at 6 and 19 months of age 59

Table 3.1: Details on culture media and time of trypsin treatment for the different cell lines used in the experiments. 62

Table 3.2: Primer pairs used for the generation of the various *FOXN1* constructs by site directed mutagenesis. 71

Table 3.3: Primer pairs used for the qRT-PCR analysis discussed in chapters 3.3.1 and 6.3.1 72

Table 4.1: Primer sequences used for cloning 103

Table 4.2: List of guide RNAs used for the CRISPR screen. 111

Table 4.3: List of putative FOXN1 binding partners. 127

Table 6.1: Reaction conditions for PCR amplification 160

Table 6.2 List of antibodies used for the FACs phenotypic analysis and FACs cell sorting 165

ABBREVIATIONS

3PP: 3rd Pharyngeal Pouch

AIRE: AutoImmune REgulator

APC: Antigen Presenting Cells

APECED: Autoimmune Polyendocrinopathy Candidiasis Ectodermal Dystrophy

APS1: Autoimmune Polyglandular Syndrome Type 1

AU: Alopecia Universalis

BMP: Bone Morphogenetic Protein

CBP: Creb Binding Protein

CCR5: C-C chemokine Receptor type 5

CCR7: C-C chemokine Receptor type 7

CCR9: C-C chemokine Feceptor type 9

CDR3: Complementary Determining Region 3

CGH: Comperative Genome Hybridization Array

ChIP-Seq: Chromatin ImmunoPrecipitation coupled with DNA sequencing

CMJ: CorticoMedullary Junction

CMV: CytoMegaloVirus

Co-IP: Co-immunoPrecipitation

CRISPR: Clustered Regularly Interspaced Short Palindromic Repeats

cTECs: cortical Thymic Epithelial Cells

CTLA4: Cytotoxic T-lymphocyte Associated Protein 4

CXCR4: C-X-C Motif Chemokine Receptor 4

DCs: Dendritic Cells

DGS: DiGeorge Syndrome

DLL4: DeLta Like protein 4

DN: Double Negative

EBV: Epstein-Barr Virus

EMSA: Electrophoretic Mobility Shift Assay

EpCAM: Epithelial Cell Adhesion Molecule

ESCs: Embryonic Stem Cells

Eya1: Eyes Absent Homolog 1

EYFP: Enchanced Yellow Fluorescent Protein

FCS : Fluorescence Correlation Spectroscopy

FDR: False Discovery Rate

FGF7: Fibroblast Growth Factor 7 also known as Keratine Growth Factor KGF

FGFR2IIIb: Fibroblast Growth Factor Receptor 2

Foxn4: Forkhead box N4

FOXO3: Forkhead box O3

FOXP3: Forkhead box P3

FRAP: Fluorescence Recovery After Photobleaching

Fs: frameshift

Fzd6: Frizzled Class Receptor 6

GFP: Green Fluorescence Protein

gMFI: geometric Mean Fluorescent Intensity

HEK239: Human Embryonic Kidney 293

HELA: HEnrietta LAcks

HLA: Human Leukocyte Antigen

HNF3α: Hepatocyte Nuclear Factor 3 alpha

Hoxa2: Homeobox A2,

HOXC13: homeobox C13

human keratine 14: hK14

ILCs: Innate-Lymphoid Cells:

IP: ImmunoPrecipitation

LC/MS-MS: Liquid Chromatography/ Mass Spectrometry-Mass Spectrometry

LRBA: Lippopolysacaccharide Responsice Beige like Anchor protein

luc: luciferase

MHC: Major Histocompatibility Complex

mTECs: medullary Thymic Epithelial Cells

Natural Killer cells: NK cells

NGS: Next Generation Sequencing

PAMPs: Pathogen Associated Molecular Patterns

Pax1: Paired box 1

Pax1: Paired box 1

Pax9: Paired box 9

PDGF-B: Platelet-Derived Growth Factor B

PDPN: Podoplanin

PGE: Promiscuous Gene Expression

PID: Primary ImmunoDeficiency

PKC: Protein Kinase C

PRRs: Pattern Recognition Receptors

PSMA7: Proteasome Subunit Alpha 7

R: arginine

RAG1/2: Recombination Activating Genes 1/2

Rb: Retinoblastoma

SCID: Severe Combined ImmunoDeficiencies

sgRNA: single guide RNA

Six1: Sine Oculis Homeobox Homolog 1

SP: Single Positive

SPCD4: Single Positive CD4

SPCD8: Singe Positive CD8

TBX1: T BoX transcription factor 1

TCR: T Cell Receptor

TDT: Terminal Deoxynucleotide Transferase

TECP: TEC progenitor

TECs: Thymic Epithelial Cells

TF: Transcription Factor

TRA: Tissue Restricted Antigens

TRECs: T cell Receptor Excision Circles

Treg: T-regulatory

Trp63: Transformation related protein 63

VEGF-A: Vascular Endothelial Growth Factor A

W: tryptophan

WB: Western Blot

WGS: Whole Genome Sequencing

WIMM: Weatherall Institute of Molecular Medicine

Wnt1: Wnt family member 1

WT: Wild Type

X: stop codon

YBX1: Y-box binding protein

β5t: thymoproteasome subunit β5

CHAPTER 1

INTRODUCTION

Preface	22
1.1 The immune system	23
1.2 The thymus as a primary site for T-cell development	23
1.3 Generation of a TCR with unique antigen specificity	28
1.4 Severe combined immunodeficiencies	28
1.5 The Forkhead box protein N1 (FOXN1)	30
1.6 Absence of FOXN1 results in the “nude” phenotype	31
1.7 FOXN1 is a member of the forkhead family of transcription factors	34
1.8 The role of FOXN1 in thymus organogenesis and development	35
1.9 The role of FOXN1 in thymus maintenance and involution	38
1.10FOXN1 is a master transcriptional regulator in TECs	40
1.11 Foxn1’s regulation in TECs	41
1.12 Efforts to correct thymic epithelial cell defects through the manipulation of FOXN1	44
1.13 Outstanding questions in FOXN1 biology	48
1.14 Hypothesis and aims	49

PREFACE

The thymus gland was known to the ancient Greeks. Its name originates from the greek word Θυμός (tʰyː.mós, ‘’soul, spirit, as the principle of life, feeling and thought, esp. of strong feeling and passion’’ from the Henry George Liddell, Robert Scott, A Greek-English Lexicon). Homer referred to the thymus as the source of all emotions, the human soul. The ancient Greeks believed the thymus to be the place where emotions are generated, perhaps due to its location above the heart. Until very recently the thymic function remained an enigma. It was considered a vestigial organ full of lymphocytes, whose existence there –as Sir Peter Medawar had stated- ‘’has absolutely no significance’’[1]. Tremendous progress in the study of the function of thymus over the last 50 years has changed this view. We now know that the thymus, rather than the seat of the soul, has a central role in generating mature, functional and self-tolerant T cells.

1.1 The immune system

The immune system provides the body's defence against diseases. It is made of various tissues and cell types that collaborate closely to mount an effective immune response against foreign pathogens, such as bacteria, viruses and parasites but also against tumours or other harmful substances like toxins. The potency of this defence system relies on the interplay and regulation between the innate and adaptive immunity. Innate immunity recognises structural components of pathogens, known as pathogen associated molecular patterns (PAMPs), via a limited number of germline-encoded receptors (pattern recognition receptors or PRRs). Adaptive immunity involves pathogen-specific responses facilitated by the interplay between antigen-presenting cells (i.e. dendritic cells), T lymphocytes and B lymphocytes. T and B lymphocytes carry antigen-specific receptors that have been generated via somatic gene rearrangements and can recognise antigenic components of all potential pathogens. Adaptive immunity is also characterised by immunological memory following subsequent encounters with the same pathogen. T cells are critical in orchestrating protective immune responses involving multiple cell types of both the innate and adaptive immunity. To successfully fulfil this role, during their development they are trained to discriminate between potentially injurious non-self and benign self-antigens. The focus of this thesis will be on the thymus, the site where tolerance to self is instructed on developing T cells, designated thymocytes.

1.2 The thymus as a primary site for T cell development

The thymus is the primary lymphoid organ of the immune system, responsible for the generation, differentiation and repertoire selection of T lymphocytes[2]. It serves as

the primary site for T cell development in all jawed vertebrates[3]. This unique function is primarily dependent on the thymic stroma that consists of a highly specialized thymic epithelial cell (TECs) population and various other cell types including dendritic cells (DCs), macrophages, mesenchymal cells and vascular endothelium[4]. TECs form a unique three-dimensional (3D) network [5] that creates the appropriate microenvironment for thymocyte development. The tissue is subdivided into two broad regions, namely the cortex and the medulla, each containing distinct TEC sublineages, cortical (c) and medullary (m) TEC respectively[4]. Each TEC sublineage possesses unique functional and structural characteristics that are responsible for different stages of T cell development[6]. cTECs occupy the outer parts of the tissue, while mTECs reside in the organ's centrally located medullary islands. In between the two compartments lies the corticomedullary junction (CMJ) controlling the entry of lymphoid progenitors into the thymus from the vasculature and the emigration of mature T cells (Figure 1.1)[7, 8].

The physical movement of developing T cells within the thymus during their maturation is illustrated in Figure 1.1. The different thymocyte developmental stages can be distinguished by a set of specific cell (surface) markers. The most important are the co-receptors CD4 and CD8 as well as molecules of the T Cell Receptor (TCR) complex. After entering the thymus at the CMJ, T cell progenitors are attracted to move across the cortex to the subcapsular area where they intensely proliferate for several days. [9, 10] (1 in Figure 1.1). During this early phase, neither CD4, CD8 or the TCR are expressed and the thymocytes at this stage are referred to as double negative (DN), i.e. lacking expression of CD4 and CD8. Blood-born DN progenitors express the chemokine receptors CXCR4 (C-X-C Motif Chemokine Receptor 4), CCR7 (C-C

chemokine receptor type 7), and CCR9 (C-C chemokine receptor type 9) that bind to their respective ligands expressed by the thymic stroma and this directs the entry of the cells from the blood to the thymus[11-13]. Several distinct and successive DN stages (DN1-4) are known, each defined by a distinct set of surface markers. Successive DN stages (DN1-DN4) are accompanied by a progressive movement towards the outer cortex (stage 2 in Figure 1.1). At the DN2 stage, thymocytes are committed to the T cell fate following signals received from DLL4 (delta like protein 4) present on cTECs that activates a Notch signaling response[14] (stage 2 in Figure 1.1). Notch signaling triggers DN proliferation and differentiation throughout DN development [15]. During these early developmental stages, DN thymocytes activate the RAG1/2 genes (recombination activating genes) that initiate the TCR rearrangement resulting in a TCR locus with unique antigen specificity (detailed in chapter 1.3). T-committed DN3 cells with a productively rearranged TCR β-chain, pass the first checkpoint, known as β-selection, and expand through proliferation (reviewed in[16]) (stage 3 in Figure 1.1). Thymocytes that successfully pass β-selection upregulate the concomitant expression of CD4 and CD8 coreceptors and are designated as double positive (DP). In parallel TCRa chain's rearrangement is initiated and together with TCRb chain they form a complete TCRαβ. DP cells have a short life span of three to four days which is extended '' rescued ''upon successful and correct interaction of their now complete αβ TCR with self-peptide:MHC complexes (MHC: Major Histocompatibility complex) presented by cTECs, a process termed positive selection (reviewed by[17]). The result of positive selection is the generation of two classes of thymocytes according to their TCR's MHC restriction, MHC class I–restricted $CD8^+$ and MHC class II–restricted $CD4^+$ cells, known as single positive (SP) CD4 or single

positive (SP) CD8 T cells. Committed to the different effector lineages, the thymocytes will transition from the cortex to the medulla[18] (4 in Figure 1.1).

The thymic medulla is the site where central tolerance is instructed by mTECs and DCs. mTECs as a population express almost all protein coding genes while still able to retain their TEC identity[19, 20]. This unique property of mTECs, known as promiscuous gene expression (PGE) entails the expression of proteins usually expressed in peripheral tissues, so called tissue-restricted antigens, TRAs)[21, 22] (stage 5 in Figure 1.1). TRAs are presented by mTECs to developing thymocytes. DCs play also an active role in negative selection[23]. Conventional DCs are located primarily in the medulla where they acquire TRAs from mTECs and present them to T cells [23]. Two other subsets of DCs (plasmacytoid and migratory DCs) develop in the periphery where they take up antigens and migrate to the thymus to present these antigens to developing T cells[23]. Newly selected single positive (SP) T cells bearing an αβ TCR that triggers high affinity signalling upon interaction with self-peptide MHC complexes undergo programmed cell death (apoptosis) in the medulla or are diverted to the T-regulatory (Treg) lineage. This process is known as negative selection and helps to eliminate self-reactive T cells (reviewed in [17]). Negative selection can also occur by APCs in the cortex[24].

PGE that facilitates negative selection of autoreactive T cells differs significantly from the conventional control of gene expression in the corresponding peripheral tissues. A transcriptional facilitator known as the autoimmune regulator (AIRE) is partly responsible for PGE[25]. *Aire* is expressed in mature mTECs expressing high cell surface concentration of MHC II and CD80 (designated as $mTEC^{hi}$). PGE was dramatically reduced in mature mTECs in the absence of AIRE and consequently, AIRE-deficient

mice were defective in the negative selection of autoreactive T cells and suffered from organ specific autoimmunity [22, 25]. In humans, mutations in the AIRE gene result in Autoimmune Polyendocrinopathy Candidiasis Ectodermal Dystrophy (APECED); also known as Autoimmune polyglandular syndrome type 1 (APS1) [26]. Patients with APECED have severe autoimmune manifestations against a variety of organs including parathyroid and adrenal glands. Apart from AIRE there are other AIRE-independent mechanisms that control the expression of TRAs, that are still poorly understood. Functionally competent SP $CD4^+$ or $CD8^+$ T cells that have successfully survived negative selection, undergo a process of post selectional maturation and will subsequently exit the thymus to the periphery as naïve T cells [8, 27-30] (stage 6 in figure 1.1).

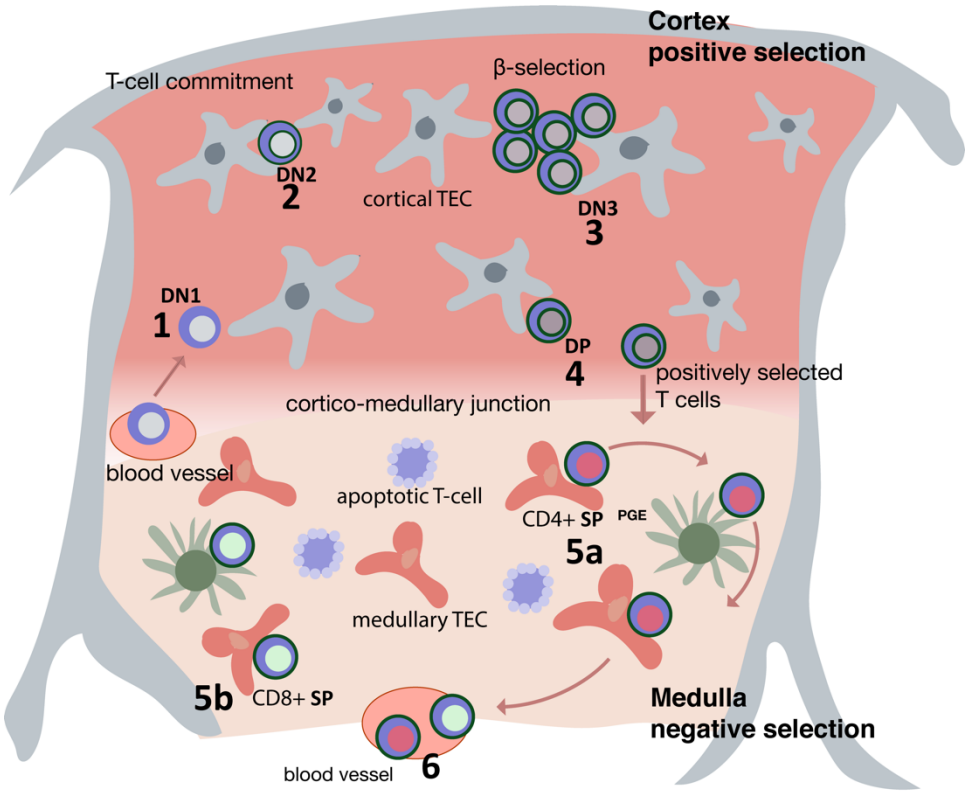


Figure 1.1: Schematic representation of the thymus' cellular architecture and the journey of developing thymocytes (details in chapter 1.2) through the thymic microenvironment. Numbers (1-6) represent the different stages of T cell development in the tissue starting from T cell precursors entering the tissue to SP $CD4^+$ and $CD8^+$ T cells exiting the thymus.

1.3 Generation of a TCR with unique antigen specificity

A T cell's antigen specificity is determined by its TCR. In all jawed vertebrates there are four TCR gene loci, TRA, TRB, TRG and TRD[31-33]. Each locus contains a number of variable (V) and joining (J) segments, while for TRB and TRD there are also additional diversity segments (D). During thymocyte maturation in the thymus, these loci undergo a process of somatic DNA rearrangement containing single individual V, D and J regions to produce a TCR clonotype with a novel sequence (reviewed in [34]). This novel configuration produces a TCR with unique specificity for a given antigen. The gene rearrangement process involves a series of DNA splicing reactions controlled by the RAG1/2 (recombination activating gene) proteins[35]. Because the splicing is not precise, it results in nucleotide deletions and/or de-novo insertions at the junctional sites of splicing (the latter known as n-nucleotides). These nucleotide additions are catalysed by the enzyme terminal deoxynucleotide transferase (TDT)[36]. In addition to this level of imprecision short palindromic segments can also be inserted (known as p-nucleotides), which add an extra level of variability at the V-D-J junctional sites[37]. Overall, the entire process results in variations in the amino acid sequence of the TCR's complementary determining region 3 (CDR3), the site that is mainly responsible for antigen recognition[38].

1.4 Severe combined immunodeficiencies

Severe combined immunodeficiencies (SCID) constitute of group of monogenic disorders with a rare incidence rate of approximately 1/50,000 live births. These pathologies manifest early in life and are characterised by a defective T lymphocyte differentiation that depending on the specific genetic aetiology may also affect both B

cell and NK cellularity and function [39-41]. Patients with SCID suffer from severe and recurrent infections caused by both opportunistic and non-opportunistic pathogens such as the fungus Pneumocystis jirovecii (PJP) and the water parasite Cryptosporidium. These infections are usually life threatening in SCID patients but not in the healthy population [42].

In most cases, the observed immunodeficiency in SCID patients arises due to intrinsic defects in T lymphocytes. An exception is the Nude/SCID syndrome where a defect in TEC differentiation results in failure in thymus organogenesis abrogating normal T cell development. There is a high degree of molecular heterogeneity among SCID syndromes due to the variety of underlying genetic causes. To date, sixteen distinct genes have been associated with the diagnosis of SCID (summarised in [39]).

Early diagnosis of SCID has recently been made possible through new-born screening using dried blood spots on conventional filter paper cards, where DNA is eluted from the cards and tested for the presence of T cell Receptor Excision Circles (TRECs) [43]. TRECs are DNA circular by-products of TCR rearrangement in the thymus and can be readily amplified and quantified by PCR. Low or absent TRECs suggest impaired thymic T cell development, a finding which is then further followed up by more sophisticated methods[43]. These include the determination of absolute lymphocyte counts, T cell function and genetic analysis to determine the molecular causes [39]. Early diagnosis is imperative for the correct management of these patients before life-threatening infections occur which increase significantly the mortality rate [39]. The definitive therapy of SCID caused by a defect in hematopoietic cells requires a hematopoietic stem cell transplantation or gene replacement therapy whereas a thymus transplantation is indicated for patients with a NUDE SCID defect[39].

1.5 The Forkhead box protein N1 (FOXN1)

The formation of a functional thymus critically depends on the transcription factor FOXN1, which acts as a master regulator of thymic epithelial cell development, function, homeostasis and regeneration [44]. Bi-allelic loss of function mutations in the *FOXN1* gene result in humans, mice and rats in the nude severe combined immunodeficiency (Nude/SCID) phenotype known also as lymphoid cystic thymic dysgenesis (ORPHA169095)[45-48]. The precise molecular cause of this rare autosomal recessive pathology was first identified in 1994 to be due to a deletional mutation in the *Foxn1* gene (at the time still referred to as winged-helix nude, *Whn*) [48, 49]. The *Foxn1* transcript in the nude mouse carries a single base pair deletion leading to premature termination of translation and an altogether absence of the FOXN1 protein[48]. Studies in mice inserting a LacZ M2 neo cassette into exon 3 of *Foxn1* alleles, phenocopied the ''nude'' mouse, due to a loss of functional FOXN1 expression [9]. This studies thus confirmed that *Foxn1* is the gene mutated in nude mice[9].

In addition to the thymus, *Foxn1* is also expressed in the skin, where it is expressed at the onset of terminal differentiation of keratinocytes and regulates their balance between proliferation and differentiation [50]. In the skin, FOXN1 regulates the expression of various genes involved in cell cycle progression such as protein kinase C *(PKC)* [51] and epithelial cell differentiation markers like keratin 1[52].

The FOXN1 protein consists structurally of three functionally distinct domains. Structure: function analysis has demonstrated that the N-terminus of FOXN1 is critical for TEC differentiation at least on experimental conditions in the mouse, whereas the C-terminus contains an acidic activation domain required for target gene

transcriptional activation [53-55] (Figure 1.2a). Between these two domains lies the highly conserved forkhead domain that mediates DNA binding and defines the membership to the forkhead family of molecules[49, 56].

1.6 Absence of FOXN1 results in the "nude" phenotype

The clinical presentation of absent thymus (athymia), alopecia universalis (AU) and nail dystrophy[47, 57-61] are the hallmarks of the so-called nude phenotype (Nude-SCID). This collection of features occurred spontaneously in 1966 in the so-called nude mouse, and was associated with a severe failure to thrive and increased mortality [62-64] due to the athymia, recognised at that time to be the most likely explanation for the latter.

The human equivalent of the mouse nude phenotype was reported 30 years later in two sisters from Southern Italy who presented with athymia, reduced T cell counts, an absence of hair and nail dysplasia [45, 57]. Before the genetic cause could be identified one of the two sisters received an HLA-identical total bone marrow transplantation and appeared to be healthy for at least the six years of follow up. In contrast, the other sister died from infections prior to the initiation of treatment[65]. To date, eleven cases of human NUDE/SCID have been reported (estimated incidence of <1/1,000,000)[45, 57, 59-61, 65, 66]. The reported human *FOXN1* mutations are located either in the N-terminus or the forkhead domain of the protein and are uniformly predicted to result in loss-of-function (figure 1.2). The R255X and S188fs mutations cause a premature stop codon in the N-terminus or the forkhead domain, respectively leading to a non-sense mediated decay of the mRNA[45, 59]. The R320W mutation is a single amino acid substitution in the forkhead domain and is predicted

to disrupt the DNA binding ability of the mutated FOXN1 [66]. Adults heterozygous for one of these mutations have normal peripheral T cell numbers, with slightly reduced $CD8^+$ T cells and they are not susceptible to recurrent infections. The presence of a thymus was however not assessed in those patients. While, almost 60% of them were also reported to have nail dystrophy [67].

A recent study characterised a total of 12 heterozygous *FOXN1* mutations found in 21 adult or paediatric patients that were located in the C-terminus of the *FOXN1* gene [67]. The majority of these mutations were single base pair deletions, located at various positions in the C-terminus that in silico are predicted to generate a truncated FOXN1 protein. Patients with these mutations have T cell lymphopenia primarily affecting the CD8 compartment and a range of pathologies. Some of them were healthy while others had recurrent infections that in cases were particularly severe. The location of the mutation didn't seem to correlate with the presence or absence of thymic tissue or the severity of the infections. It is particularly striking that the same single base pair deletion lead to athymia in one patient but presence of a thymus in another.

Mutations in the rat *Foxn1* gene generate a protein lacking 175aa from the C-terminus resulting in the equivalent of the nude phenotype [48]. In Birman cats a generation of a homozygous premature stop codon at protein position 547aa and when homozygous results in hypotrichosis and reduced lifespan. However, it is not known whether this mutation results in underlying immunodeficiency in these species[68].

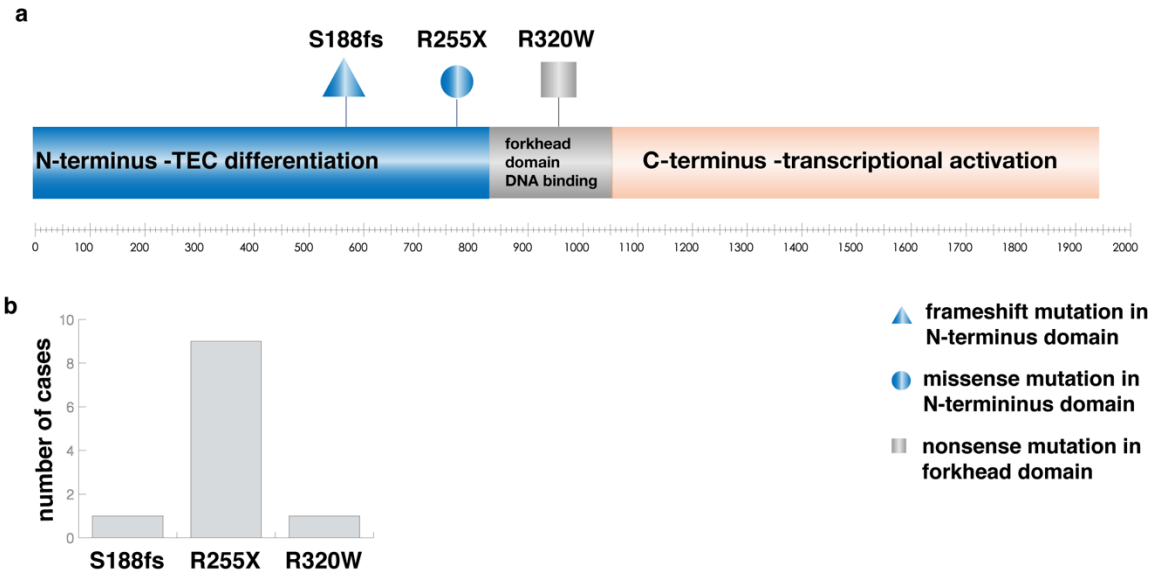


Figure 1.2: Known NUDE mutations in the human *FOXN1* gene a) Functional domains of the human FOXN1 protein with NUDE mutations indicated b) Number of cases reported for the NUDE mutations (adapted from[46]) . Numbered scale represents base pairs.

1.7 FOXN1 is a member of the forkhead family of transcription factors

FOXN1 is a member of the forkhead family of transcription factors (TF) with more than 2000 FOX members identified in 108 species[69-71]. All members of this family have pivotal roles in development, function, and aging of various tissues and organs– including the immune system [69, 72]. For example, FOXP3 (Forkhead box P3) is indispensable for the normal functional of regulatory T cells (Treg cells)[73, 74] and FOXO3 (Forkhead Box O3) is required for the proliferation and apoptosis of lymphocytes [75, 76]. All FOX family members have in common a highly conserved DNA binding domain known as the forkhead domain, that is the only sequence of the protein that can be confidently aligned across all FOX members[49, 77]. This kind of DNA binding domain was first identified in 1990, in the rat hepatocyte nuclear factor 3 alpha (*HNF3α*) (now known as FOXA1) [78].

The prototypical forkhead DNA binding domain consists of three α-helices (H1-3), three β-sheets (S1-3) and two wing region/loops (W1-2) in the following order H1-S1-H2-H3-S2-W1-S3-W2[79, 80]. The DNA binding specificity of each FOX member is determined by the variable regions between the α-helices and the wing loops[81]. The specific functions of each FOX protein in this family lie in the protein parts outside the DNA binding domain that have almost no homology among the FOX family members [72]. Further functional diversity is achieved by different interaction partners or distinct spatio-temporal expression patterns [77]. FOX factors can bind to DNA as monomers [79], multimers[82], homodimers[83], or heterodimers[82]. FOX family members might have different post-translation modifications such as phosphorylation, of serine, threonine or tyrosine residues[84], acetylation of lysine[85] or ubiquitination[86]. These post translational modifications can determine

the activity, cellular localisation and stability of these proteins and have been shown to fine-tune their DNA binding efficiency[69, 87, 88]. All the above determine the ability of FOX factors to act as effector molecules in several signalling pathways[69]

FOXA transcription factors were among the first pioneer TF to be identified [89, 90]. The term pioneer refers to the capacity of these factors to directly open previously compact chromatin in order to facilitate its transcription. FOXA proteins can achieve that through their C-terminal transactivation domain[89, 90]. It remains to be determined whether FOXN1 can also act as a pioneer transcription factor [44].

FOXN1 is most closely related to its paralog *FOXN4*. *Foxn4* is expressed in the pharyngeal endoderm of amphioxus suggesting that it contributed to the evolutionary emergence of thymopoiesis [91]. While both *Foxn1* and *Foxn4* are expressed in the thymi of all jawed vertebrates; *Foxn4 (Forkhead box N4)* gene expression is very low in higher order organisms[92]. However, it has been shown that the role of *Foxn1* for thymus development in jawed vertebrates cannot be substituted by *Foxn4* [92]

1.8 The role of FOXN1 in thymus organogenesis and development

FOXN1 is critical for TEC development and function at any age. In the mouse embryo *Foxn1*'s expression becomes prominent only by E11.25 [93]. In humans, the thymic primordium is evident by week 6 of gestation while *FOXN1* expression can be detected by mid-week 6 [94]. Histological analysis in mice concluded that *Foxn1's* expression is not required for the formation of a thymus primordium[95] or TEC lineage specification[95-97]. Indeed, the thymus primordium in nude mice and WT mice is

very similar[91]. By E15 the nude fetal thymus contains $K5^{hi}$ $Cld4^{hi}$ areas associated with mTEC lineage suggesting that their specification is also *Foxn1* independent [91].

From the moment thymocyte progenitors seed the thymic primordium (E11.5-E12), *Foxn1* expression and thymocyte:TEC crosstalk play a critical role in the processes that ultimately form a regular thymus [98]. The exact role of FOXN1 during the later stages of development is only partially characterised. Experimental evidence suggests that FOXN1 is involved in TEC proliferation[99] and the attraction of both hematopoietic and endothelial progenitors to the thymic rudiment[99-101]. FOXN1 has also been shown to control the migration of neural crest cells to the thymus anlage forming its mesenchymal stromal component [91]. Finally, FOXN1 regulates the normal vascularisation of the tissue as in its absence vascular endothelial growth factor A (VEGF-A) and platelet-derived growth factor B **(**PDGF-B) expression is reduced leading to fewer capillaries in the thymic rudiment, leaky blood vessels and a collapse in normal vascular organisation[102].

FOXN1 function is dose-dependent throughout different stages of development as shown by the use of *Foxn1* hypomorphic alleles[54, 91] or the analysis of the temporal control of *Foxn1* expression levels[103]. In a homozygous mouse model where *Foxn1* hypomorphic alleles only transcribe 15% of WT *Foxn1* levels, T cell development and cellularity are significantly decreased[91]. Interestingly, these lower *Foxn1* levels allow for an initial TEC differentiation to occur but later developmental stages are not obtained [54, 91]. Decreased *Foxn1* levels have also been associated with fewer TEC progenitors, fewer mature mTECs (MHC-II^{hi} $CD80^{+}$ $CD86^{+}$), and increased numbers of negatively selected thymocytes[104].

Distinct TEC subsets express different levels of *Foxn1*[103, 105]. Adult mTECs express lower levels of *Foxn1* compared to cTECs while mTEC^{hi}, as defined by high MHC II and CD80 cell surface display, express higher levels when compared to mTEC^{lo} [91, 106, 107]. MTEC^{lo} cells consist an mTEC subpopulation, defined by low expression of MHC II and CD80 and serve as precursors to mTEC^{hi} [108, 109]. It appears from a single study that adult mTEC when compared to cTEC, are more sensitive to the loss of FOXN1, because its postnatal deletion results in dramatic tissue atrophy primarily affecting the medulla[110], other experiments could not confirm this observation [97], which however may be explained by the difference in the methods used.

As detailed in chapter 1.9, continuous expression of *Foxn1* is necessary for the maintenance of TECs throughout life [103, 111-113]. All embryonic TECs, after E11.5, express *Foxn1*; however, in the aging thymus *Foxn1* expression progressively declines concurrent with the accumulation of FOXN1$^{-/low}$ TECs [106]. FOXN1 negative TECs arise from FOXN1 positive precursors as shown by lineage tracing studies[112, 114, 115]. The emergence of these negative cells signals the onset of thymic involution as elegantly shown using FOXN1-eGFP reporter mice[114].

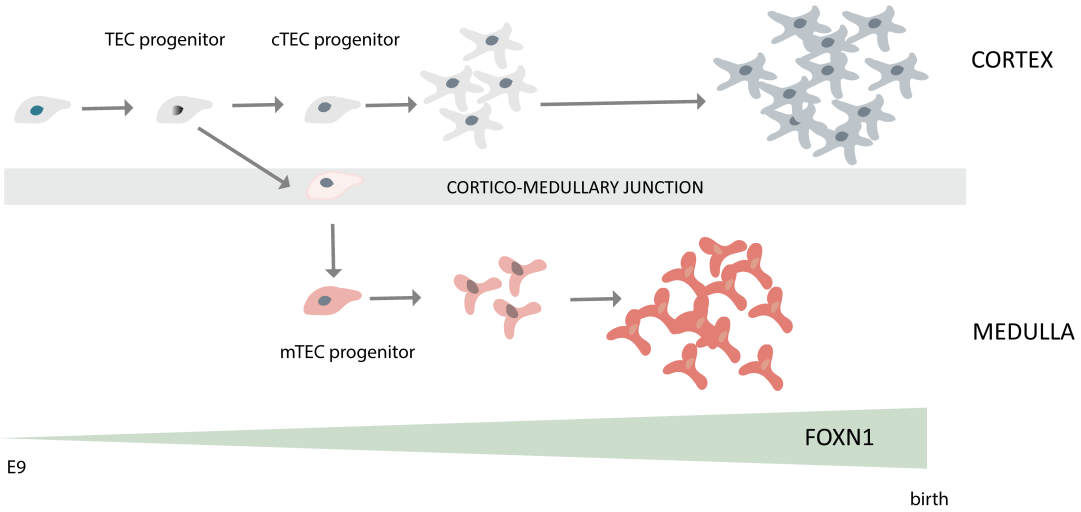


Figure 1.3: Distinct FOXN1 dosage requirements over different stages of TEC development. Both mTEC and cTEC arise from a common bipotent progenitor with cTEC like characteristics, designated TEC progenitor (TECP). This cell is initially localised in the cortex and later also in the corticomedullary junction[116-118]. TECP express the thymus specific thymoproteasome subunit β5 (β5t), are podoplanin (PDPN) positive and can give rise to β5t-negative mTEC as well as β5t-positive cTEC[119]. One study defines adult TECP as EpCam^{+}UEA1^{-}Ly-51^{+}PLET1^{+}MHC II^{hi}. TECP comprise 0.5% of the adult TEC population and their existence persists *in vivo* in mice for up to 9 months of age[120]. mTEC sub-lineage-restricted progenitors have been identified in the fetal thymus and they are able to generate AIRE^{+} mTEC (essential for central tolerance)[121-123]. Similarly, a putative fetal cTEC-restricted progenitor was also identified[124]. Throughout, TEC differentiation process distinct FOXN1 dosage levels are detected.

1.9 The role of FOXN1 in thymus maintenance and involution

Thymus function, as measured by naïve T cell output, reaches its peak during embryonic life and shortly after birth. However, after the first years of life and mainly after puberty the thymus undergoes a premature age-related degeneration, characterised by loss of tissue architecture and decline in T cell output[125]. The tissue senescence is considered to be primarily a consequence of TECs [103, 126, 127] as their numbers decline dramatically and are replaced over time by fibroblasts and adipocytes[128-130]. During the process of thymic involution a reduction in TEC turnover has been observed. In the mouse for example, the number of proliferating TECs (i.e Ki67^{+}), falls from 30%, in the perinatal period, to 5% at 4 weeks of age [130].

This change is accompanied by a decrease in the expression of cell-cycle associated genes, like *E2f3* [107]. Ageing TECs also progressively lose their expression of fibroblast growth factor 21 (FGF21), a factor involved in fatty acid metabolism and known to prevent TEC degeneration in aged mice[131]. Moreover, FGF21 has also been shown to downregulate other molecules necessary of TEC- T cell crosstalk such as MHC-II and IL-7[130].

Foxn1 expression progressively decline in TECs with age which has been considered as one of the hallmarks of thymic involution [106, 132]. The forced expression of *Foxn1* (i.e transgenic) attenuates this process [133] thus supporting the critical role of FOXN1 in postnatal thymus homeostasis and involution. For example TEC progenitor cells in *Foxn1* nude mice display a developmental block that can be restored in neonatal and adult mice by engineered *Foxn1* expression [134]. In an experimental mouse model in which a LacZ transgene has been placed into exon 9 of *Foxn1*, *Foxn1* expression levels are normal during embryonic and early postnatal development. However, at 5 weeks of age *Foxn1* expression declines to 20-30% of wild type. perturbating TEC homeostasis and eventually leading to premature thymus involution. [103]. Interestingly, TEC subsets expressing higher levels of *Foxn1* were the cells most affected by this decline highlighting a FOXN1 dosage sensitivity for TEC [103]. Upon deletion of *Foxn1*, postnatal thymi rapidly involute further strengthening the role of FOXN1 in the maintaining adult thymic tissue[111, 112, 135]. This conclusion is further supported by observations in physiological conditions as *Foxn1* expression declines with age leading to the accumulation of *Foxn1* $^{-/low}$ TECs. This study took an advantage of a newly generated antibody against the C-terminus of FOXN1 [106] which so far has not been independently verified by others. Lineage tracing of FOXN1 TECs

demonstrated that these cells arise from *Foxn1*-expressing cells [112, 114, 115]. In summary, the aforementioned studies suggest that declining *Foxn1* expression regulates the onset and progression of age-related thymus involution.

1.10 FOXN1 is a master transcriptional regulator in TECs

A series of studies have associated FOXN1 with the expression of genes linked to TEC identity. These include genes involved in TEC differentiation and function, like the transcription factors *Trp63* (transformation related protein 63), *Pax1* (paired box 1), *FGFR2IIIb* (fibroblast growth factor receptor 2*)*, chemokines like *IL-7*, and other genes characteristic of TECs like *Dll4, CD40, CD80* as well as several genes of the Wnt signaling pathway like *Wnt1* (wnt family member 1) and *Fzd6* (Frizzled Class Receptor 6) [91, 104, 136, 137]. Ectopic overexpression of *Foxn1* in mouse embryonic fibroblasts results in the reprogramming of these cells into functional TECs expressing genes involved in TEC identity like *EpCAM* (epithelial cell adhesion molecule) and *Keratin* 8[138]. Using a combination of ChIP-Seq (chromatin immunoprecipitation coupled with DNA sequencing) and RNA-Sequencing in a mouse model expressing a FLAG-tagged FOXN1, 450 high confidence FOXN1 targets were identified[104].

The direct transcriptional regulation of a few of these genes by FOXN1 was confirmed in two studies [104, 139]. One of these studies [139] identified a highly conserved FOXN1 binding sequence upstream of the *β5t* coding sequence. Point mutations in that binding site abrogate *β5t* upregulation confirming that FOXN1 is involved in the direct control of its expression[139]. Fully in accordance with this result, the disruption of the FOXN1 binding sites within the promoters of *β5t* and *CD83* disrupted the ability to drive the expression of luciferase in HEK293 cells co-transfected with

a *Foxn1* expression plasmid and a luciferase construct downstream of the *β5t* and *Cd83* promoters. These studies confirmed FOXN1 as a master transcriptional regulator of TEC development, proficient to initiate and maintain the transcriptional network that determines the identity of TECs.

1.11 *Foxn1*'s regulation in TECs

Little is known about the upstream transcriptional regulators of *Foxn1*. There is strong evidence in TECs for a positive autoregulatory loop for *Foxn1* expression. In a FOXN1 transgenic mouse where *Foxn1* expression was driven under the control of the human keratin 14 promoter (hK14), the transgene could upregulate endogenous *Foxn1*[133]. However, it is yet unknown whether this loop is further controlled by other regulators. It is however of note that a FOXN1 DNA binding motif can be detected upstream of the *Foxn1* coding sequence (A. Handel personal communication).

The loss of gene expression for several transcription factors results in athymia in mice[140]. ''Knock out'' of *Pax9* (paired box 9) or *Pax1* (paired box 1) transcription factors both expressed in the endoderm of the 3rd Pharyngeal Pouch (3PP) from where TECP derive, results in athymia or thymic hypoplasia, respectively[141, 142]. While loss of *Hoxa2* (homeobox A2), *Eya1* (Eyes Absent Homolog 1) or *Six1* (Sine Oculis Homeobox Homolog 1) disrupt normal TEC development [143-145]. However, these factors have not been shown to directly bind to *Foxn1* regulatory regions *in vivo*.

The T box transcription factor 1 (TBX1) is, early in development, a putative negative *Foxn1* regulator. Mutations in the *TBX1* gene cause the DiGeorge syndrome (22q11 deletion syndrome) which is characterised among others by thymic hypoplasia or aplasia with subsequent impaired thymocyte development [146]. Ectopic *Tbx1*

expression in FOXN1 expressing cells of the E11.5 3PP leads to downregulation of *Foxn1* [147] indicating that TBX1 suppresses TEC differentiation. This finding is further corroborated in fetal thymi where a forced *Tbx1* expression blocks TEC differentiation[147]. Given that TBX1 binding sites have not been found in the *Foxn1* promoter candidate region, it remains to be determined whether TBX1 suppresses FOXN1 function indirectly through modulating a direct yet unknown FOXN1 regulator[147].

E2F3 and E2F4, members of the E2F family of transcription factors, have been shown to bind *in vitro* to their consensus binding motif upstream of *Foxn1* in a region considered as the *Foxn1* promoter[148]. E2F3 and E2F4 proteins regulate cell cycle progression and are downregulated by Retinoblastoma tumor suppressor (Rb) proteins [148]. *In vivo*, increased E2F3 expression results in an increase in *Foxn1* expression. Mice that lack the *Rb* and *p103* genes, both members of the Rb family, exhibit severe thymus hyperplasia correlated with an increase in *Foxn1* expression. Reduction in *Foxn1* levels reversed the hyperplastic thymus providing strong evidence of FOXN1 regulation by RB-E2F axis[148].

In the skin and hair follicles, *Foxn1* is regulated by HOXC13. However, it has not been determined whether HOXC13 (homeobox C13) regulates *Foxn1* also in TECs[149]. In TECs, BMP (Bone morphogenetic protein) and Wnt signalling have been associated with the regulation of FOXN1 expression but the exact molecular mechanisms are currently not elucidated[150-157].

The regulatory regions controlling *Foxn1* expression in TECs are not fully characterised. A 26kb region containing only the *Foxn1* coding exons and 8.5kb upstream and 3kb downstream of this sequence could only rescue the skin phenotype but failed to

restore the thymus development in nude mice, suggesting a differential regulatory network for *Foxn1* expression in skin and thymus[158]. A 110kb region with the entire *Foxn1* locus in addition to 75kb and 12kb flanking sequences upstream and downstream respectively was able to rescue the nude phenotype *in vivo,* documenting that this region contains all the *Foxn1* regulatory elements[159]. Examining chromatin marks consistent with active regulatory regions, a 1.6kb region within the first intron of *Foxn1* was identified that is indispensable for *foxn1* expression in TEC [160].Deletion of this region lead to athymia and a nearly complete loss of T cells in the periphery. However, *foxn1* expression in the skin was unaffected and mice lacking this 1.6kb regulatory region developed normal hair and nails.

1.12 Efforts to correct thymic epithelial cell defects through the manipulation of FOXN1

Given FOXN1's critical role in thymic maintenance and involution, it is not surprising that recent studies with the goal to achieve thymus regeneration focus on efforts to manipulate FOXN1.

Using the R26-*Foxn1ERT2 mouse strain*, where *Foxn1* tissue-specific expression can be regulated by tamoxifen[136], it was shown that overexpression of *Foxn1* in TECs of aged animals (12 to 24-month-old) can lead to thymus regeneration. This conclusion was drawn from a restored thymic architecture and enhanced functionality, as measured by an increase in the numbers of peripheral naïve T cells, that was comparable to that found in younger mice. The expression of genes important for TEC identity and function including *Dll4*, *Ccl25*, *Kitl*, *Cxcl12, Ctsl, CD40, CD80, Pax1*, *Trp63*, *Fgfr2IIIb*, and *Aire* was fully restored to levels of young mice. In addition, there was an increase in proliferation of TEC progenitors[136]. This study renders FOXN1 as the main target for age-related thymic involution making it a top candidate for strategies aiming to rejuvenate the thymus.

Zook et al. studied the delay of age-related *Foxn1* decline by generating a mouse model where mouse *Foxn1* cDNA under the control of the human K14 promoter was introduced randomly into the genome. This lead to a 20-fold over-expression of *Foxn1*. Using this model, high levels of FOXN1 could be maintained throughout ontogeny. However, an age-related thymic involution still occurred in these mice but its initiation was significantly delayed suggesting that FOXN1 is not the only orchestrator of this process[133].

Bredenkamp et al. have been successful in reprogramming mouse embryonic fibroblasts into TECs by *Foxn1* overexpression. These FOXN1-induced TEC (iTECs), when grafted under the kidney capsule of nude mice, promote T cell development which may constitute a promising method to re-generate a functional thymic tissue in aged individuals [138]. Efforts have also been directed to develop protocols that drive the differentiation of embryonic stem cells into TEC progenitors. These approaches foresee the progressive differentiation of embryonic stem cells (ESCs) into definitive endoderm following the exposure to the endoderm inducing factors, activin A or WNT3a. The subsequent differentiation into TECP employs stimuli that trigger *FGF, BMP4,* retinoic acid (RA) and EGF signaling, which have previously been shown to be involved in TEC development[161-163].

TECs can transiently degenerate due to stress, infection, chemotherapy, or radiotherapy. This process differs from the age-related thymic involution as the aforementioned factors act directly on T cells and affect TEC only indirectly due to the lack of crosstalk. For example, infections can trigger a stress response that increases glucocorticoid levels which in turn induce apoptosis of DP thymocytes that express high levels of glucocorticoid receptors. This sequence of events results in acute thymic involution[164, 165]. In a similar way, chemotherapy and radiotherapy deplete hematopoietic cells, including T cell progenitors. As a consequence, this perturbated the TEC- thymocyte crosstalk and as a result the TEC compartment [166].

FGF7 and IL-22 play a critical role in thymus regeneration after injury. In particular, it was shown that treatment with FGF7 (also known as keratine growth factor KGF) stimulates TEC proliferation and differentiation[167]. Similarly, IL-22 secreted by

innate-lymphoid cells (ILCs) upon tissue damage promotes TEC proliferation and survival[168].

A schematic overview of chapter 1.12 is shown in Figure 1.4.

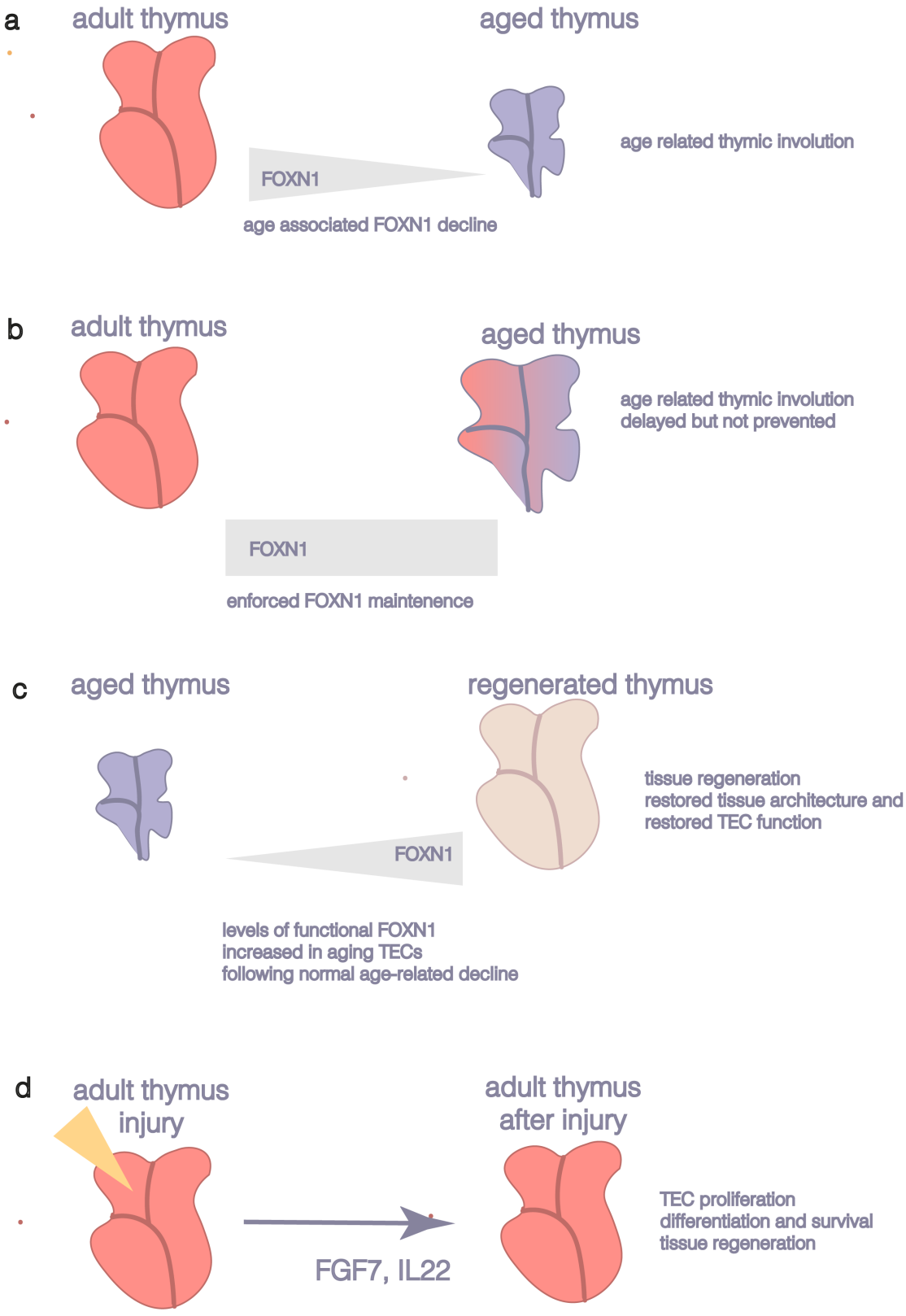


Figure 1.4 FOXN1 levels determine thymic involution and regeneration a) Age-related thymic involution, occurring during normal aging, is associated with the decrease in FOXN1 expression levels that is accompanied by a decrease in tissue size, tissue organization and TEC functionality b) Enforced maintenance of FOXN1 levels achieved by transgenic overexpression of FOXN1 delays but does not prevent the onset of age-related thymic involution c) Induction of increased levels of functional FOXN1 in a fully involuted aged thymus leads to restored thymic architecture and functionality comparable to that found in younger mice d) Systemic treatment of mice with an injured thymic tissue using FGF7 or IL-22 stimulates TEC proliferation and survival. Adapted from Vaidya et al [44]

1.13 Outstanding questions in FOXN1 biology

The pivotal role of FOXN1 in thymus development, maintenance and function has unequivocally been established by the identification of this molecule as a master transcriptional regulator of TEC biology. However, the molecular mechanism(s) by which FOXN1 exerts its regulatory function still remains to be elucidated. It is yet not known whether FOXN1 acts alone or in concert with other transcriptional regulators in order to drive the transcription of hundreds of target genes. Moreover, the longstanding question whether and how FOXN1's interactome changes over different embryonic and postnatal developmental stages remains un-answered. Studies have correlated a dose-dependent function of FOXN1, with individual requirements for distinct TEC populations throughout development. How this differential requirement is established is not understood.

The regulation of *FOXN1* expression in TECs is still incompletely characterised. Although the genomic regulatory region has been now broadly defined, the exact sequences of the promoters or putative enhancers of *FOXN1* are not yet known. The same holds true for the regulatory network upstream of *FOXN1* expression. Although the loss of expression of multiple transcription factors affects *Foxn1* expression, a direct regulatory mechanism awaits to be uncovered.

Answers to these questions will not only provide a better understanding of FOXN1's function as a master TEC regulator, but it will also contribute to a broader appreciation on how this master regulator coordinates gene expression vital for thymus biology.

1.14 Hypothesis and aims

FOXN1 has a critical role in thymus development and function as its homozygous loss of normal expression due to mutations severely affects TEC development and function. Patients with such mutations fail to develop a functional thymus and therefore present with forms of severe immunodeficiency. In this thesis, I investigate a novel mutant *FOXN1* allele (designated *Δ550* FOXN1) detected in a family trio with absent thymus but only mild immunodeficiency. This allele generates a truncated form of the FOXN1 protein which lacks part of the C-terminus transcriptional activation domain. The patients were found to be heterozygous for this allele. We therefore hypothesise that the *Δ550* FOXN1 mutant exerts a dominant negative effect on its wild-type counterpart thus abrogating normal FOXN1 function. The aim of this thesis is to explore the underlying molecular mechanism(s) by which wild-type and mutant FOXN1 drive thymus development and tissue dysfunction, respectively.

Specific aims of the thesis project are:

1. To explore the molecular characteristics and the transcriptional competence of the *Δ550* mutant allele (chapter 3).
2. To characterise the molecular interaction partners of wild type FOXN1 and investigate the potential impact of the *Δ550* FOXN1 mutation on these interactions (chapter 4).
3. To determine whether the *Δ550* FOXN1 mutation affects the factor's ability for DNA binding (chapter 5).
4. To investigate the impact of the *Δ550 FOXN1* mutant on thymus organogenesis by creating and analyzing an in vivo mouse model with an equivalent mutation

(chapter 6)

The research in this thesis expands our knowledge on how FOXN1 exerts its key role as a master regulator of TEC development, maintenance and function.

CHAPTER 2

CLINICAL AND IMMUNOLOGIC PHENOTYPE OF A PATIENT WITH A NOVEL MUTATION IN THE *FOXN1* GENE

2.1 Introduction and aims 52

2.2 Materials and methods 53

2.2.1 Whole genome sequencing analysis pipeline 53

2.2.2 MiSeq sequencing to determine the length of the CDR3 region of TCR alpha- and beta-chains 54

2.3 Results 55

2.3.1 Clinical and immunologic phenotype in carriers of *Δ550* FOXN1 mutation 55

2.3.2 CDR3 length distribution for Valpha (Vα) and Vbeta (Vβ) TCR chain is similar for T cells from the patient and a healthy control 60

2.3.3 TCR repertoire diversity is decreased in the patient 62

2.4 Discussion 63

INTRODUCTION and AIMS

Homozygous loss of function mutations in the human *FOXN1* gene result in a rare form of severe combined immunodeficiency (SCID) characterised by athymia with consequent T cell deficiency, absence of visible hair, and nail dystrophy known as NUDE-SCID. To date, three different autosomal recessive NUDE *FOXN1* mutations have been reported in ten individuals, located either in the N-terminus or the DNA binding domain of the protein[45, 46, 58, 65, 66]. Adults heterozygous for one of these mutations have normal peripheral T cell counts, with slightly reduced CD8 T cells and they are not susceptible to recurrent infections[67].

We identified a female paediatric patient presented with a lack of thymic tissue at birth, peripheral T cell lymphopenia and a skewed and contracted T cell antigen receptor repertoire (TCR). Whole genome sequencing (WGS) revealed that the girl was heterozygous for a previously unrecognized point mutation in the C-terminal domain of *FOXN1* gene (c.1370delA, p.H457fs*93).

Chapter 2 details the clinical and immunological findings of the patient and investigates how peripheral T cells can be detected despite an absence of thymic tissue at birth.

2.2.1 Whole genome sequencing analysis pipeline

The following analysis was performed by Alistair Pagnamenta and Carme Camps, at the National Institute for Health Research Biomedical Research Centre of the University of Oxford. Briefly, after obtaining parental informed consent, DNA was extracted from peripheral blood mononuclear cells (PBMCs) of the father, sibling and the index patient using a magnetic bead method and the QIAsymphony automated extraction system (Qiagen). Whole Genome Sequencing was performed with the HiSeq2500 (Illumina) platform using the SeqCap EZ Human Exome Library v3.0 (NimbleGen). Base pair reads were mapped to hs37d5 using Stampy version 1.0.22 [169](www.well.ox.ac.uk/stampy). Variants calling was performed with Platypus version 0.5.2 [170](www.well.ox.ac.uk/platypus) and coverage was calculated on deduplicated BAM files using bedtools and CODOC[171].

The sequencing data was extensively examined using Ingenuity Variant Analysis (version 3.1.20150207, www.ingenuity.com/products/variant-analysis) to identify shared variants. Genetic filters were set to identify *FOXN1* variants that fitted a heterozygous, compound heterozygous, hemizygous and haploinsufficiency model. Data were also investigated for other variants. The population allele frequency filter was set to 0.1% in the 1000 Genome Frequency (v5) and ExAC database. The filter 'predicted deleterious' included variants that either could be pathogenic or likely pathogenic and could introduce a frameshift, in-frame ''indels'', a stop codon, missense variants, splice site variants and variants which are reported in HGMD (the Human Gene Mutation Database, version 2014.4).

2.2.2 MiSeq sequencing to determine the length of the CDR3 region of TCR alpha- and beta-chains

A MiSeq analysis was performed in collaboration with Dr Athina Soragia Gkazi at Great Ormond Street Institute of Child Health, University College London. Briefly, RNA was extracted from PBMCs of the patient and an aged-matched control using the Qiagen RNA blood Mini kit (Qiagen). DNase treatment of the extracted RNA was performed (RQ1 DNAse Promega) following the manufacturer's instructions to remove any residual genomic DNA. A library preparation was performed as previously described following a protocol for quantitative TCR sequencing [172]. The prepared libraries were pooled at a final 12pM concentration and sequenced employing the Illumina MiSeq platform, using a version 2 chemistry 2x250PE kit. Data were analysed by Dr Athina Soragia Gkazi as previously described[172]. Shannon entropy was used as a diversity measure of the data. As detailed in reference [172] Shannon entropy was calculated using the *vegan* package (version 2.4.2) to quantify diversity by incorporating both evenness and richness of a variable. The *ggplot2* package (version 2.2.1) was used for all data visualizations

RESULTS

2.3.1 Clinical and immunologic phenotype in carriers of *Δ550 FOXN1* mutation

A six-month old patient, second child to non-consanguineous parents, was presented to Great Ormond Street Hospital in London with severe dermatitis, a history of chronic diarrhoea and an acute chest infection caused by rhinovirus. Peripheral blood testing revealed a T cell lymphopenia [32% of total lymphocytes, normal range 51–77%] and reduced TCR diversity measured by TCR-spectratyping as part of the standard immunological work-up (Table 2.1). Subsequent testing found no TRECs (T cell receptor excision circles) suggesting impaired thymic T cell development [43]. Chest ultrasound revealed the absence of a thymus. Immunological diagnostics demonstrated normal T cell proliferative responses to mitogens (PHA; phytohemagglutinin) as well as normal total serum IgG levels. The patient's phenotype was reminiscent of a patient with primary immunodeficiency of a yet to be further characterised aetiology[173].

To identify the genetic defect underlying the observed immunopathology, further genetic work-up was performed to exclude a 22q1 deletion. Deletions in a specific region of chromosome 22 (at a location designated q11.2.) have been associated with thymic hypoplasia or aplasia and accompanied immunodeficiency, a condition known as DiGeorge Syndrome (DGS) [11]. This chromosomal deletion affects multiple genes and results in an abnormal development of the 3rd and 4th pharyngeal arches leading to a complex syndrome characterised by thymic hypoplasia or aplasia, cardiac defects, facial abnormalities and other developmental defects [174]. Such chromosomal rearrangements or abnormalities in the index patient were excluded by Comparative

Genomic Hybridization array (CGH). Other known genetic variants were excluded using targeted sequencing for a panel of 72 genes associated with primary immunodeficiencies (PID).

Because the vast majority of PID are inherited disorders [175] the diagnostic workup also included the rest of the family members. The 4-year-old sister was also found to have a reduction in naïve T cells [naïve $CD4^+$: 25% (normal range is 53-86%), naïve $CD8^+$:21% (normal range 86% (69-97)], absent TRECs and a missing thymus. The child was otherwise thriving and was clinically well. The 30-year-old father also lacked TRECs, but he was clinically well. A sonographic assessment of the thymic tissue was however not informative for the father, given that the thymus involutes with age starting as early as the second year of life[176]. Reflecting a compromised immune defence, both the father and the sister had also high Epstein-Barr virus (EBV) serum load though had not developed any further symptoms. The mother was healthy and a basic assessment of her immune system was normal. The wider family medical history was otherwise not informative (Table 2.1 for peripheral lymphocyte counts in all family members).

% parental	Index patient				SISTER				FATHER	
	6 mo		Control 3-6 mo		4y		Control 4y		31y	adult control
	$x10^9$/L	%	$x10^9$/L	%	$x10^9$/L	%	$x10^9$/L	%	$x10^9$/L	$x10^9$/L
WBC	**4.88**	**-**	9.20 (6.70-14.00)	-	5.93	-	7.10(5.2-11.00)	-	7.17	
lymphocyte count	**1.93**	**-**	6.30 (3.90-9.0)	-	2.50	-	3.60 (2.3-5.4)	-	1.80	1.8 (1.1-2.5)
$CD3^+$	**0.62**	**32**	3.93 (2.50-5.60)	66 %(51-77) %	**1.38**	**55 %**	2.39 (1.4-3.7)	66 %(56-75)	1.17	1.2 (0.7-1.9)
$CD3^+CD4^+$	**0.60**	**31**	2.8 (1.7-4.1)	46%(35-56)	**0.60**	**24 %**	1.3 (0.7-2.0)	38%(28-47)	0.61	0.7 (0.4-1.3)
$CD3^+CD8^+$	**0.04**	**2**	1.1 (0.7-1.8)	16% (12-23)	0.58	23 %	0.8 (0.5-1.4)	23%(16-30)	0.41	0.4 (0.2-0.7)
$CD4^+CD45RA^-CD27^+$ (MEM)	**0.52**	**86**	8 (3-16)	8% (3-16)	**0.38**	**64 %**	0.36(0.22-0.66)	16% (9-26)	ND	-
$CD4^+CD45RA^+CD27^+$ (NAI)	**0.02**	**3**	2.32 (1.3-3.7)	90% (77-94)	**0.15**	**25 %**	0.98(0.43-1.50)	71% (53-86)	ND	-
$CD4^+CD45RA^+CD27^-$ (EFF)	**0**	**0.4**	0.15 (0.06-0.28)	4% (2-9)	**0.00**	**0.1 %**	0.09 (0.05-0.18)	5% (2-9)	ND	-
$CD8^+CD45RA^-CD27^+$ (MEM)	unable to analyse		3(1-7)	3% (1-7)	**0.43**	**74 %**	0.19 (0.09-0.44)	9% (4-16)	ND	-
$CD8^+CD45RA^+CD27^+$ (NAI)	unable to analyse		0.91 (0.55-1.40)	94% (85-98)	**0.12**	**21 %**	0.67 (0.38-1.1)	86%(69-97)	ND	-
$CD8^+CD45RA^+CD27^-$ (EFF)	unable to analyse		0.08(0.03-0.17)	7% (3-16)	**0.01**	**1%**	0.14(0.07-0.42)	13%(5-29)	ND	-
$CD19^+$	0.87	45 %	1.55 (0.43-3)	25% (11-41)	0.75	30 %	0.75 (0.39-1.4)	21% (14-33)	0.41	0.2 (0.1-0.4)
$CD16^+CD56^+$	0.33	17 %	0.42 (0.17-0.83)	6% (3-14)	0.33	13 %	0.3 (0.13-0.72)	9%(4-17)	0.20	0.3 (0.1-0.4)

Table 2.1: Peripheral lymphocyte absolute counts and their percentages in the patient, her sister and father. Values that lie outside the reference range are in bold. The normal values as given for each age group (mean followed by the 10-90 percentile

within the parenthesis). The reference ranges were previously published in [177]. mo=months, y=years, ND=not determined

Whole genome sequencing (WGS) on isolated peripheral blood mononuclear cells from the patient, father and elder sister revealed a common single base pair deletion in exon 7 of *FOXN1*. This mutation (c.1370delA, p.H457FS*93) results in a frameshift and the generation of a premature stop codon in exon 8. *In silico* analysis of the mutation predicted the generation of a truncated protein that is shortened in the C-terminus by 98 amino acids. Hence, we refer to this novel *FOXN1* variant as ***Δ550 FOXN1*** (Figure 2.1 for family pedigree).

Following the initial symptoms, the index patient remained well and did not require further medical attention. At nineteen-months of age the patient's lymphopenia had improved (Table 2.2). The frequency of $CD3^+$ lymphocytes had risen from 32% at six-months of age to 55.6% at nineteen-months of age, falling now within a normal range for age matched individuals. The frequency of $CD8^+$ had also improved during the same period from initially 2% with no naïve $CD8^+$ to 21.4% of which a third had a naïve phenotype. Similarly, the frequency of naive $CD4^+$ T cells had also marginally improved from 3% to 8.2% but the total $CD4^+$ T cell frequency had further decreased at this point (table 2.2). The frequency of Natural Killer cells (NK) defined as $CD16^+CD56^+$ increased significantly from 17% to 40.5% (normal range for the age 3%-15%) most likely due to homeostatic proliferation in response to peripheral T cell lymphopenia. Neither the father nor the sister demonstrated a comparable increase in NK cells.

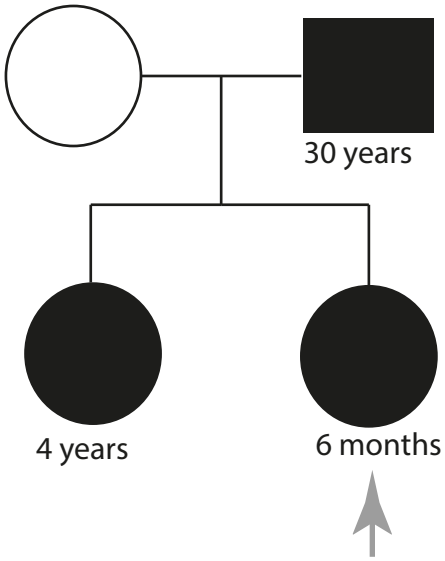


Figure 2.1 Family pedigree of *Δ550 FOXN1* mutation. Squares represent male and circles female family members. Filled symbols indicate individuals with the *Δ550 FOXN1* mutation. Arrow points at the index patient.

Lymphocyte subset	Proband 6months	Healthy control 6 months	Proband 19months	Healthy control 19 months
$CD3^+$	**32%**	66 %(51-77)	55.6%	65 %(53-75)
$CD3^+CD4^+$	**31%**	46%(35-56)	**26.4%**	41 %(32-51)
$CD3^+CD8^+$	**2%**	16% (12-23)	21.4%	20 %(14-30)
$CD4^+CD45RA^+$ $CD27^+$ (naïve)	**3%**	90% (77-94)	**8.2%**	81 %(63-91)
$CD4^+CD45RA^+$ $CD27^-$ (effector)	**0.4%**	4% (2-9)	**0.1%**	5% (2-9)
$CD4^+CD45RA^-$ $CD27^+$ (memory)	**86%**	8% (3-16)	**86.3%**	12 %(7-20)
$CD8^+CD45RA^+$ $CD27^+$ (naïve)	**Unable to analyse**	94% (85-98)	**31.7%**	89% (71-98)
$CD8^+CD45RA^+$ $CD27^-$ (effector)	**Unable to analyse**	7% (3-16)	**0.8%**	15 %(5-30)
$CD8^+CD45RA^-CD27^+$ (memory)	**Unable to analyse**	3% (1-7)	**66.8%**	6% (2-12)
$CD19^+$ (B cells)	45%	25% (11-41)	16%	25 %(16-35)
$CD16^+CD56^+$ (Natural Killer cells)	17%	6% (3-14)	40.5%	7% (3-15)

Table 2.2 The patient's peripheral lymphocyte frequencies at 6 and 19 months of age. Values outside the normal reference range are in bold. The normal values as given for each age group (mean followed by the 10-90 percentile within the parenthesis). The reference ranges were previously published in [177]

2.3.2 CDR3 length distribution for Valpha (Vα) and Vbeta (Vβ) TCR chain is similar for T cells from the patient and a healthy control

The patient had a low number of peripheral T cells despite apparent athymia. We therefore hypothesized that thymic tissue must have been present early in gestation but had vanished by the age of six months. To determine the timing of T cell generation in the patient we measured the CD3-length of their TCR. TDT (terminal deoxynucleotidyl transferase) is an enzyme that adds N nucleotides in the CDR3 region of the TCR's Vα and Vβ chain [36]. In humans, TDT starts to be expressed at the end of the 2nd trimester of pregnancy. T cells that have been generated earlier will have a shorter CDR3 length.

To assess the CDR3 lengths of both the α and β TCR chain we employed MiSeq. As shown in Figure 2.2 a comparable distribution of CD3 length was observed for T cells from the patient and the control. This strongly supports that the patient was able to produce T cells following the expression of TDT, suggesting that the thymus must have involuted thereafter. However, and reflecting the dynamics of significant lymphopenia, the CDR3 length distribution revealed oligoclonal expansions of T cells with CDR3 length of 7 and 10 amino acids (Figure 2.2, red arrows).

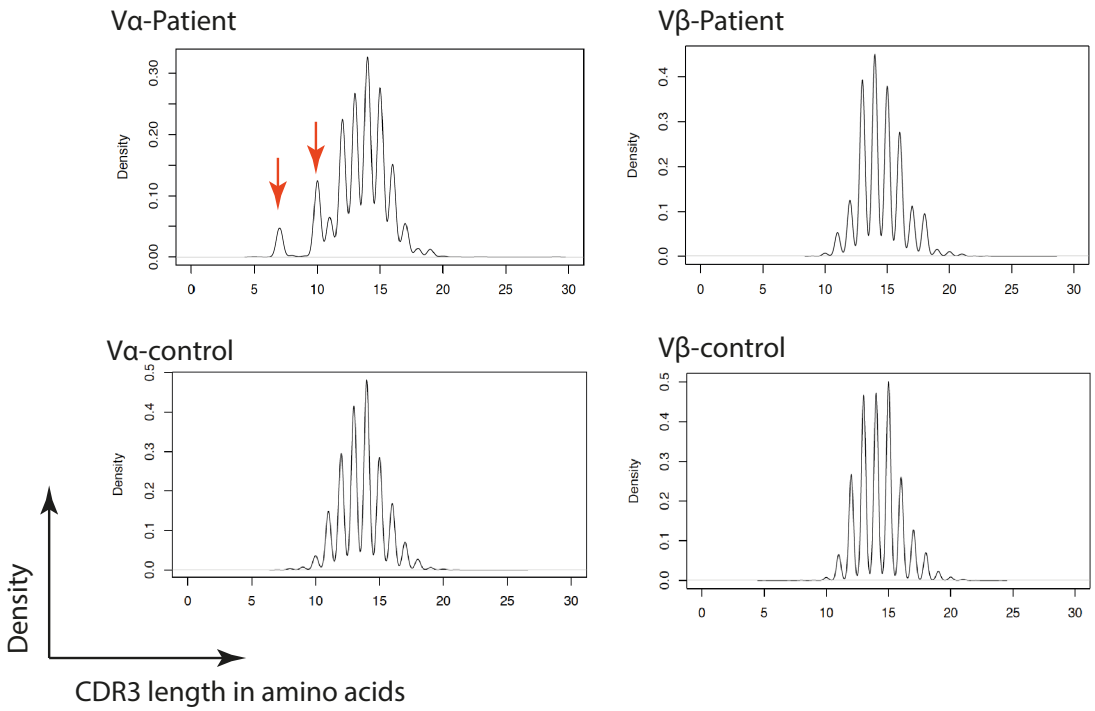


Figure 2.2: CDR3 length distribution for Vα and Vβ chain in the patient and an aged-matched healthy control. X axis depicts CDR3 length measured in amino acids. The red arrows indicate oligoclonal expansion of T cells with CDR3 length of 7 and 10 amino acids respectively.

2.3.3 TCR repertoire diversity is decreased in the patient

Further analysis of the diversity of the TCR's Vα and Vβ chains of the patient's T cell repertoire in comparison to an age matched control, revealed an almost 50% reduction in the number of unique CDR3 regions for either TCR chain (Table 2.3). The mean frequency of unique CDR3 regions was increased by approximately 50%, reflecting, possibly, the homeostatic expansion of a limited number of peripheral T cells (Table 2.3). Overall, TCR diversity as calculated by the Shannon index was decreased in the proband (Table 2.3).

	α chain		β chain	
	Patient	Healthy control	Patient	Healthy control
Number of unique CDR3 regions	7777	13877	10229	18266
Mean frequency of unique CDR3 regions	4.02906	1.977589	2.814547	1.535147
Total number of CDR3 regions per sample	31334	27443	28790	28041
TCR diversity (Shannon entropy)	10.23692	12.71595	11.00125	13.22756

Table 2.3: TCR diversity in proband and aged-matched control. Table shows the total number and frequency of unique CDR3 regions and total TCR diversity as calculated by the Shannon entropy. The lower the shannon index, the lower the diversity. This analysis was performed with blood taken from patient and aged matched healthy control at 6 months of age.

DISCUSSION

The loss of a single nucleotide in exon 7 of the *FOXN1* locus encoding part of the C-terminus transcriptional activation domain resulted in a frameshift and a premature stop codon. Here, we propose that this previously unrecognised mutation (*Δ550* FOXN1) plays a causative role in the striking phenotype of the index patient who presented with athymia, an absence of thymic output and T cell lymphopenia. Similar clinical features were observed in the sibling. $CD3^+$ single positive T cells were primarily affected by the mutation with reduced numbers of naïve T cells for both $CD4^+$ and $CD8^+$ subsets and a reduced TCR repertoire diversity. The observed lymphopenia improved with age which correlated with a stable medical course. Interestingly both, the father and the older sister of the patient, were clinically healthy despite the absence of TRECs and lymphopenia.

A similar phenotype has been recently described in a series of patients with heterozygous mutations in the C-terminus of the *FOXN1* gene[67]. The majority of these mutations are single base pair deletions at various positions within the C-terminus and *in silico* are predicted to generate a truncated FOXN1 protein of the same length as the *Δ550* FOXN1 mutant. Early in life, patients with these mutations had T cell lymphopenia in both the $CD4^+$ and the $CD8^+$ compartment, present or absent thymus and a range of pathologies. Some of them were healthy while others had recurrent infections that in cases were particularly severe. The location of the mutation did not seem to correlate with the presence of thymic tissue or the severity of the infections. The $CD4^+$ T cell lymphopenia improved with age while in most of the cases the $CD8^+$ T cell counts remained below the normal range. The authors of this

study suggest that the normalization of the $CD4^+$ counts is due to homeostatic proliferation. A T cell immunodeficiency that improves after the first year of life has also been described in patients with partial DiGeorge Syndrome (pDGS) [174, 178]. The increased T cellularity observed with advanced age in these patients has been in part attributed to oligoclonal T cell expansion with abnormal T cell receptor spectratypes [174, 178]. Whether the improved lymphopenia seen in the *Δ550* patient at nineteen-months of age is due to an oligoclonal T cell expansion is therefore likely but requires further investigations.

Individuals heterozygous for the *Δ550* mutation are athymic at birth but are largely immunocompetent and clinically very different to NUDE SCID patients. The later, typically lack almost all T cells suffer from life threatening infections as early as shortly after birth and require a thymus transplantation to correct their condition [66]. Apart from the thymus, *FOXN1* is also expressed in the skin where it controls the balance between proliferation and terminal differentiation of keratinocytes [50]. Its absence in the NUDE SCID patients prevents the normal development of hair and nails leading to alopecia and nail dysmorphia respectively [46, 58]. A 60% of patients heterozygous for the NUDE mutations or a 45% of patients heterozygous for other mutations in the C-terminus of the *FOXN1* gene have nail dystrophy but normal hair development[67]. At the time of this study, individuals with heterozygous *Δ550* mutations did not present with dermatological symptoms, suggesting different requirements for the function of FOXN1 in keratinocytes when compared to TEC. However, this hypothesis was not further examined as part of this thesis.

A central question arises concerning the origin of T cells in athymic patients with a heterozygous *Δ550* mutation or other similar mutations located in the C-terminus of

the *FOXN1* gene. An absent or hypoplastic thymus but nearly normal T cell numbers have been rarely observed in patients with DiGeorge Syndrome (DGS)[179]. These patients, have however an ectopically positioned thymus close to or within the thyroid gland which serves as the primary lymphoid organ for the T cell development. The ectopic thymus arises as a consequence of migration defects during thymus organogenesis and usually occurs together with other developmental anomalies [179]. Interestingly, the individuals with a heterozygous *Δ550* mutation investigated here did not have radiologically evidence for an ectopic thymus or other developmental defects.

The analysis of the CDR3 length demonstrated that the patient's T cells continued to be generated after the end of the second trimester of pregnancy. This provides strong evidence that a fully functional thymus was present for a couple of weeks able to dispense functionally competent T cells. As discussed extensively in section 1.11 of the Introduction, FOXN1's function is required for normal thymic tissue maintenance and its declined expression correlates with thymic senescence and involution. We hypothesised that the *Δ550* mutation disrupts the normal FOXN1 function consequently leading to premature tissue involution. This hypothesis is examined further in chapter 6 using a mouse model mimicking the situation of the athymic *Δ550* patient.

The phenotype of previously described patients heterozygous for mutations in the C-terminus of the *FOXN1* gene was comparable to the phenotype of mice heterozygous for a loss of function *FOXN1* allele[67]. This led the authors to hypothesise that these *FOXN1* variants are loss of function mutants and the phenotype seen in those patients Is due to haploinsufficiency[67]. However, the possibility that some of these variants

are dominant negative mutants was not excluded[67]. As part of this thesis we examined whether the *Δ550* variant is a dominant negative mutant *in vitro* (Chapters 3,4 and 5).

The incidence of patients with mutations in the C-terminus of the human *FOXN1* gene has recently increased, mainly due to the introduction of the TREC assay as part of the routine newborn screening[67]. The disease prevalence in the European populations is expected to be higher than initially thought due to the mild phenotype this mutation causes. Our study can provide a better understanding of the impact of the novel *Δ550 FOXN1* variant and similar variants on the immunocompetence of patients with such mutations.

CHAPTER 3

THE IMPACT OF THE *Δ550* FOXN1 MUTATION ON FOXN1 BIOLOGY

3.1 Introduction and Aims 68

3.2 Materials and Methods 69

3.2.1 Cell culture 69

3.2.2 Generation of C-terminally myc-tagged or FLAG-tagged wild type FOXN1 70

3.2.3 Site-directed mutagenesis for the generation of human and mouse FOXN1 variants 70

3.2.4 Transfection of human and mouse cell lines 71

3.2.5 RNA, cDNA synthesis and qRT-PCR 71

3.2.6 Immunohistochemistry 72

3.2.7 Protein preparations and Western blot 73

3.2.8 Luciferase reporter assay 74

3.2.9 RNA-sequencing of the human thymic epithelial 4D6 cell line transfected with either wild-type or *Δ550* mutant FOXN1 75

3.3 Results 76

3.3.1 The *Δ550* mutant allele encodes for a protein of reduced molecular weight compared to the WT protein 76

3.3.2 The *Δ550* mutant localises to the nucleus similar to the wild-type protein 78

3.3.3 The frameshift in the *Δ550* mutant disrupts the evolutionary conserved domain in the c-terminus of the FOXN1 protein 79

3.3.4 FOXN1's function is dose dependent 81

3.3.5 The *Δ550* FOXN1 exerts a dominant negative effect. 83

3.3.6 The *Δ550's* aberrant protein domain makes it a dominant negative mutant 85

3.3.7 The *Δ550* FOXN1 mutant impairs the transcriptionally activity of the WT FOXN1 88

3.3.8 Assessing the pathogenicity of different FOXN1 variants found in two paediatric patients with immunodeficiency. 92

3.4 Discussion 97

3.1 INTRODUCTION and AIMS

Previously described heterozygous *FOXN1* variants within the C-terminus of the *FOXN1* gene have been characterised as loss of function mutants, as the phenotype of the heterozygous patients resembles the phenotype of mice heterozygous for a loss of function *Foxn1* allele[67]. However, the exact molecular mechanism of any of these variants has not been examined in further detail therefore the possibility that some could act as dominant negative mutants cannot be excluded. In this chapter I present evidence that the *Δ550* FOXN1 variant can act as a dominant negative mutant in-vitro. To study the molecular characteristics of the *Δ550*-FOXN1 mutant, we employed site-directed mutagenesis to engineer a human *FOXN1* gene sequence carrying the same single-base pair deletion as identified in heterozygous *Δ550* patients. By overexpressing this mutant (designated *Δ550* FOXN1) in different thymic epithelial cell lines, we were able to determine its transcription and translation characteristics as well as its subcellular localisation and compare those to WT FOXN1. Furthermore, we used a luciferase reporter assay and RNA-sequencing to determine the ability of the mutation to disrupt FOXN1 controlled transcription and the mechanism by which this seemingly dominant negative activity is effected. In the last section of this chapter, I describe how we employed our methodology to help in characterising novel single point mutations in *FOXN1* identified in two paediatric patients with absent thymus and immunodeficiency, that ultimately contributed to their clinical management.

3.2 MATERIALS AND METHODS

3.2.1 Cell culture

Cells were handled using standard tissue cultured techniques in a sterile Class II laminar flow hood. All cell lines were cultured in appropriate media (Table 3.1), passaged at 90% confluency and counted using a haematocytometer (Neubauer) and Trypan blue (Thermo Fisher Scientific) to distinguish dead from livencells. Attached cells were harvested by incubation with 0.25% Trypsin-EDTA (Gibco) for 1-15min at 37°C depending on the cell line (Table 3.1).

Cell line	Culture media	Trypsinisation time
Human TEC4D6 (human derived thymic epithelial cells)	RPMI (Thermo Fisher scientific) 10%FCS (Fetal Calf serum, Sigma), 1%P/S (Penicillin Streptomycin, ThermoFisher scientific) 1%L-Glut (L-Glutamine, ThermoFisher scientific) 1%NEAA (Non essential amino acids ThermoFisher scientific) 1%HEPES (N-2-hydroxyethylpiperazine-N-2-ethane sulfonic acid, ThermoFisher scientific)	30sec
Mouse TEC1.2 (mouse derived thymic epithelial cells)	IMDM (ThermoFisher scientific) 10%FCS, 50µM 2-Mercaptoethanol (ThermoFisher scientific)	15min
HEK293	EMEM (ThermoFisher scientific) 10% FCS, 1%P/S	1min
HELA	DMEM (ThermoFisher scientific) 10% FCS, 1% P/S	1min

Table 3.1: Details on culture media and time of trypsin treatment for the different cell lines used in the experiments.

3.2.2 Generation of C-terminally myc-tagged or FLAG-tagged wild type FOXN1

Human FOXN1 cDNA was purchased from Genecopoeia (sequence accession number BC140423) cloned into the pdonor vector backbone pENTR223.1. Full length FOXN1 cDNA without a stop codon was cloned into a vector with a C-terminus FLAG (pCSF107mT-GATEWAY-3'-FLAG, Addgene) or myc tags (pCSF107mT-GATEWAY-3'-Myc tag, Addgene) using the Gateway cloning technology. Briefly the Gateway cloning technology is based on a site-specific recombination system used by phage I to integrate its DNA into bacterial chromosomes. The recombination is facilitated by specific recombination sequences found in the donor and host known as attP and attB respectively. When used for cloning purposes the recombination enzyme LR is used to catalyse the recombination reaction.

3.2.3 Site-directed mutagenesis for the generation of human and mouse FOXN1 variants

Insertion of single base pair changes for the generation of human and mouse FOXN1 variants (Table 3.2) was achieved by site-directed mutagenesis using the Phusion site-directed mutagenesis kit (#F-541, Thermo Fisher Scientific). Specific primers for the introduction of single base pair deletions or single base pair changes were designed using the following software http://www.genomics.agilent.com/primerDesignProgram.jsp?toggle=uploadNow&mutate=true&_requestid=295758. Correct incorporation of single base pair changes was verified by Sanger sequencing.

FOXN1 mutants	Species	Base pair and amino acid change	Forward (F) and Reverse (R) primers
Δ550	human	Deletion A at c.1370	F: 5'CAGACATACTTGCACCTCTCACCAGG3' R: 5'CCTGGTGAGAGGTGCAAGTATGTCTG3'
Δ457	human	C>G at c.1365 Tyrosine to Stop	F:5'GGTGAGAGGTGCAA**C**TATGTCT 3' R: 5'AGACATA**G**TTGCACCTCTCACC3'
Δ564	human	C>G at c.1691 Serine to stop	F:5'TGACCT**G**ATCCCCGACATCATC3' R: 5'GATGATGTCGGGGAT**C**AGGTC3'
Δ550b	human	A >T at c.1647 Lysine to stop	F:5' CGGTTCGATAGTAGGA**T**GTTGACAAG 3' R:5'CTTGTCAAC**A**TCCTACTATCGAACCG3'
325 FOXN1	human	T>C at c.974 Leucine to proline	F:5'AAGCACTTGTTG**G**GGGATAGGTTGTGC' R:5'ACAACCTATCCC**C**CAACAAGTGCTTCGA G3'
350 FOXN1	human	C>T at c.1049 Proline to leucine	F:5'GTCGATCTTGGCC**A**GATTGAGG3' R:5'CCTCAATC**T**GGCCAAGATCGAC3'
Δ505	human	C>G at c. 1514 Leucine to stop	F:5'AGTGCCAAGCTA**G**TGGCCGAG3' R:5'TCGGCCA**C**TAGCTTGGCAC3'
Δ505	mouse	Deletion A at c.1370	F:5'ACCTACCCACACCTTTCCCCCAG3' R:5'TGGGGGAAAGGTGTGGGTAG3'

Table 3.2: Primer pairs used for the generation of the various FOXN1 constructs by site directed mutagenesis. Base pair changes are shown in bold, deleted base pairs are shown in grey.

3.2.4 Transfection of human and mouse cell lines

Cells were seeded in 6-well or 24-well plates (Corning) and allowed to grow overnight in order to reach 70% confluency by the time of transfection. Within 18-20 hours after seeding, cells were transfected with the combination of plasmid(s) of interest using Fugene (Promega) as per manufacturer's recommendations. Four hours post transfection, the cell culture media was replaced by fresh media. Cells were then harvested 24, 48 or 72 hours post transfection for the planned downstream analysis.

3.2.5 RNA, cDNA synthesis and qRT-PCR

RNA isolation was performed using the RNeasy Mini (Qiagen) or RNeasy Plus Micro kit (Qiagen) following manufacturer's recommendations. RNA samples were used

immediately or stored at -80°C until subsequent use. cDNA was synthesised using SensiFAST cDNA kit (Bioline) following the manufacturer's recommendations.

qPCR experiments were conducted in the StepOnePlus Real-Time PCR system (Applied Biosystems). A mastermix was prepared using 1µl of template, 100 nM of each relevant primer (table 3.2) and SensiMix SYBR Hi-Rox (Bioline) as per manufacturer's recommendations. Expression levels of each gene were normalised against *GAPDH* expression and fold change was calculated using the $2^{-\Delta CT}$ equation or $2^{-\Delta\Delta CT}$[180].

Gene	Species	Forward primer	Reverse primer
GAPDH	human	5′-AACAGCCTCAAGATCATCAGC-3′	5′-CTGTTGCTGTAGCCAAATTCG-3′;
FOXN1	human	5′-TTCCTTACTTCAAGACAGCAC-3′	5′-GGTTCTTGCCAGGAATGG-3′.
Gapdh	mouse	5'GGTGAAGGTCGGTGTGAACG3'	5'ACCATGTAGTTGAGGTCAATGAAGG3'
Foxn1	mouse	5'TCTACAATTTCATGACGGAGC3'	5'TCCACCTTCTCAAAGCACTTGTT3'

Table 3.2: Primer pairs used for the qRT-PCR analysis in chapter 3.3.1 and 6.3.1

3.2.6 Immunocytochemistry

Prior to the immunofluorescent staining, 12 well cell culture plates were prepared by adding one ethanol (EtOH) embedded coverslip per well. EtOH was left to evaporate and wells were washed three times with PBS. Lysine (1:10 dilution in PBS, Sigma) was added in each well for at least 5min, washed twice with PBS and left to dry for 2hours. Cells were plated and left to adhere for 18-20hours before transfection. Cells were then transfected as per 3.2.3.

For the immunofluorescent staining cells were fixed with 4% paraformaldehyde solution (Sigma) for 30 min and permeabilised with 0.2% Triton X-100 (Sigma) for 15min at room temperature (RT). Cells were then blocked with 10% goat serum (Sigma) for 1 hour at RT. Slides were subsequently stained with primary antibodies:

Mouse anti-FLAG (1:500) (monoclonal M2, Merck) or rabbit anti-myc (1:200) (monoclonal 71D10, cell signaling) in blocking solution [1x PBS, 1% BSA (Bovine Serum Albumin, Sigma), 5% goat serum (Sigma)] for 2hours at 37°C, washed twice with 1X PBS, and stained with secondary antibodies [goat anti rabbit Alexa 488 (Sigma), goat anti-mouse Alexa 647(Sigma)] at 1:500 dilution for 30min at 37°C. Slides were washed twice in 1X PBS before being stained with DAPI (1:500.000, Thermo FIsher Scientific) in PBS and mounted with mounting media. Coverslips were sealed with clear nail polish (Various) and were allowed to dry for at least 20 min before analysis. A ZeissLSM 880 inverted confocal laser scanning microscope (Carl Zeiss AG, Oberkochen, Germany) was used to visualise the cells. Images were acquired and analysed by Fiji (ImageJ software).

3.2.7 Protein preparations and Western blot

Prior to the western blot analysis cells were lysed in lysis buffer [25mM Tris-HCL pH7.5 (prepared in house), 50mM NaCl (Sigma), 0.1%NP-40 (Thermo fisher Scientific), 0.1% SDS (Sigma), 10% Glycerol (Sigma), Protease Inhibitors 1 tablet/10ml (Roche)] for 20min on ice with mild shaking. Precipitates were removed by centrifugation (12.000 rpm for 20minutes at 4°C). Protein concentrations were determined using Pierce BCA Protein Assay Kit (Thermo Fisher Scientific) and lysates were kept on ice for immediate use or stored at -80°C for subsequent use.

For the western blot analysis 5µl of sample buffer [(250 mM Tris-HCl [pH 6.8], 10% [w/v] SDS, 35% [v/v] glycerol, 0.05% BPB (bromophenol blue, Biorad, 0.7 M (final concentration=1%) 2-mercaptoethanol (14.3M) added right before use] were added in 15µl of sample and samples were boiled at 95C for 5min.

3.2.8 Luciferase reporter assay

Cells were seeded in 24-well cell culture plates such that they reach 70-80% confluence by the time of transfection (usually 16 to 20 hours post after seeding). Cells were transfected with a combination of plasmids, using Fugene as per 3.2.3. Each condition was transfected with a renilla control plasmid (pRL Promega), a luciferase reporter plasmid pGL4.10 (Luc2, Promega) under the control of a minimal wild type β5t promoter (β5t-luc) or a mutated β5t promoter with mutated FOXN1 binding sites (β5t-mut-luc) (Figure 3.1) and a FOXN1 construct of interest in a ratio of 1:10:10. The minimal β5t promoter contains two FOXN1 binding sites, both within 415bp upstream of the translation initiation codon and has been used in previously published work from this laboratory [104]. Each transfection was performed in triplicate. Cells were incubated for 24hours (at 37°C, 5% CO_2) prior to luciferase assay. Cell lysates were prepared for the luciferase assay following the manufacturer's protocol (Promega Dual Luciferase reporter assay system) and using 80µl/well of PLB lysis buffer provided by the kit. Luciferase readings were performed at a Promega Glo Max luminometer. Luciferase and renilla plasmids were kindly provided by Dr Saulius Zuklys (Department of Biomedicine, University of Basel). Reporter activity was corrected by calculating the luciferase to renilla ratio for each well. The catalytic activity of luciferase was reported as relative luciferase units (RLU).

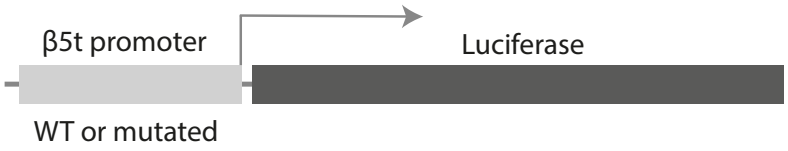


Figure 3.1: Schematic representation of the luciferase reporter construct used for all reporter assays. The luciferase gene was cloned downstream of the β5t promoter sequence (β5t-luc) or the same β5t promoter sequence mutated at the FOXN1 binding site (β5t-mut-luc).

3.2.9 RNA-sequencing of the human thymic epithelial 4D6 cell line transfected with either wild-type or *Δ550* mutant FOXN1

4D6 thymic epithelial cells were transfected with plasmids encoding 1) WT-FOXN1 alone 2) *Δ550*-FOXN1 mutant alone, 3) WT and *Δ550* or 4) empty vector only along with a GFP-expressing vector in a 4:1 ratio, to facilitate sorting of positively transfected cells. Three biological replicates were prepared for each sample (12 samples in total). A total of 75.000 GFP-positive cells were FACS sorted and RNA was extracted using the RNeasy Plus Micro kit (Qiagen 74034). RNA was processed using the RNA-Seq Poly A method and 100 bp paired-end RNA-Seq was performed on the Illumina HiSeq4000 platform (Wellcome Trust Centre for Human Genetics, University of Oxford).

Data analysis was performed by Dr Adam Handel (Department of Paediatrics and Nuffield Department of Clinical Neurosciences, University of Oxford, United Kingdom). Briefly, reads were aligned against the Ensembl transcriptome and genome (GRCh38.EBVB95-8wt.ERCC) using STAR (version 2.5.3a). The allocation of reads to protein coding gene meta-features was done using HTSeq. Differential expression analysis on genes, with at least 1 aligned fragment, was performed using general linear modelling in edgeR with trimmed-M-of-means library size correction and tagwise dispersion estimates. Differentially expressed genes were identified using the default edgeR threshold (FDR<0.05). Gene ontology analysis was performed using ClusterProfiler. The third biological replicate of the *Δ550* sample was removed as an outlier due to a low number of detected genes and initial exploratory analysis using multi-dimensional scaling of inter-sample differences.

3.3 RESULTS

3.3.1 The *Δ550* mutant allele encodes for a protein of reduced molecular weight compared to the *WT FOXN1*

To study the molecular characteristics of the *Δ550*-FOXN1 mutant, we employed site-directed mutagenesis to engineer a human *FOXN1* gene sequence carrying the same single-base pair deletion as the one identified in the paediatric patient heterozygous for the *Δ550* mutant. Subsequently, human (TEC4D6) and mouse (TEC1.2) thymic epithelial cell lines were transfected with either human WT or human *Δ550 FOXN1*. qRT-PCR analysis of WT and *Δ550* FOXN1 transcripts, showed that relative mRNA levels of *Δ550 FOXN1* were consistently higher compared to those of WT *FOXN1* in both the mouse (Figure 3.2 a,) and human TEC cell lines (Figure 3.2 b).

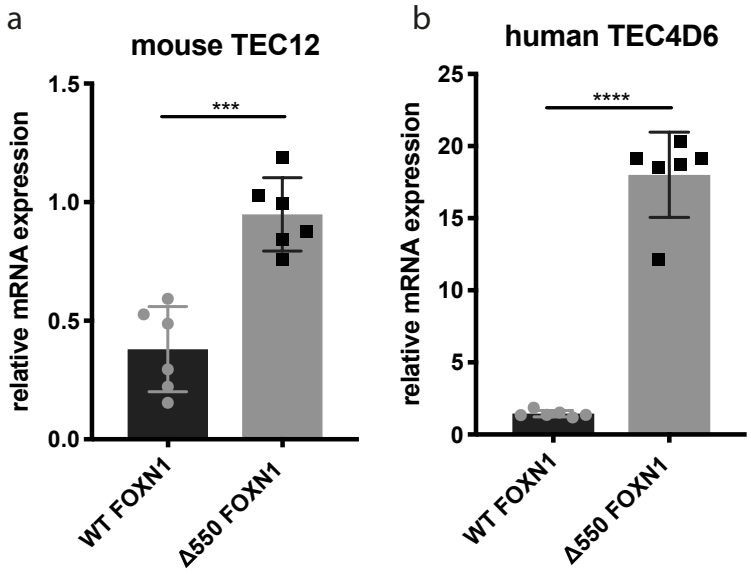


Figure 3.2 Transfection with the *Δ550*-FOXN1 results in higher *FOXN1* relative mRNA expression levels compared to the WT FOXN1 in a) mouse TEC1.2 n=6, b) human 4D6 cells n=6. qRT-PCR analysis was performed 48hours post transfection. *** p<0.005, **** p<0.0001, *P* values calculated by unpaired *t*-test. *FOXN1* expression was calculated relative to *GAPDH.*

We next sought to determine whether the mutant *FOXN1* mRNA escapes non-sense mediated decay and would successfully be translated into a protein. To this end, the human TEC 4D6 cell line was transfected with either the human WT or the mutant *Δ550* FOXN1 tagged with a FLAG tag. Western blot analysis using an anti-FLAG antibody showed that *Δ550*-FOXN1 mRNA was translated into a protein of considerably reduced molecular weight (MW~50 kDa) when compared to the WT FOXN1 protein (predicted MW 68.9kDa, observed MW~85 kDa) (Figure 3.3a). Protein levels of *Δ550*-FOXN1 were also decreased in comparison to WT FOXN1 as assessed by densitometer analysis (Figure 3.3b) and subsequently confirmed by mass spectrometry proteomics analysis (Chapter 4).

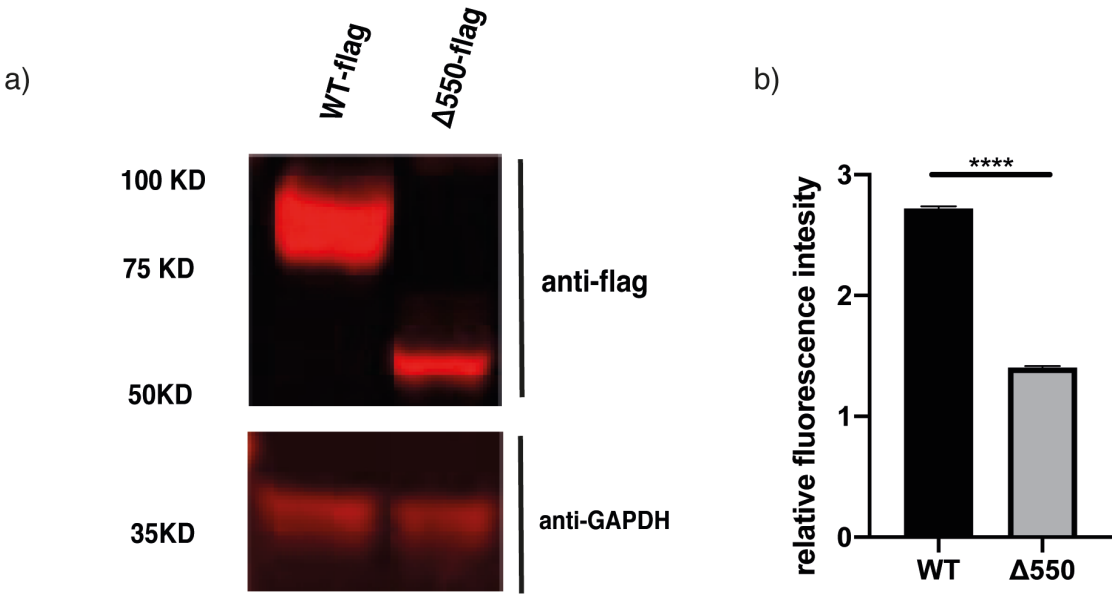


Figure 3.3 *Δ550* FOXN1 protein expression levels are decreased compared to WT protein levels a) A representative Western blot image of WT and *Δ550*-FOXN1 protein in 4D6 cell line using anti-FLAG is shown. GAPDH was used as a loading control n=2 b) Quantification of WT and *Δ550* protein band intensities from Figure 3.3.a using Fiji. The fluorescence intensity of the wild type (FI_WT) and mutant (FI_Δ550) bands was calculated relative to the fluorescence intensity of the GAPDH loading control (FI_GAPDH) in each sample after subtracting the fluorescence intensity of the background (FI_B). Relative fluorescence intensity = [(FI_WT) -(FI_B)]/ [(FI_GAPDH)- -(FI_B)] **** p<0.0001, *P* values calculated by unpaired *t*-test.

3.3.2 The *Δ550* mutant localises to the nucleus similar to the wild-type protein

It is known that mutations can disrupt the subcellular localization of proteins[181]. To investigate whether the *Δ550* mutation can cause aberrant subcellular localization of FOXN1, TEC4D6 cells were co-transfected with the human WT-myc and the mutant *Δ550*-FLAG construct. Cells were stained and visualized by confocal microscopy. Immunocytochemistry staining for myc-tagged WT-FOXN1 and FLAG-tagged *Δ550*-FOXN1 revealed that mutant FOXN1molecule correctly localises to the nucleus (DAPI nuclear stain) with a similar pattern to that observed for the WT-FOXN1 (Figure 3.4).

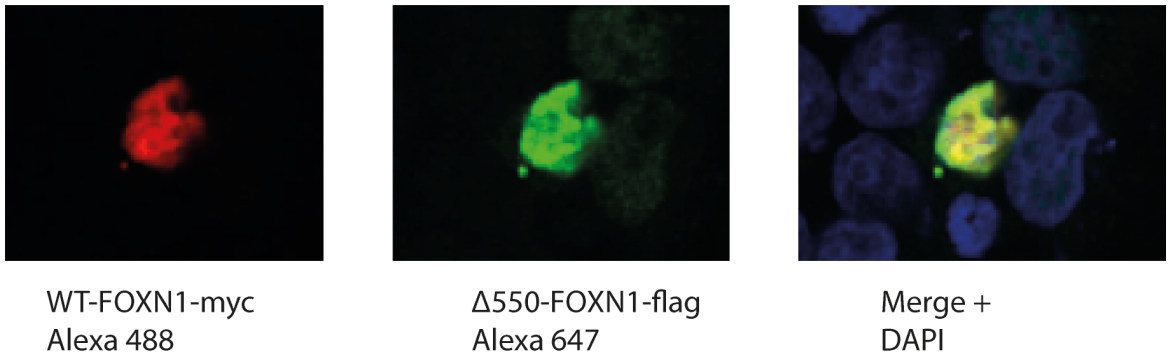


Figure 3.4 *Δ550* FOXN1 localises to the nucleus similar to WT FOXN1. 4D6 cells transfected with either WT-myc or Δ550-FLAG constructs were fixed and stained with rabbit anti-myc and mouse anti-FLAG antibodies, respectively. Alexa 488 anti-rabbit and Alexa 647 anti-mouse were used as secondary antibodies. DAPI nuclear stain. Representative confocal images images from two independent experiments are shown.

3.3.3 The frameshift in the *Δ550* mutant disrupts the evolutionary conserved domain in the C-terminus of the FOXN1 protein

As discussed in chapter 2, the *Δ550* mutation is characterised by a single base pair deletion at the Histidine-457 (his 457) residue, that generates a protein frameshift and a premature truncation of the protein at residue 550. The his457 residue and the protein region surrounding it, are not evolutionary conserved (Figure 3.5a). However, the following protein region from residue 517 to 557, is enriched for fully conserved amino acids or for amino acids with conserved properties (Figure 3.5b). The sequence conservation is true for species that possess a functional thymus specialised in T cell development, while is absent in the *S.canicula* jawed vertebrate (Figure 3.5b) that contains a thymus supporting both B and T cell development[92].

Using a β-galactosidase transcriptional reporter assay Thomas Bohem and colleagues assessed the transcriptional potency of FOXN1 constructs lacking parts of the C-terminus. With these experiments they positioned the transcriptional activation domain of the rat FOXN1 protein within residues 507 to 562[182]. The same sequence was also later found in the mouse FOXN1 protein [183] . Figure 3.5 b illustrates that the properties of the amino-acids making up this transcriptional activation domain are conserved among species. This region is enriched for acidic amino acids (21.5%) (Figure 3.5c), a feature that is characteristic of the transcriptional activation domains of other transcription factors like Tp53 and Fos and that has been linked to the molecule's transcriptional activity[184]. In the *Δ550* mutant this region is replaced by a new sequence that does not align with any other FOXN1 known ortholog (Figure 3.5b). Interestingly, the content of acidic amino acids in the mutant's aberrant region is five times lower when compared to that of WT FOXN1 (Figure 3.5c). As will be

further examined in the following sections of this chapter, the above data suggest that the mutation disrupts a protein sequence with an essential role in the transcriptional competence of the FOXN1 protein.

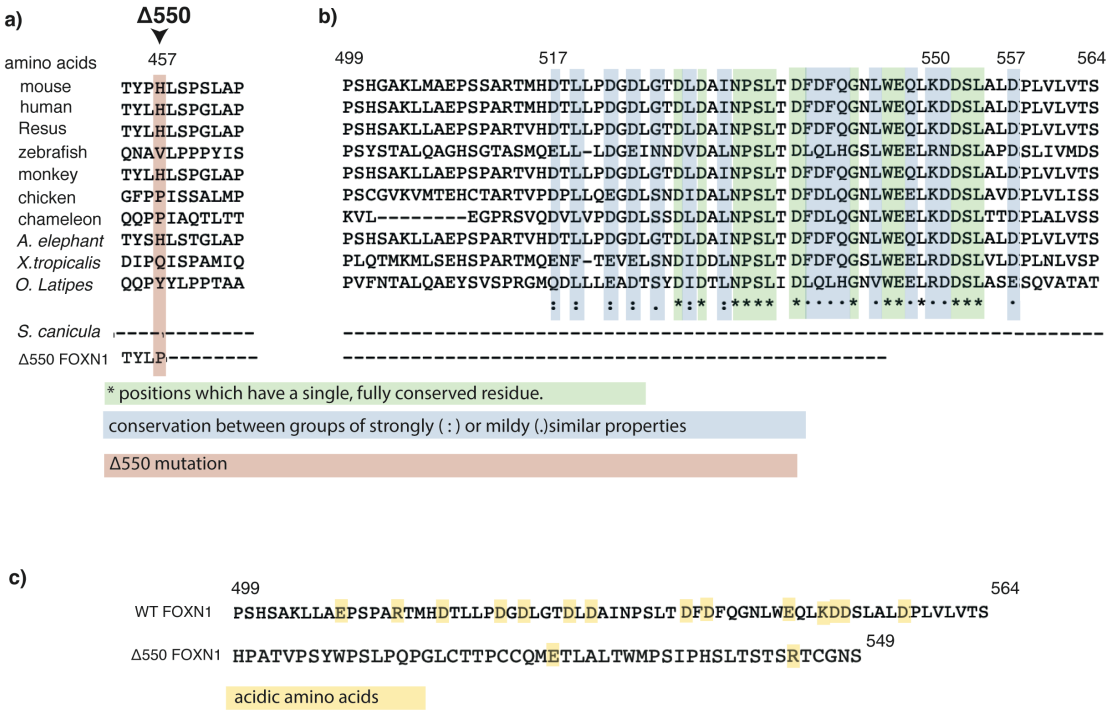


Figure 3.5 Amino acid sequence conservation of the C-terminus domain among species a) sequence conservation surrounding the *Δ550* mutation at residue 457 b) conserved region within residues 499-564 of the C-terminus of the protein. Sequence alignments were performed with UniProt c) acidic amino acid content within residues 499-564 of the human WT and residues 544-549 of the *Δ550* FOXN1.

3.3.4 FOXN1's function is dose dependent

To test the transcriptional competence of the various FOXN1 mutants, a luciferase assay was developed and used. The 4D6 human thymic epithelial cells were transfected with decreasing amounts of WT, *Δ564* or *Δ550*-FOXN1. A plasmid containing the β5t promoter (β5t-luc), a recently described FOXN1 target[104], followed by the gene encoding the luciferase (chapter 3.2.8) was also co-transfected. As a negative control a mutant β5t promoter with a mutated FOXN1 binding site (β5t-*mut*-luc) was used.

The *Δ564* construct [564amino acids (aa) long] contains the conserved transcriptional activation domain (chapter 3.3.4) as characterised for mouse [183] and rat FOXN1[182] proteins but is otherwise of shorter length compared to WT-FOXN1 (648 aa long) (Figure 3.6a). The *Δ550* mutant was found to be transcriptionally inactive while the *Δ564* mutant showed a 20-30% reduced transcriptional activity compared to the WT FOXN1 (Figure 3.6b). *In vivo* mouse studies demonstrated that FOXN1 functions in TECs in a dose-dependent manner [54, 91] [103]. In agreement, we also observed a linear dose response for WT and *Δ564*-FOXN1 in our *in vitro* studies (Figure 3.6b).

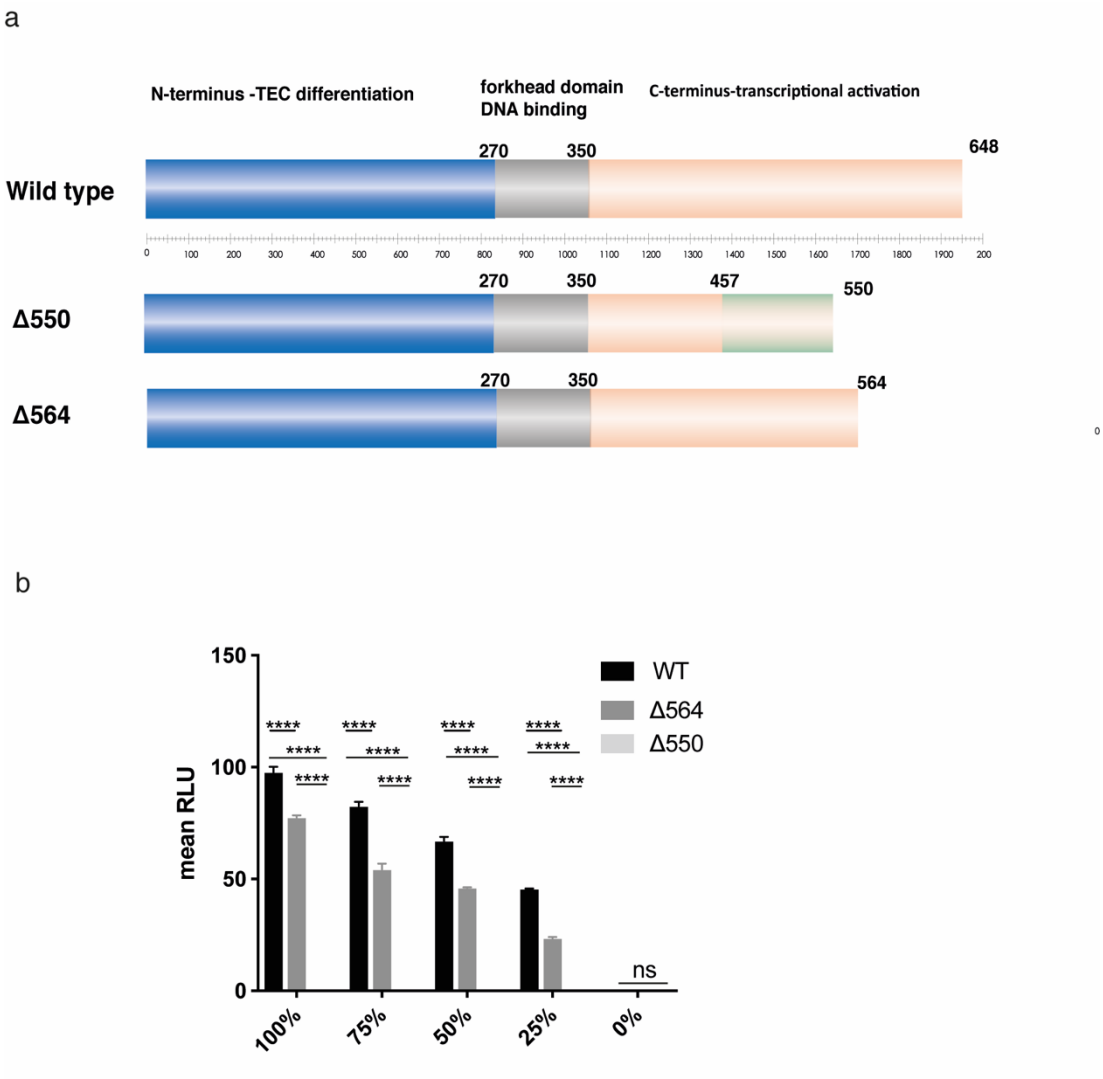


Figure 3.6 Functionality of different FOXN1 mutants a) Schematic representation of WT, *Δ550* and *Δ564* FOXN1 constructs, numbered bar represents base pairs b) Transcriptional competence was assessed by a luciferase reporter assay. Linear dose response for WT and *Δ564* FOXN1 and loss of transcriptional activity for *Δ550* FOXN1. Reporter activity was corrected by calculating the luciferase to renilla ratio for each well. RLU=relative light units, **** p<0.0001, *P* values were calculated by unpaired *t*-test, n=3.

3.3.5 The *Δ550* mutant exerts a dominant negative effect.

We next sought to evaluate the impact of the *Δ550* mutant on the transcriptional activity of WT-FOXN1 with the in vitro luciferase reporter assay described above. To this end, 4D6 cells were co-transfected with WT FOXN1 and/or *Δ550*-FOXN1 plasmids and the luciferase β5t reporter plasmid bearing the canonical FOXN1 binding site (β5t-luc). As a control a mutant β5t promoter with a mutated FOXN1 binding site (β5t-*mut*-luc) was used.

As demonstrated in Figure 3.7a co-transfection of 4D6 cells with β5t-luc and WT-FOXN1 plasmid resulted in pronounced luciferase activity relative to the control assay with β5t-*mut*-luc plasmid. In sharp contrast, co-transfection with β5t-luc and *Δ550* FOXN1 resulted in absence of luciferase expression (Figure 3.7a). When both WT and *Δ550* FOXN1 were co-transfected, the transcriptional activity of the WT-FOXN1 was almost completely abrogated (Figure 3.7b). Specifically, when WT FOXN1 and *Δ550* mutant were co-transfected in a one-to-one ratio (mimicking the situation of a heterozygous cell) the activity of WT FOXN1 to activate luciferase transcription was dramatically reduced to only 3.3% of its normal activity (Figure 3.7b). Taken together, these data suggest that the *Δ550* mutant exerts a dominant negative effect on WT FOXN1.

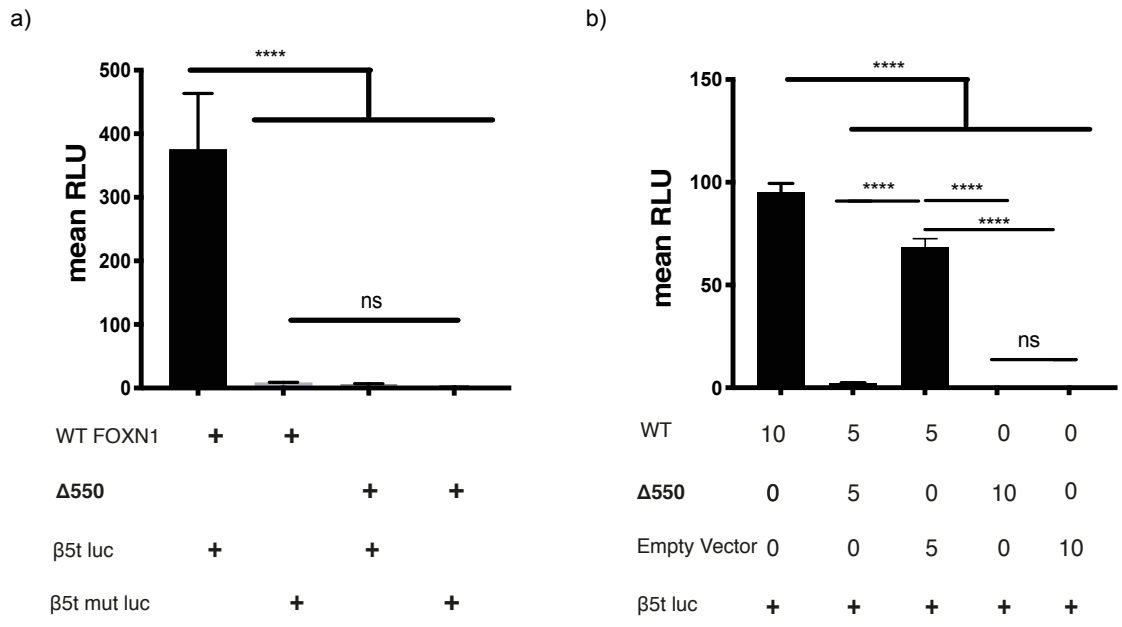


Figure 3.7 *Δ550*-FOXN1 exerts a dominant negative effect on WT-FOXN1. Luciferase assay on 4D6 human cells transfected with a) WT or *Δ550* FOXN1 along with β5t-luc or β5t-mut-luc promoter and b) with different ratios of WT FOXN1 and *Δ550* FOXN1. Co-transfection of WT-FOXN1 with an empty vector was used as a control in all cases. Reporter activity was corrected by calculating the luciferase to renilla ratio for each well. Graphs correspond to a representative experiment, out of five independent experiments, with three technical replicates each. RLU=relative light units, ****p<0.0001, *P* values were calculated by unpaired *t*-test with correction for multiple comparisons, n>3

3.3.6 The aberrant protein domain in the *Δ550* FOXN1 makes it a dominant negative mutant

To characterise the protein domain responsible for exerting the dominant negative effect observed, various FOXN1 mutant variants truncated at different positions in the C-terminus were generated (Figure 3.8).The *Δ550b* variant has the same length as the *Δ550* mutant but contains a normal sequence instead of the frameshifted region (from aa 457 to 549) found in *Δ550.* The *Δ564 variant*, retains the transcriptional domain but is of shorter length (only composed by 564 amino acids) compared to WT-FOXN1. The *Δ457* variant is truncated at the site of the single base pair deletion found in the naturally occurring *Δ550* variant.

Luciferase reporter assays were performed to assess the transcriptional activity and the dominant negative potential of these individual variants (Figure 3.9). The effect of the *Δ550* and *Δ564* mutants were previously described in section 3.3.4. As shown in Figure 3.9 a and b, *Δ550b* was transcriptionally inactive but exerted only a moderate repressive effect on transcription activation of the WT FOXN1. Similar findings were obtained with *Δ457* mutant. (Figure 3.9 c,d). Taken together, these data suggest that the *Δ550* mutant's frameshifted region (from 457 aa to 549 aa) is responsible for its dominant negative effect. When this region was added at the C-terminus of a full length WT FOXN1 (designated *WT+ scramble* construct), the generated construct was unable to exert a dominant negative effect (Figure 3.9 e,f) indicating that the protein conformation of the *Δ550* mutant and not only the altered sequence, is critical for exerting a dominant negative effect.

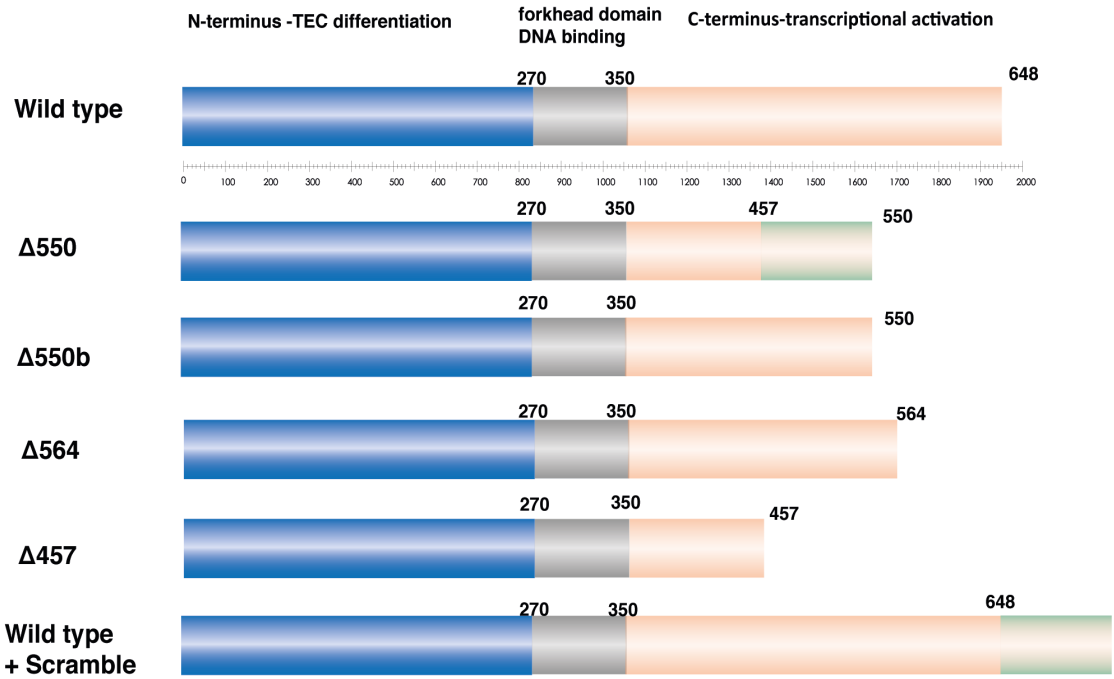


Figure 3.8 Schematic representation of FOXN1 constructs differentially truncated at the C-terminus. Detailed description of each construct can be found in section 3.3.6. Numbered bar represents base pairs

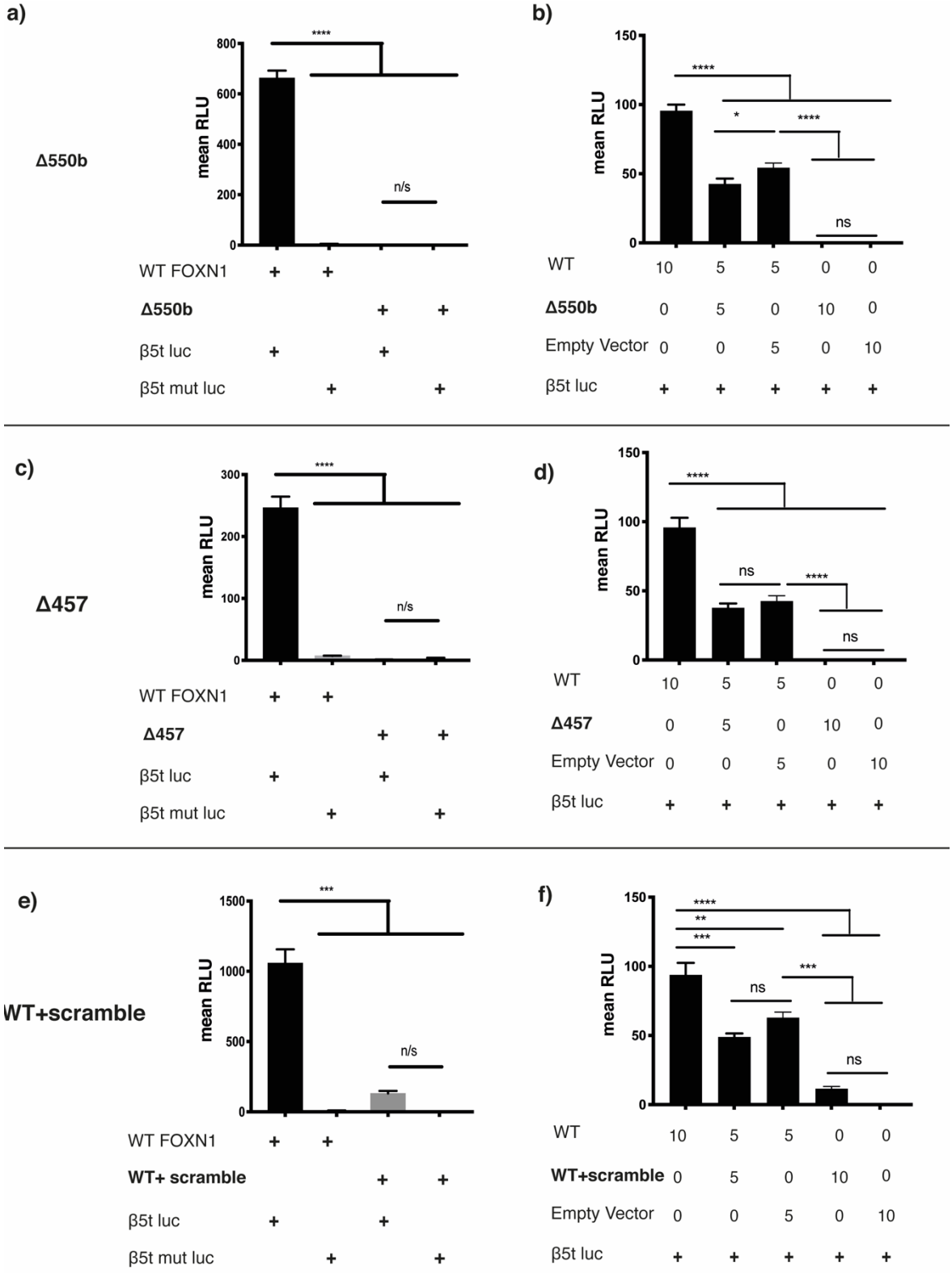


Figure 3.9 Dominant negative activity of different FOXN1 constructs. Luciferase reporter assay in 4D6 cells transfected with a) WT or *Δ550*b FOXN1 along with β5t-luc and β5t-mut-luc b) different ratios of WT and *Δ550*b FOXN1 c) WT or Δ457 FOXN1 along with β5t-luc or β5t-mut-luc promoter d) different ratios of WT and Δ457 FOXN1 e) WT FOXN1 or WT+scramble FOXN1 along with β5t-luc or β5t-mut-luc promoter f) different ratios of WT and WT+scrambled. Co-transfection of WT FOXN1 with empty vector (grey bar) was used as a control in all cases. Reporter activity was corrected by calculating the luciferase to renilla ratio for each well. Graphs correspond to a representative experiment, out of two independent experiments, with three technical

replicates each RLU=relative light units. *p<0.05; **p<0.01; ***p<0.005,****p<0.0001. *P* values were calculated by unpaired t-test.

3.3.7 The *Δ550* FOXN1 mutant impairs the transcriptionally activity of the WT FOXN1

To more directly address how the *Δ550* FOXN1 mutant affects the transcriptional activity of the wild-type FOXN1, we performed RNA-sequencing in 4D6 cells transfected with either WT-FOXN1 alone, *Δ550*-FOXN1 alone, a combination of both or an empty-vector as a negative control.

Overexpression of WT-FOXN1 in 4D6 human thymic epithelial cells resulted in the significant upregulation of 62 genes and downregulation of 68 genes compared to the empty vector control (Figure 3.10a). Among the 62 upregulated genes there was an enrichment for proteins involved in transcription factor binding and transcriptional activity, such as HES1 (hes family bHLH transcription factor 1) and FOXQ1 (Forkhead box Q1) (Figure 3.10b). Conversely, genes downregulated in the presence of WT-FOXN1 encoded for proteins involved in cellular response to pathogens, including various interferon related genes (Figure 3.10c).

In contrast, overexpression of the *Δ550* mutant resulted in the significant downregulation of only one gene (*BHLHE41*, Basic helix-loop-helix family, member e41) (Figure 3.10d). These findings strongly suggest that the *Δ550* mutant is transcriptionally inactive and further supported the results obtained with the luciferase assay (chapter 3.3.6).

Dual transfection with WT and *Δ550* FOXN1 resulted in the significant induction /repression of 29 genes. 14 of those (48.3%) were the same genes that were differentially regulated by WT FOXN1 alone (Figure 3.10e). The remaining 15 genes (51.7%) encoded for seemingly unrelated proteins, not enriched for specific biological

functions; including the chemokine CXCL8, growth factors (for example Proheparin-binding EGF-like growth factor HBEGF), histones (for example HIST1H2AB), kinases (for example G1/S-specific cyclin-D2 CCND2). Most importantly, in the presence of the *Δ550* mutant the WT was unable to differentially regulate 116/130 (89%) of the genes that would normally regulate. In conclusion, although *Δ550* FOXN1 is transcriptionally inert, co-transfection with WT FOXN1 is insufficient to rescue the transcriptomic phenotype.

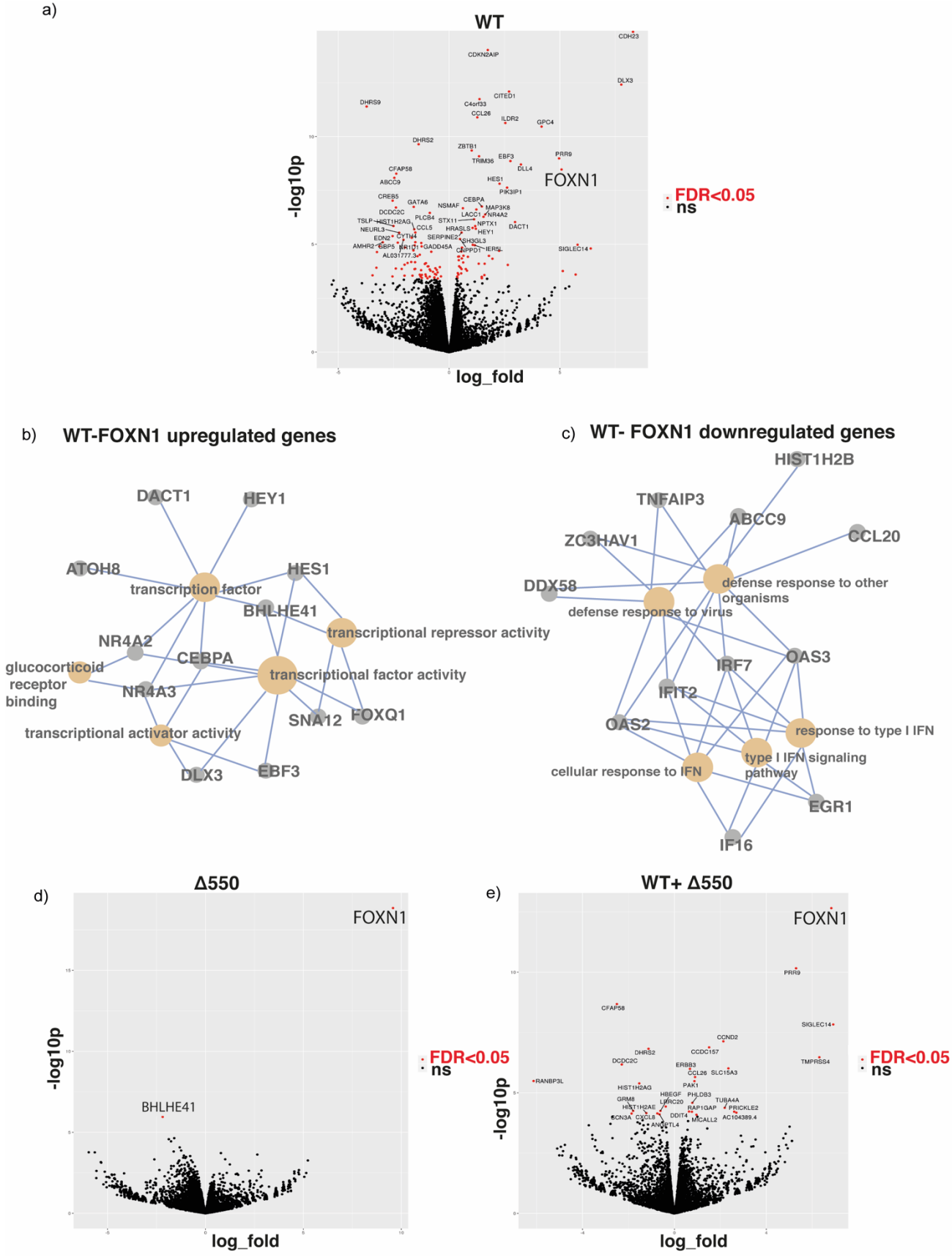


Figure 3.10 Analysis of gene expression changes in the 4D6 cell line transfected with WT, *Δ550* or both. a) Volcano plot analysis of differential gene expression in 4D6 cells transfected with WT compared to empty vector. Positive values on the x-axis indicate upregulated transcripts presented as $\log_2$ fold changes, whereas negative values specify downregulated transcripts shown as $\log_2$ fold change. The y-axis represents a

log scale of the p-values for a two-way ANOVA of the differences between samples. ClusterProfiler networks with gene set enrichment analysis for b) upregulated genes presented in Figure 3.10a and c) downregulated genes after WT overexpression presented in Figure 3.10a, FDR<0.05. Volcano plot analysis of differential gene expression in 4D6 cells transfected with d) *Δ550* e) WT and *Δ550* compared to empty vector. Positive values on the x-axis indicate upregulated transcripts presented as $\log_2$ fold changes, whereas negative values specify downregulated transcripts shown as $\log_2$ fold change. The y-axis represents a log scale of the p-values for a two-way ANOVA of the differences between samples.

3.3.8 Assessing the pathogenicity of different *FOXN1* variants found in two paediatric patients with immunodeficiency.

We have generated an in vitro model to interrogate the molecular mechanisms that underpin the clinical presentation of two unrelated paediatric patients with athymia or thymic hypoplasia and immunodeficiency. Both patients, had among other genetic variants, heterozygous point mutations in their *FOXN1* gene of unknown functional consequence. As the other genetic variants identified, concerned genes involved in haematopoiesis, the precise molecular cause of the observed immunodeficiency was initially unknown. However, it is this information that assists in clinical decision making and determines the management of these patients. More specifically, as to whether a bone marrow or a thymus transplant is indicated as the best treatment of choice.

We therefore established a diagnostic tool that allows the functional assessment of *FOXN1* mutations. Using this approach, we assessed the pathogenicity of *FOXN1* variants found in the two paediatric patients.

Patient 1-Clinical history:

A 6-month old male infant was presented in the clinic with viral recurrent diarrhoea, recurrent fever, oedema and joint swelling. A blood analysis revealed profound T cell lymphopenia (22% of total lymphocytes, normal range 51-77%). The relative frequency of $CD4^+CD45RA^+$ naïve cells was reduced (5% of $CD4^+$, normal range: 20-60%) while he had no $CD8^+$ T cells. Proliferative response to the mitogen PHA (phytohemagglutinin) was reduced by 80-90%. Further clinical work-up revealed a reduced thymus size (for their age) by CT scan. Genetic testing for 207 known molecular causes of primary immunodeficiency genes revealed several genetic variants of unknown clinical significance. Among which there was a

heterozygous *FOXN1* mutation c.974 C>T. p. 325Pro>Leu that we will be referring to as 325FOXN1 (Figure 3.11).

Patient 2-Clinical history:

An 11-year old male patient was presented to the thymus transplantation team at Great Ormond Street Hospital, London with absent thymus and severe T cell immunodeficiency with absent naïve T cells and negligible TREC levels. He had a normal T cell proliferative response to PHA mitogen and a normal response to vaccinations. The past medical history revealed a lymphoproliferative disease most likely caused by EBV infection but there was no other history of serious infections. Diagnostic work using Next Generation Sequencing (NGS) identified the patient to be compound heterozygous for two separate *FOXN1* mutations (c.246 C>A and c.1049 C>T, respectively). The first mutation was predicted to result in an early stop codon at protein residue 246. The second mutation lead to a proline to leucine substitution at residue 350 but was of unknown significance (we will be referring to the second mutation as 350 FOXN1) (Figure 3.11). In addition, multiple polymorphic variants in LRBA (Lipopolysacaccharide-responsive, beige-like anchor protein) and CTLA4 *(cytotoxic T-lymphocyte associated protein 4)* were detected. While functional assays suggested low *CTLA4* expression. Overall, it was unclear whether his clinical phenotype resulted from the mutations observed in LRBA, *CTLA-4* and/or *FOXN1*.

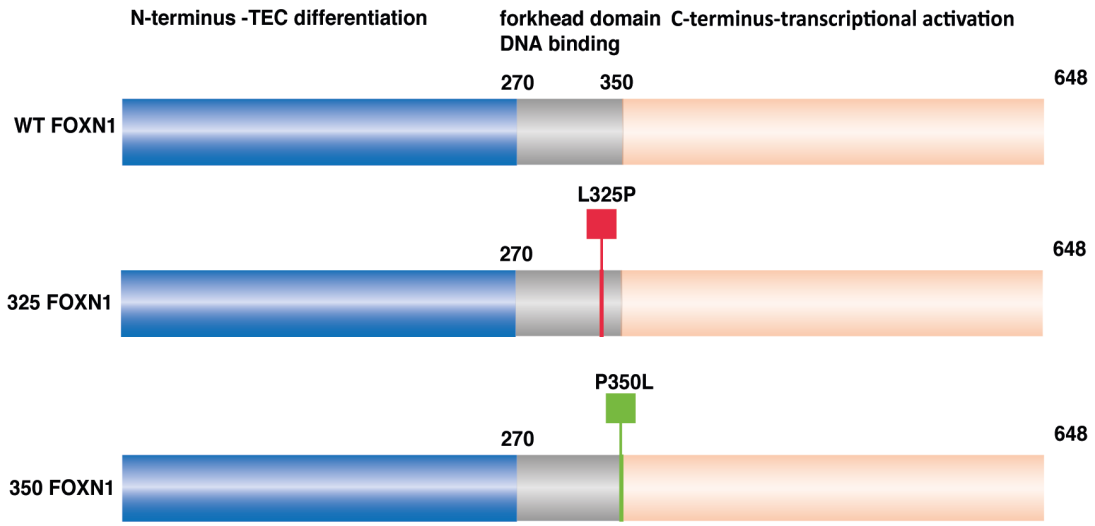


Figure 3.11 Schematic representation of FOXN1 variants found in two paediatric patients with athymia or thymic hypoplasia and immunodeficiency

Using site-directed mutagenesis (chapter 3.2.3) we introduced the respective mutations found in patient 1 and 2 into the WT *FOXN1* open reading frame (ORF). By luciferase reporter assay we assessed the transcriptional competence of these variants and their dominant negative activity as previously described for the *Δ550* FOXN1 variant.

1) In the 325FOXN1 variant, there is a leucine-to-proline substitution within the DNA binding forkhead domain of FOXN1, In a region very close to the actual DNA recognition site of FOXN1[87]. This substitution is predicted to disrupt the hydrogen bonding thus affecting the protein conformation change. That may ultimately impact on how FOXN1 binds to DNA, making 325FOXN1 a loss-of-function mutant. Using the luciferase assay to probe functionality, we found that 325FOXN1 was transcriptionally inactive (Figure 3.12a) but lacked a dominant negative potential (Figure 3.12b). Individuals that are heterozygous carriers of loss of function mutations in the *FOXN1* gene are immunocompetent. Therefore, we hypothesised that the immunodeficiency

of this patient was most likely the consequence of other genetic variants and not directly due to the *FOXN1* mutation.

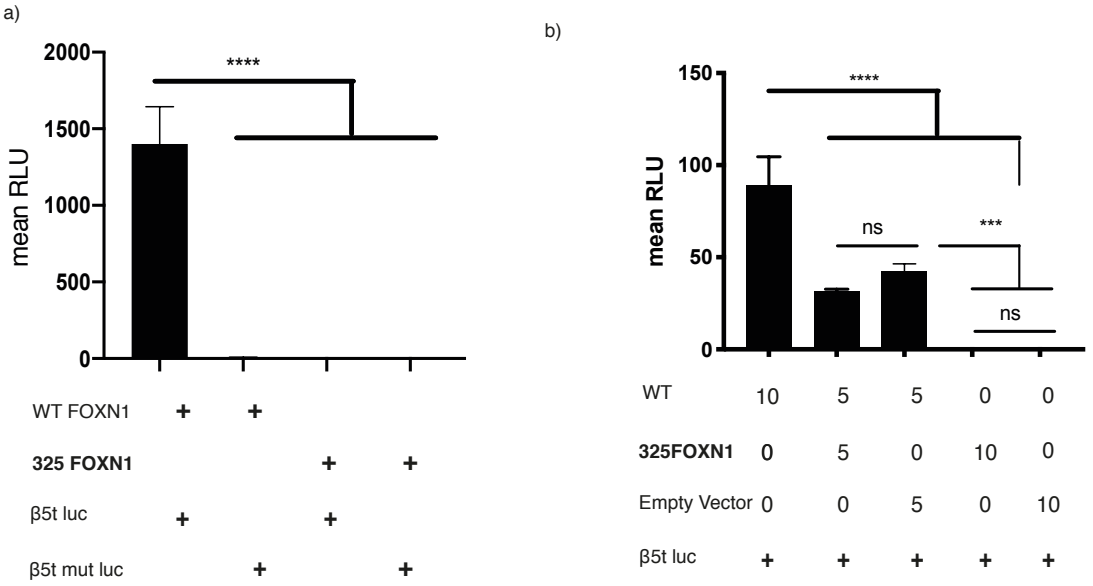


Figure 3.12 Assessing the pathogenicity of the 325 FOXN1 variant found in a patient with athymia and immunodeficiency. Luciferase reporter assay in 4D6 cells transfected with a) wild type FOXN1 (WT) or 325FOXN1 along with a wild type β5t promoter or a mutated β5t promoter and b) WT and 350FOXN1 at different ratios. Co-transfection of WT with empty vector (grey bar) was used as a control. RLU=relative light units. Reporter activity was corrected by calculating the luciferase to renilla ratio for each well. Graphs correspond to a representative experiment, out of three independent experiments, with three technical replicates each RLU=relative light units. *p<0.05; **p<0.01; ***p<0.005,****p<0.0001. *P* values were calculated by unpaired t-test.

2) The 350 FOXN1 mutation found in the patient 2 was located in the second winged helix, which is part of the DNA binding forkhead domain but is distant to the sequence that determines the DNA-protein interface[87]. From a structural point of view, the proline to leucine substitution is not predicted to impact on the secondary structure of FOXN1. Using our functional in vitro assay, we demonstrated that 350FOXN1 constitutes a hypomorphic variant (Figure 3.13). The other allele in the patient had a

non-sense mutation at residue 246 that generated a truncated FOXN1 protein of 246 amino acids length. The generated protein does not contain a DNA binding domain or a transcriptional activation domain and is not functional. This patient had therefore only one functional allele which was however strongly hypomorphic thus explaining their athymia. The patient ultimately underwent thymus transplantation and is currently in recovery phase.

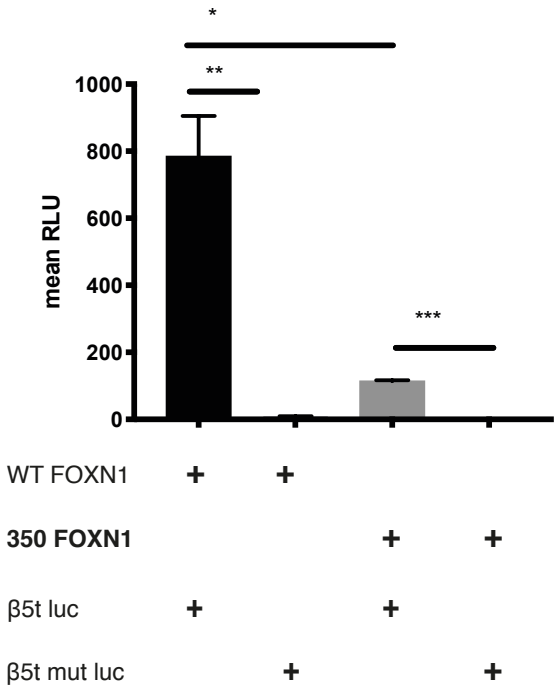


Figure 3.13 Assessing the pathogenicity of 350 FOXN1 variant found in a patient with thymic hypoplasia and immunodeficiency. Luciferase reporter assay in 4D6 human cells transfected with either wild-type FOXN1 (WT) or 350FOXN1 along with β5t-luc or β5t-mut-luc luciferase plasmids. Reporter activity was corrected by calculating the luciferase to renilla ratio for each well. RLU=relative light units. Graphs correspond to a representative experiment, out of three independent experiments, with three technical replicates each RLU=relative light units. *p<0.05; **p<0.01; ***p<0.005. *P* values were calculated by unpaired t-test.

The study described in chapter 3.3.9 was done in collaboration with Dr Fatima Dhalla, Department of Paediatrics, University of Oxford and Prof Graham Davies' clinical team at the Great Ormond Street Hospital, London.

DISCUSSION

The role and unique importance of FOXN1 as a master regulator of the transcriptional network that determines TEC identity has been previously established [44, 91, 104, 136, 137, 139]. The transcriptional activation domain of the mouse and rat FOXN1 was defined to lie within residues 509 -563 of the protein's C-terminus [182, 183] and shown to be required to promote the expression of FOXN1 target genes. In this chapter, I showed that the transcriptional activation domain of FOXN1 is enriched for acidic amino acids, a feature also found in other transcriptional activation domains, including those of TP53 and Fos [184]. This very domain of FOXN1 is also evolutionary conserved among species that contain a thymus specialized in T cell production. Using a luciferase assay to measure the transcriptional competence of differentially truncated FOXN1 constructs, we showed that the human FOXN1 protein relies on the same sequence to control the transcriptional activation of target genes.

When overexpressed in human thymic epithelial 4D6 cells, human FOXN1 exerts a dual role, namely that of a transcriptional activator and a repressor of gene transcription controlling the expression of 130 genes, as verified by RNA-Seq. This is in line with previous studies that show *Foxn1* to activate and suppress gene transcription in mouse primary TECs [104]. *Foxd3* (forkhead box protein D3), another member of the forkhead family of transcription factors, with a key role in neural crest development, can facilitate both transcriptional activation and repression of a large number of target genes[185]. At initial stages of this development, these opposing mechanisms occur concomitantly. Over time however, there is a gradual shift towards a repressive

activity [185]. Whether FOXN1 preferentially acts as a transcriptional repressor or activator at different stages of thymus organogenesis remains to be determined.

What is the consequence of the *Δ550* mutation for the formation and function of the FOXN1 protein? To answer this question, we compared the molecular characteristics of the WT and mutant and showed that *Δ550*-FOXN1 mRNA escapes non-sense mediated decay and is translated into a protein of reduced molecular weight. *Δ550's* mRNA levels were found to be consistently increased in comparison to those encoding the WT protein. This could be due to an increased mRNA stability or alternatively, secondarily to a positive feedback mechanism whereby an increased degradation of the mutant protein drives *FOXN1* transcription. Two studies provide evidence of positive autoregulation of *FOXN1*. In one of these reports, *FOXN1* transgene expression was driven by the human keratin 14 promoter in mouse TECs[133]. Under these experimental conditions and using a set of primers recognising the transcripts of either the transgene or the endogenous FOXN1 locus, they were able to show that enforced FOXN1 overexpression upregulated endogenous FOXN1 transcription. In another study, mouse *Foxn1* overexpressed in mouse fibroblasts could upregulate endogenous *Foxn1* [138]. However, these studies didn't determine whether the observed upregulation of endogenous *Foxn1* occurred via a direct or indirect mechanism.

The *Δ550* mutant correctly localised to the nucleus similar to that of WT FOXN1. FOXN1's nuclear localization signal has not yet been identified but this study places the sequence to be outside of the region affected by the mutation (residues 457-648). However, the frameshifted sequence and the pre-mature termination resulted in a

protein that was transcriptionally inactive as it has lost its transcriptional activation domain.

Despite its transcriptional incompetence, *Δ550* exerts a dominant negative effect on the WT FOXN1 shown by both RNA sequencing and a luciferase assay. We could demonstrate that this FOXN1 mutant could impair the transcriptional activity of the WT protein and thus the up and down regulation of FOXN1 related gene expression in a TEC line. We propose that the mutant's aberrant amino acid sequence is responsible for driving the dominant negative effect probably due to an abnormal 3D folding of the C-terminal part of the protein. This in turn may change the protein's physiological interaction with important co-factors or may affect the factors ability to bind to DNA. Examples in the literature support either explanation. One report [186] describes a dominant negative mutation in the CD3ε subunit of the T cell receptor (TCR) that prevents a protein conformation required for the transduction of the activation signaling and thus impairs subsequent T cell maturation. This mutation reduces the correct interaction of the TCR subunits and negatively affects the recruitment of downstream signaling molecules[186]. In a second report, a conformational change of p53 alters its ability to interact with DNA[187]. It is therefore conceivable that the *Δ550* mutation could alter the interaction of the mutant with other protein co-factors that are necessary for WT FOXN1 activity or provide the mutant with a DNA binding advantage. Both hypotheses are examined in chapter 4 and chapter 5, respectively.

CHAPTER 4

CHARACTERISATION OF THE FOXN1 INTERACTOME

4.1 Introduction and Aims 102

4.2 Materials and Methods 103

4.2.1 Generation of a C-terminally tagged FOXN1 constructs 103

4.2.2 Immunoprecipitation of tagged FOXN1 variants 104

4.2.3 Live cell imaging 104

4.2.4 Fluorescence recovery after photobleaching 105

4.2.5 Fluorescence correlation spectroscopy of wild type and Δ550 FOXN1 105

4.2.6 Mass spectrometry proteomics analysis 106

4.2.7 Generation of the EYFP$^{\beta 5t}$FOXN1^{CMV} 4D6 reporter cell line 107

4.2.8 Cloning of sgRNAs in Cas9 expressing vector and transfection of 4D6 EYFP$^{\beta 5t}$FOXN1^{CMV} reporter cells. 110

4.3 Results

4.3.1 Wild-type FOXN1 forms multimers in vivo in 4D6 TEC cells 113

4.3.2 Live behavior of GFP tagged wild type FOXN1 114

4.3.3 Wild-type FOXN1 requires the specific environment of thymic epithelial to form multimers. 116

4.3.4 Wild-type FOXN1 does not form multimers in the presence of the Δ550 mutant 117

4.3.5 Nuclear movement of Wild-type FOXN1 in the presence or absence of the Δ550 FOXN1 120

4.3.6 Identification of putative FOXN1 partners by co-immunoprecipitation and mass spectrometry proteomics analysis 122

4.3.7 Validation of candidate FOXN1 interacting proteins using the EYFP$^{\beta 5t}$FOXN1^{CMV} reporter cell line 129

4.4 Discussion 134

4.1 INTRODUCTION AND AIMS

The FOXN1 interactome is not yet known. Indirect evidence of co-factors facilitating the FOXN1 function comes from Chromatin Immunoprecipitation experiments followed by DNA Sequencing (ChIP-Seq) studies in primary mouse TECs[104]. This study identified transcription factor binding motifs that were positioned in close proximity to canonical FOXN1 binding sites, including binding motifs for TP63 (tumour protein p63) and CREB *(cAMP response element-binding protein)*. However, any physical or functional association of FOXN1 with these proteins has not yet been identified.

The focus of this chapter is the characterization of the FOXN1 interactome. Employing standard co-immunoprecipitation (co-IP) and live cell imaging we interrogated whether FOXN1 forms larger protein complexes and whether the *Δ550* mutation disrupts such interactions. To identify candidates that assist the function of FOXN1 we employed mass spectrometric proteomics analysis of FOXN1 pull downs. To verify the function of selected candidate proteins, we used CRISPR/Cas9 to delete their expression, in a reporter cell line that monitors FOXN1 function.

4.2 MATERIALS AND METHODS

4.2.1 Generation of a C-terminally tagged FOXN1 constructs

The open reading frames (ORFs) of human wild-type (WT) and *Δ550* FOXN1 were cloned into an expression vector to be tagged with a C-terminal GFP (https://www.addgene.org/70219/), FLAG (https://www.addgene.org/67619/) or myc tags (https://www.addgene.org/67617/) following standard cloning protocols. Briefly, each ORF was amplified using primers with restriction site overhangs (table 4.1). Amplicon and vector were digested using the appropriate restriction enzyme combination that matches the primer overhangs (table 4.1) making sure that the insertion of the amplicon was in the correct orientation and in frame with the tag. Amplicon and vector were ligated overnight according to the NEBioligator (https://nebiocalculator.neb.com/#!/ligation), transformed into Top10 competent cells and plated on agar plates with antibiotic selection. Colony PCR was performed on selected colonies using a combination of suitable primers spanning the ORF and tag. Correct insertion of ORF into the vector was confirmed by Sanger sequencing. The generation of WT FOXN1 tagged with myc or FLAG tags is described in chapter 3.2.2 and was done using the GATEWAY cloning technology.

Insert	Vector backbone	Forward primer	Reverse primer	Restriction enzyme combination
Δ550 FOXN1	FLAG (https://www.addgene.org/67619/)	NotI 5'AAGCGGCCGCatggtgtcgctacccccg3'	SalI: 5'AAGTCGACcatggtgtcgctacccccg	NotI SalI
WT FOXN1	GFP (https://www.addgene.org/70219/)	KpnI 5'AAGGTACCatggtgtcgctacccccg3'	BamHI: 5'AAGGATCCTTttatgccagggccacgg3'	KpNI BamHI

Table 4.1: Primer sequences used for cloning

4.2.2 Immunoprecipitation of tagged FOXN1 variants

The 4D6, HEK293 or HELA cells were transfected and co-transfected as indicated, with either WT-FLAG or *Δ550*-FLAG, WT-FLAG and WT-Myc in the presence or absence of untagged *Δ550* as detailed below. Cells were lysed as described in chapter 3.2.6 and precipitates were removed by centrifugation at 15.000 g for 10 min 4°C. A few microliters of the lysate were kept as input for downstream western blot analyses. The remaining lysates were incubated with an anti-FLAG or anti-Myc antibodies and protein G magnetic beads for 2 hours at 4°C while slowly rotating. A few microliters of the supernatant were kept as flow through samples. IPs were washed three times with wash buffer using a magnetic rack. If pull downs were to be analysed by WB, beads were boiled at 95°C with denaturating sample buffer [250 mM Tris-HCl [pH 6.8], 10% [w/v] SDS, 35% [v/v] glycerol, 0.05% BPB, 0.7 M 2-mercaptoethanol (14.3M)] and stored at -20°C until further use. For mass spectrometry proteomic analysis the beads were eluted using 3x FLAG peptide by incubating 40 µg of FLAG peptide with 200 µl of IP sample for 45 min at 4°C under rotation. FLAG-peptide eluates were stored at -80°C for further use.

4.2.3 Live cell imaging

The 4D6 cells were plated on 35 mm glass bottom dishes (Ibidi, cat. no. 81158) at a density of 0.15 x 10^6 cells per dish. Cells were then transfected with various combinations of the WT and mutant FOXN1 constructs. Twenty-four hours after transfection the culture medium was exchanged with Leibovitz L15 medium without phenol red (Thermo Fisher, cat. no. 21083027) and the cells were imaged with a ZeissLSM 880 inverted confocal laser scanning microscope (Carl Zeiss AG, Oberkochen

Germany). The live cell imaging was performed in collaboration with Dr Erdinc Sezgin, Weatherall Institute of Molecular Medicine.

4.2.4 Fluorescence recovery after photobleaching

Fluorescence recovery after photobleaching (FRAP) used a focused laser beam to irreversibly photo-bleach fluorescent molecules in a specific area of the nucleus. The time to recover the fluorescent signal was subsequently measured, reflecting the diffusion of adjacent unbleached fluorescent molecules to replace the bleached molecules[188]. FRAP was performed in defined areas of the nucleus of 4D6 cells transfected with WT-FOXN1 GFP. FRAP analysis was performed in collaboration with Dr Erdinc Sezgin, Weatherall Institute of Molecular Medicine.

4.2.5 Fluorescence correlation spectroscopy of Wild type and *Δ550* FOXN1

For Fluorescence correlation spectroscopy (FCS), cells were prepared as described in section 4.2.3. For each cell where an FCS measurement was planned a fluorescence image was first taken of the cell's nuclei containing fluorescently labelled FOXN1. Subsequently, the nuclear location for the FCS analysis was selected and changes in fluorescence were measured at this position as a function of time. For each selected position five FCS measurements were taken of 10 sec each. FCS curves from single runs were individually sorted to determine whether they meet the designated criteria which stipulated i) photobleaching during acquisition time is less than 10% ii) shape or amplitude of curves from the same acquisition spot display differences that are less than twice the standard deviation in shape or amplitude of the curve)[189]. Curves that did not meet these criteria were excluded from further

analysis. Selected FCS curves from each run were combined and fitted using the FoCuS-point software[190]. FCS analysis was performed in collaboration with Dr Erdinc Sezgin, Weatherall Institute of Molecular Medicine.

4.2.6 Mass spectrometry proteomics analysis

The 4D6 or HEK293 cells were transfected with either WT-FLAG or *Δ550*-FLAG vectors. Three experimental replicates were prepared for each experimental condition. Cells were lysed and FLAG immunoprecipitation was performed as described in section 4.2.2. Part of the sample was analysed by silver staining (Pierce™ silver staining kit, ThermoFisher scientific) according to the manufacturer's recommendations, to confirm the presence of proteins other than FOXN1. For the mass spectrometric analysis, frozen samples were thawed and subjected to two rounds of chloroformmethanol precipitation. An in-solution trypsin digestion was followed as detailed by Fischer and Kessler, 2015[191]. After digestion and desalting, samples were resuspended in 20 µL 2% acetonitrile, 0.1% formic acid and subjected to nano-flow liquid chromatography tandem mass spectrometry (LC-MS/MS, here referred to as MS) as described by Fischer and Kessler, 2015[191]. LC MS/MS analysis was performed on an Orbitrap Fusion Lumos instrument, coupled to an Ultimate 3000 nUPLC with an EASY-Spray column (50 cm). The raw MS data were processed with Progenesis QI for Proteomics v. 4.1.6675.48614 to generate label-free relative quantitation.

The raw quantitation values were further analysed in R version 3.5.1 by Dr. Philip Charles from the Target Discovery Institute, University of Oxford. For each protein, correlation with FOXN1 was assessed by Spearman's ρ, and associated p-values were

calculated by the algorithm AS89[192]. False discovery rate (FDR) estimates at each p-value cutoff (q-values) were calculated from the list of p-values using the fdrtool package[193] (R package version 1.2.15 https://CRAN.Rproject.org/package=fdrtool). An FDR cutoff of 5% was applied.

4.2.7 Generation of the EYFP$^{\beta5t}$FOXN1^{CMV} 4D6 reporter cell line

To generate a reporter cell line for the screening of putative FOXN1 interacting partners identified by MS analysis, 4D6 cells were transformed with the lentivector EYFP$^{\beta5t}$FOXN1^{CMV} . Stable integration of this lentivector into the genome of 4D6 cells allows the constitutive expression of FOXN1 under the control of CMV promoter. Functional FOXN1 will bind to the β5t promoter (β5t is a well characterized FOXN1 target and the same promoter used for the luciferase assays described in chapter 3.2.8) to drive the expression of EYFP. The recombinant lentivector designated EYFP$^{\beta5t}$FOXN1^{CMV} was purchased from Vectorbuilder (Figure 4.1a for vector's map). Once expressed in cells it allows for the constitutive expression of *FOXN1* under the CMV promoter and the expression of EYDP under the transcriptional control of the β5t promoter.

Lentiviral supernatant was produced by Ryan Beveridge at the WIMM Virus Screening Facility. Briefly, 1.2 x10^7 HEK-293T cells were plated onto a 15 cm tissue culture dish. Twenty-four hours after plating, cells were co-transfected with the lentiviral transfer vector (EYFP$^{\beta5t}$FOXN1^{CMV}) and the psPAX2 and pMD2.G viral packaging vectors at a ratio of 044:0.33:0.22 using PEIPro (PolyPlus Transfection) following the manufacturer's protocol. Culture media was exchanged with 10 mL of fresh DMEM, (complemented with 10% FCS, NEAA, penicillin/streptomycin and L-glutamine) 6

hours post-transfection. Lentiviral supernatant was collected at 48- and 72- hours post transfection, pooled and filtered with a 0.45 µm cellulose acetate syringe filter (Sartorius). Supernatant was then overlaid onto 5 mL of 20% sucrose and ultracentrifuged at 24,000 rpm for 2.5 hrs (Beckman XPN80, SW32.Ti). The viral pellet was resuspended in PBS, aliquoted and stored at −80°C until further use.

For the generation of the FOXN1-EYFP reporter cell line, 4D6 cells were virally transduced with the $EYFP^{\beta 5t}FOXN1^{CMV}$ expression vector. The transduction was performed by Ryan Beveridge at the WIMM Virus Screening Facility. A range of MOIs (multiplicity of infection - reflecting the ratio of viral particles to target cells) was used to determine the virus titer required to achieve a 5% transduction efficiency in order to ensure a single integration of the construct in successfully transduced cells. Transduction was performed in the presence of 8 µg/mL hexadimethrine bromide (Polybrene). The resulting stable cell line was evaluated, 72 hours post transduction, for EYFP expression levels using flow cytometry. Transduced cells were repetitively sorted by FACs to obtain a population with at least 75% EYFP positive cells, as successfully transduced cells displayed the tendency to decrease the frequency of EYFP positive cells over time (Figure 4.1b and c)

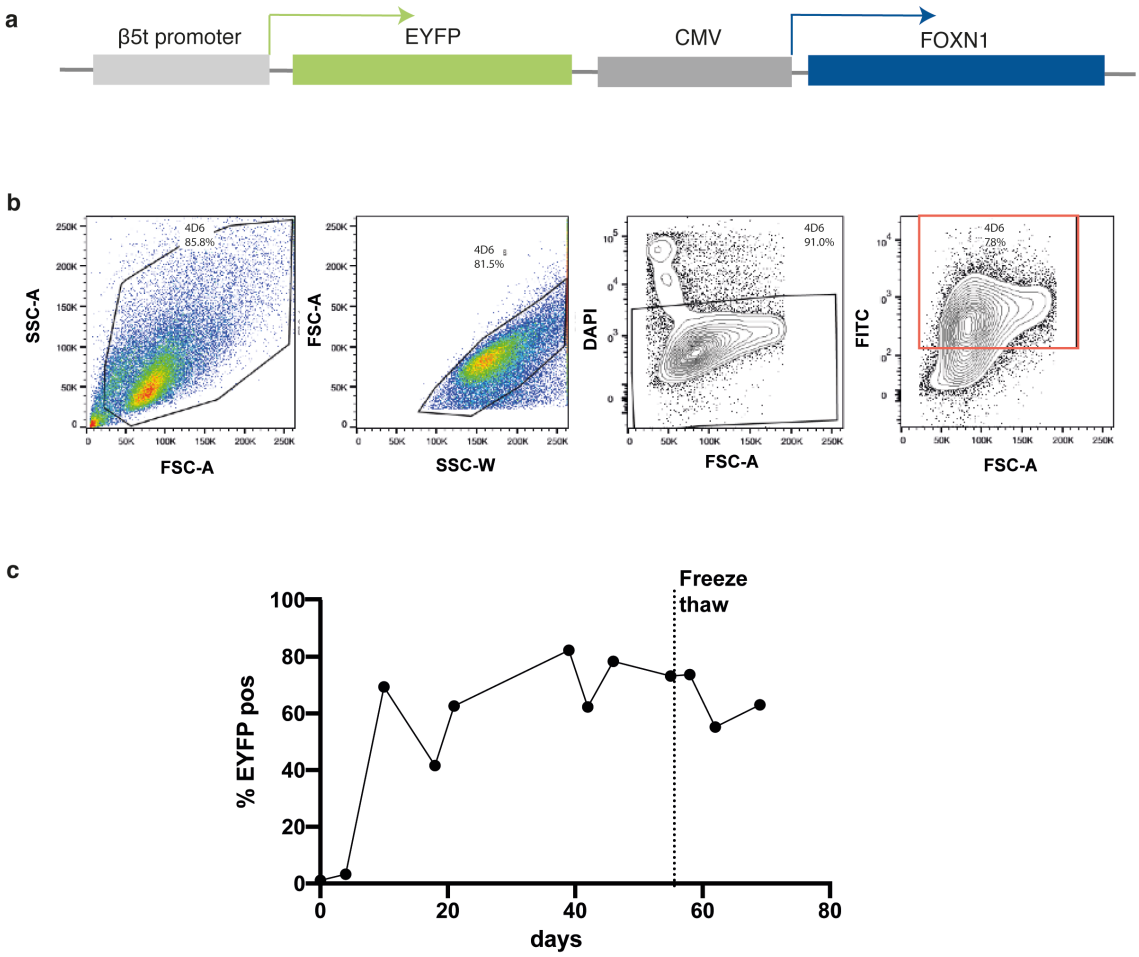


Figure 4.1 Generation of the EYFP$^{\beta 5t}$FOXN1^{CMV} reporter cell line a) A schematic representation of the EYFP$^{\beta 5t}$FOXN1^{CMV} construct b) Enrichment of EYFP positive 4D6 cells. Cells were first gated for their cell size (defined by their FSC/SSC), doublets were then excluded by gating according to Side Scatter-Width (SSC-W)/Forward Scatter-Area (FSC-A) parameters and an additional gate was placed to avoid dead cells (DAPI positive cells). The red square in the last plot indicates the gate used for sorting to obtain EYFP^{pos} cells c) Enrichment for EYFP^{pos} cells following multiple rounds of FACS sorting. The cells were sorted on the day to obtain a >95% EYFP-positive population of transduced 4D6 cells. Reinvestigation over the following days revealed the spontaneous silencing of the transduced sequence.

4.2.8 Cloning of sgRNAs in Cas9 expressing vector and transfection of 4D6 EYFP$^{\beta5t}$FOXN1^{CMV} reporter cells.

Single guide RNAs (sgRNAs) targeting FOXN1, YBX1 and CBP were selected from the GeneScript database https://www.genscript.com/gRNA-detail/1387/CREBBP-CRISPR-guide-RNA.html (table 4.2). Each pair of guides was cloned into the Cas9-2A-mRuby2 vector (https://www.addgene.org/110164/ Addgene #110164 a gift from Philip Hublitz) following the Feng Zhang lab protocol (https://media.addgene.org/cms/filer_public/e6/5a/e65a9ef8-c8ac-4f88-98da-3b7d7960394c/zhang-lab-general-cloning-protocol.pdf). Briefly, guides were designed to be complementary to both strands of the targeted sequence followed by an NGG Protospacer adjacent motif (PAM) with BbsI restriction overhangs. Vector and oligos were Bbsi digested for 30min at 37C. The plasmid was gel purified using the QIAquick Gel Extraction Kit (Qiagen 28115) and eluted in EB buffer. The oligos were phosphorylated and annealed using T4 Polynucleotide Kinase (TPNK New England Biolabs M0201S) for 30min. Digested vector and the chosen oligo were ligated using quick ligase (CatM2200 new England Biolabs). Ligates were used to transform chemically competent bacteria (One shot Top 10 E.coli C404010) which were then plated on ampicillin resistant plates for o/n growth. Two colonies per guide were selected, grown overnight in liquid cultures, miniprepped and sent for sequencing to confirm the successful ligation into the Cas9-2A-mRuby2 vector.

Guide	Sequence	Targeted exon
sgFOXN1#1	F:5'CACCG**TGCTCGTCATTTGTGTCCGA**3' R:5'AAAC **TCGGACACAAATGACGAGCA** C3'	exon1
sgFOXN1#2	F:5'CACCG**CGCCCTTCCACCCGTACAAG**3' R:5'AAAC **CTTGTACGGGTGGAAGGGCG** C3'	exon1
sgFOXN1#3	F:5'CACCG**ACACTATCAGTACCAGCGAA**3 R: 5'AAAC **TTCGCTGGTACTGATAGTGT** C3'	exon2
sgCBP#1	F: 5'CACCG**AGCGGCTCTAGTATCAACCC**3' R: 5'AAAC**GGGTTGATACTAGAGCCGCT**C3'	exon2
sgCBP#2	F:5'CACCG**GAATCACATGACGCATTGTC**3' R: 5'AAAC**GACAATGCGTCATGTGATTC**C3'	exon 4
sgCBP#3	F:5'CACCG**CCCGCAAATGACTGGTCACG**3' R: 5'AAAC**CGTGACCAGTCATTTGCGGG**C3'	exon 2
sgYBX1#1	F:5'CACCG**GGACCATACCTGCGGAATCG**3' R:5'AAAC**CGATTCCGCAGGTATGGTCC**C3'	exon 2
sgYBX1#2	F:5'CACCG**GTCTTGCAGGAATGACACCA**3' R: 5'AAAC**TGGTGTCATTCCTGCAAGAC**C3'	exon 5
sgYBX1#3	F:5'CACCG**CAGTAAAATGGTTCAATGTA**3' R: 5'AAAC**TACATTGAACCATTTTACTG**C3'	exon 5

Table 4.2 List of guide RNAs used for the CRISPR screen. In bold is the sequence complementary to the sequence of the targeted gene, in regular letters are the BbsI restriction overhangs

4D6 EYFP$^{\beta 5t}$FOXN1^{CMV} cells were seeded in 24 well plates at a density of 0.33 x10^6 cells/well. The CRISPR mediated deletion of selected genes was performed by transfecting 4D6 EYFP$^{\beta 5t}$FOXN1^{CMV} cells with respective guides using Fugene (see chapter 3.2.4). Three technical replicates were prepared per sample. Cells transfected only with the EYFP$^{\beta 5t}$FOXN1^{CMV} vector, only with Fugene, or the sgCCR5 (a guide that targets a gene irrelevant for FOXN1 function) served as negative controls. Forty-eight hours post-transfection cells were collected in FACS buffer (1x PBS, 5% FCS), stained with DAPI for live/dead cell discrimination and acquired by FACS. Live cells, DAPI negative, were gated for mRuby2 positivity (detected by 561/564nm) to select successfully transduced cells (see Figure 4.2 for gating strategy). Finally, EYFP positivity within the Mruby2 positive cells.

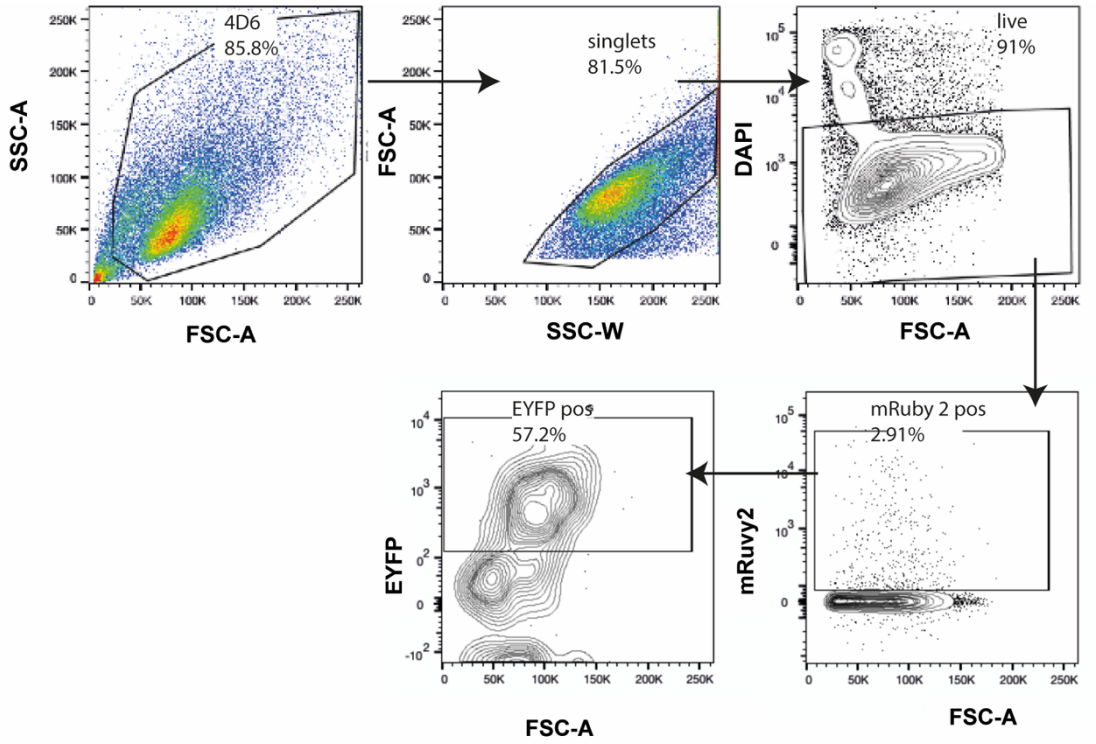


Figure 4.2 FACS gating strategy for the analysis of EYFP positive 4D6 EYFP$^{\beta 5t}$FOXN1^{CMV} cells, after transfection with the Cas9-2A-mRuby2 vector. Representative FACS-plots are shown. Cells were distinguished by their size (using the Forward SCatter (FSC)/Side SCatter (SSC) parameters). Doublets were discriminated by gating according to SSC-W/FSC-A and additional gating was performed to discriminate dead cells (DAPI positive). Positively transfected cells were selected based on mRuby2 expression. Numbers show percentages of cells within each gate.

4.3 RESULTS

4.3.1 Wild-type FOXN1 forms multimers in vivo

Transcription factors (TFs) can regulate the transcription of target genes as monomers, homodimers, heterodimers or oligomers [194]. To test whether under physiological conditions wild type (WT) FOXN1 exerts its regulatory function as either a homo-dimer or a homo-multimer we followed a standard co-immunoprecipitation (co-IP) approach. To that end, 4D6 cells were co-transfected to concomitantly express two forms of *WT FOXN1, one* tagged with a myc and one with a FLAG sequence. After transfection, cells were lysed and FOXN1 was immunoprecipitated using an anti-FLAG or an anti-myc antibody, gel electrophoresed, blotted and then developed with the converse antibody. In WT-FLAG pull downs, WT-myc could be detected in the IP lane (Figure 4.3a), while in WT-myc pull downs, WT-FLAG could be detected in the IP lane (Figure 4.3b) indicating their physical interaction. These experiments suggest that FOXN1 forms homo-dimers or multimers in thymic epithelial 4D6 cells.

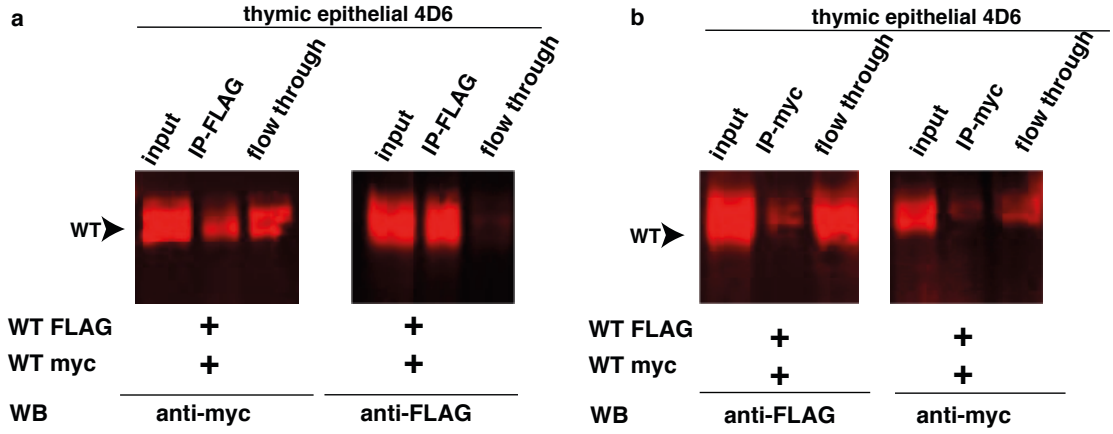


Figure 4.3: WT FOXN1 forms homo-dimers or multimers. a) WB analysis of FLAG immunoprecipitation in cell lysates from 4D6 cells co-transfected with WT-FLAG and WT-myc. b) WB analysis of myc immunoprecipitation in cell lysates from 4D6 cells co-transfected with WT-FLAG and WT-myc. The data shown are representative of three independent experiments

4.3.2 Live behaviour of GFP tagged wild type FOXN1

We next visualised WT FOXN1 in live cells using live cell imagining. To that end, 4D6 cells were transfected with WT-GFP and analysed by confocal microscopy. WT-GFP could be detected in the nucleus of 4D6 cells where it formed larger complexes revealed as bright spots (Figure 4.4) that resemble nuclear bodies [195-198]. Nuclear bodies are membrane-less organelles, defined as highly dynamic macromolecular assemblies specialised in gene regulation and genome maintenance[197]. It has been proposed that their formation is driven by the liquid-liquid phase separation of proteins containing intrinsically disordered protein domains[199]. The role of these structures is to concentrate reactive molecules and facilitate their interactions[195-198].

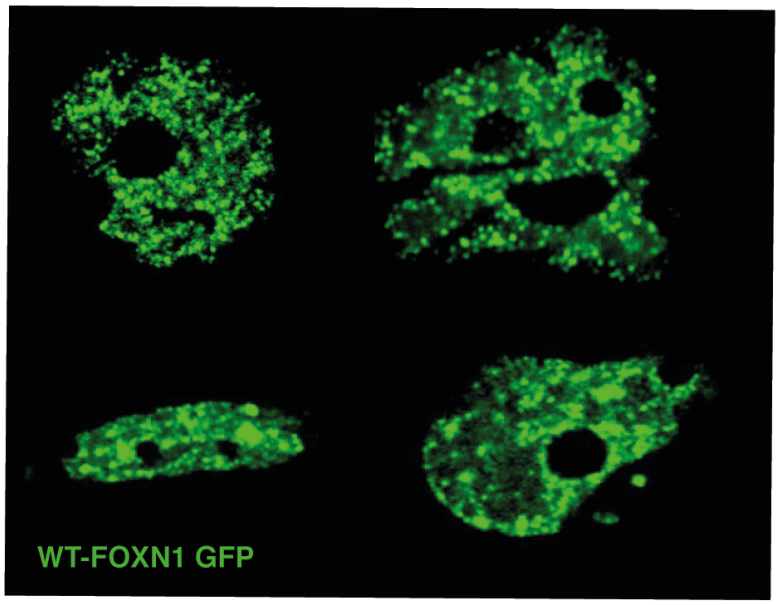


Figure 4.4: WT-GFP forms higher ordered structures seen as bright spots in the nucleus of 4D6 TEC cells. Snapshots of live cell confocal microscopy of 4D6 cells transfected with WT-GFP. The images are representative of three independent experiments with a total of 31 cells captured.

The lack of a lipid rich barrier surrounding the nuclear bodies allows their components to rapidly cycle between the organelle and the nucleoplasm[200]. To study the

dynamic exchange of WT-GFP molecules within individual nuclear bodies we used therefore Fluorescence Recovery After Photobleaching (FRAP). FRAP uses a focused laser beam to irreversibly photo-bleach fluorescent molecules in a well-defined area of choice and measures the recovery of the fluorescent signal over time, representing the diffusion of surrounding fluorescent molecules that had not been bleached into the bleached area[188]. These experiments demonstrated that the photobleaching of GFP bright spots was followed by a full recovery of the fluorescence signal over a relatively short period of time, indicating a dynamic turnover of WT-GFP molecules within and outside the spots (Figure 4.5), a characteristic property of nuclear bodies[200].

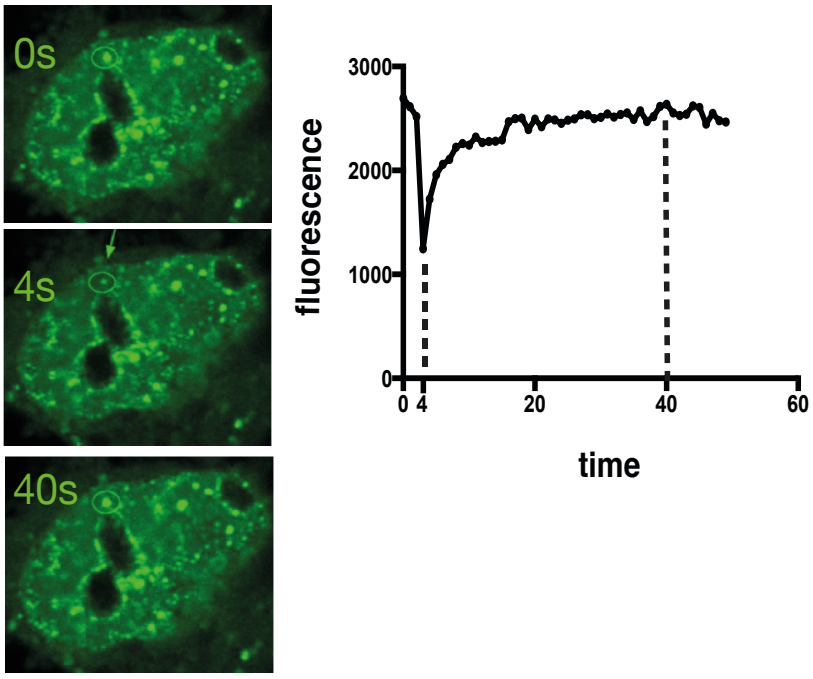


Figure 4.5: Dynamic turnover of WT -FOXN1 in nuclear bodies. Left: FRAP analysis of GFP labelled WT-FOXN1 in 4D6 cells at indicated times after photobleaching of an area indicated by the circle. The arrow shows the snapshot at which the photobleaching occured. Right: Fluorescence recovery curve of GFP labelled WT-FOXN1 as a function of time. Snapshots of cell nuclei at 0, 4 and 40 sec time points. Fluorescence recovery measured in the designated areas was used to calculate the recovery curve. The images are representative of three independent experiments.

4.3.3 Wild-type FOXN1 requires the specific environment of thymic epithelial to form multimers.

Next, we tested whether the formation of FOXN1 homo-multimers is a TEC specific property and therefore investigated whether WT FOXN1 could form homo- multimers in non-TEC cell lines. To this end, HEK293 and HELA cells were co-transfected to concomitantly express WT FOXN1 molecules that were tagged either with a myc or a FLAG sequence. Cells were lysed and FOXN1 was immunoprecipitated using an anti-FLAG. Input, IP and flow through were gel electrophoresed, blotted and FOXN1 was then revealed using the converse antibody. In HEK293 or HELA cells, WT-myc could be detected in the input and flow through lane of the FLAG-IP experiments but could not be detected in the FLAG IP lane (Figure 4.6 a and b). However, probing the same membrane for the presence of WT-FOXN1-FLAG demonstrated the efficiency of the IP in both cell lines. In conclusion, WT-FLAG could not pull down WT-myc in HEK293 and HELA cells, therefore they do not interact in those cell types. These experiments suggest that FOXN1 does not form multimeric complexes in the non-TEC cell lines HEK293 and HELA.

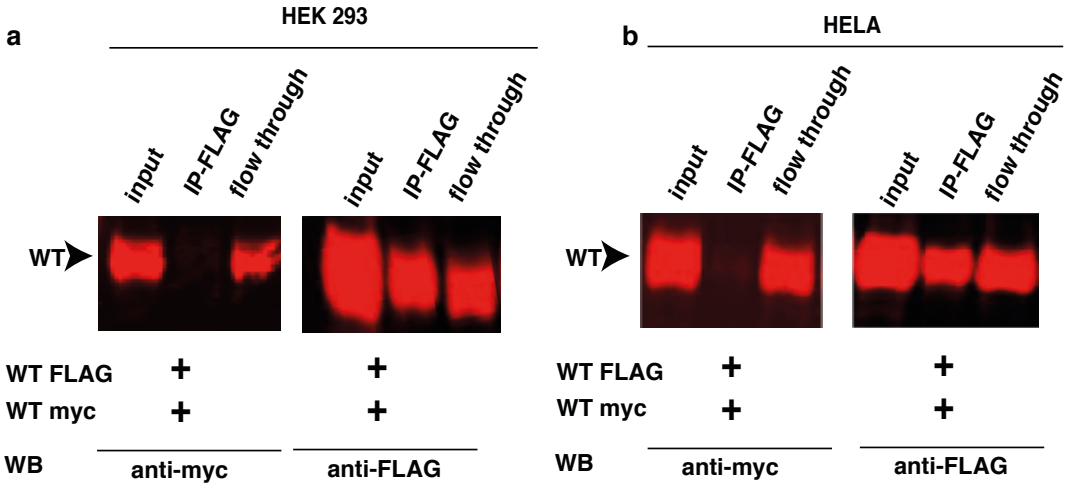


Figure 4.6: WT FOXN1 does not form homo-multimers in non-TEC cell lines HEK293 and HELA. WB analysis of flag immunoprecipitation in cell lysates from a) HEK293 or b) HELA cells co-transfected with WT-FLAG and WT-myc. myc FOXN1 can be detected in the input and flow through lane. FLAG FOXN1 can be detected in the input and IP lane showing that it has been successfully pull down during the FLAG IP. The data shown are representative of two independent experiments

4.3.4 Wild-type FOXN1 does not form multimers in the presence of the *Δ550* mutant

Dominant negative mutants can interfere with the function of the WT proteins that physiologically form homo-multimers. An example is the effect of a dominant negative Notch mutant that interferes with Notch homo-dimerisation and thus abrogates the receptors downstream activity of controlling the expression of target genes [15]. To assess whether the *Δ550* mutant could disrupt the formation of WT-FOXN1 homo-multimers, 4D6 cells were co-transfected to concomitantly express WT FOXN1 molecules that are tagged either with a Myc or a FLAG sequence and the *Δ550* FOXN1 mutant devoid of a tag. FOXN1 was then immunoprecipitated from the cell lysate using an anti-FLAG, gel electrophoresed, blotted and then developed with the converse antibody. Under these experimental conditions, WT-myc could be detected

in the input and flow through samples but was absent in the IP lane (Figure 4.7 left panle). However, FLAG-tagged FOXN1 could be detected in all three samples (Figure 4.7 right panel). Taken together these experiments suggest that WT-FLAG can no longer interact with WT-myc in the presence of the *Δ550* FOXN1 mutant.

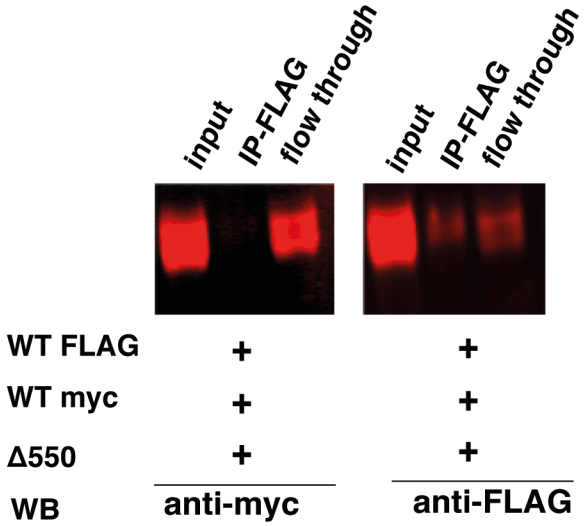


Figure 4.7: WT FOXN1 does not form homo-multimers in the presence of Δ550FOXN1. WB analysis of FLAG immunoprecipitation in cell lysates from 4D6 cells co-transfected with WT-FLAG, WT-myc and Δ550 without a tag. Myc FOXN1 can be detected in input and flow through lane. FLAG FOXN1 can be detected in input and IP lane showing that it has been successfully pull down. The data shown are representative of three independent experiments

To assess how the *Δ550* mutant affects the live behaviour of WT FOXN1 we also performed live cell imaging studies. To that end 4D6 cells transfected with WT-GFP and *Δ550* with no tag were imaged using confocal microscopy. The number of WT-GFP bright spots formed in the nuclei of 4D6 cells were significantly reduced in the presence of the *Δ550* mutant (Figure 4.8 a,b). In conclusion, the *Δ550* mutant disrupts the ability of WT FOXN1 to form homo multimers in 4D6 cells and significantly decreases the formation of WT -GFP nuclear spots in the nucleus of these cells.

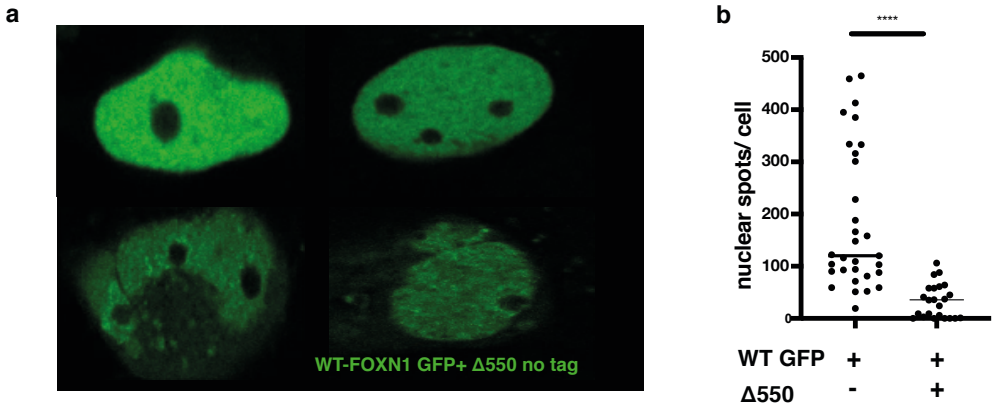


Figure 4.8: Δ550 mutant disrupts the formation of WT-FOXN1 nuclear bodies a) Live cell imaging of 4D6 cells co-transfected with WT-GFP and untagged *Δ550*. Representative images from three independent experiments. b) Quantification of FOXN1-GFP nuclear spots per cell in 4D6 cells transfected with WT-GFP (shown in figure 4.4) and in the presence or absence of *Δ550*. Individual nuclear bodies were counted by the image processing software FiJi. The graph displays the data of three independent experiments with a total of 31 nuclei analysed for 4D6 cells transfected in the absence of *Δ550* FOXN1 and 24 nuclei of 4D6 cells transfected in the presence of *Δ550* FOXN1 Statistical comparison was done using unpaired t-test *p<0.05,**p<0.01, ***p<0.001

4.3.5 Nuclear movement of Wild-type FOXN1 in the presence or absence of the *Δ550* FOXN1

To regulate the transcription of a target gene, a TF will have to diffuse in the nucleoplasm, translocate to its target DNA[201] where gene expression is initiated by recruiting other proteins of the cell's transcriptional machinery. During this movement, a TF will be involved in either transient or more stable interactions with other molecules present in the nucleoplasm that will ultimately determine its function. Within nuclear bodies, the diffusion of TF is slower compared to the rest of the nucleoplasm due to the structure's compact nature and the presence of other active molecules with which a TF engages in biologically meaningful interactions [195, 197] [202]. Therefore, studying a TF's movement in the nucleus can provide important insight into its function.

Fluorescence correlation spectroscopy (FCS) provides an indispensable tool for the measurement of protein diffusion within a cell[203]. This method can measure how a fluorescently labelled protein moves within a particular visual field over a pre-determined period of time. This movement results in a signal trace that is then translated into a correlation curve which provides information about the intensity and the diffusion of the fluorescent signal. The molecules' diffusion coefficient is inversely proportional to the width of the correlation curve and its concentration is inversely proportional to the amplitude (Figure 4.9a)[203]. In other words, FCS measures how fluorescently labelled molecules move within a subcellular compartment.

The diffusion of WT-FOXN1 tagged with GFP was therefore measured within and outside of nuclear bodies in 4D6 cells (Figure 4.9 b). WT FOXN1 was found to diffuse 200 times slower within the nuclear bodies when compared to labelled FOXN1

positioned outside of these structures (Figure 4.9 c). In the presence of Δ550 FOXN1 mutant, WT-FOXN1 largely failed to form nuclear bodies and the velocity of their diffusion rates was high corresponding to the speed observed for tagged FOXN1 molecules outside these structures (Figure 4.9 c).

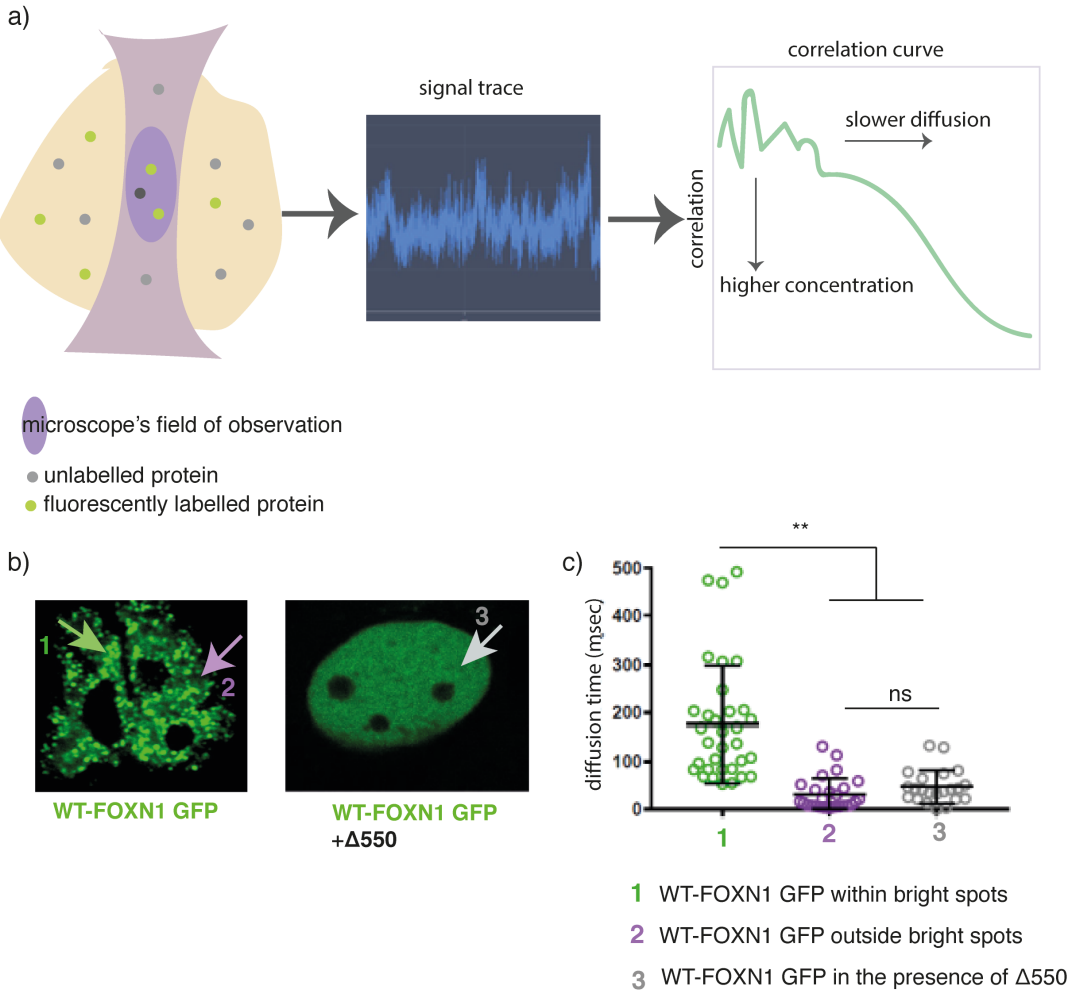


Figure 4.9 Diffusion coefficient of GFP-tagged WT-FOXN1 in the nucleus of 4D6 cells in the presence or absence of the *Δ550* mutant a) Schematic representation of FCS analysis b) nuclei of 4D6 cells transfected to express either WT-GFP alone or together with un-labeled *Δ550* mutant. Numbers indicate positions where FCS measurements were taken. The data shown is representative of three independent experiments c) diffusion time in msec of WT-GFP in the absence (1 and 2) or presence of (3) the *Δ550* mutant. Statistical comparison was done using unpaired t-test ns>0.05, **p<0.01,

4.3.6 Identification of putative FOXN1 partners by co-immunoprecipitation and mass spectrometry proteomics analysis

TFs regulate the transcription of target genes via their interaction with other molecules including other TFs, transcriptional co-activators or repressors, RNA polymerase II, chromatin remodelling proteins and/or small non-coding RNAs. To characterise the protein partners of WT and *Δ550* FOXN1, we performed FLAG pull downs in 4D6 transfected with either WT-FLAG or *Δ550*-FLAG molecules and analysed the precipitates by mass spectrometry. In previous chapters we had established that i) both WT FOXN1 and the *Δ550* FOXN1 mutant correctly localised to the nucleus (see chapter 3.3.3), ii) both molecules can be isolated by a relatively gentle method that preserves protein-protein interactions (see chapter 4.3.1), and iii) WT-FOXN1 is transcriptionally active (see chapters 3.3.4 and 3.3.7) while the *Δ550* mutant displays a dominant negative function (see chapters 3.3.5 and 3.3.7). Taken together these data, validate 4D6 cells to be suitable for elucidating the FOXN1 interactome.

Immunoprecipitation of WT-FOXN1 FLAG molecules and Δ550-FOXN1 FLAG molecules revealed proteins of different molecular weight (Figure 4.10a). The most prominent bands present in each of the silver staining corresponded to WT (85KDa) and mutant *Δ550* FOXN1 (60KDa) (Figure 4.10a). Of note, the band of the *Δ550* mutant was broader and mildly more diffused in the analysis when compared to the detection of the WT band in the corresponding sample. This finding is furthermore remarkable as the WB analysis demonstrated that WT FOXN1 has increased protein levels when compared to the mutant (chapter 3.3.2). Because silver staining detects all proteins present in a sample, if their concentration is sufficient [204], we suspected that the *Δ550* band may contains additional proteins of similar molecular size. The

aforementioned decrease of the *Δ550* mutant protein in transfected 4D6 cells was independently confirmed by mass spectrometry (Figure 4.10b).

Total pull downs from 3 biological replicates of wild type and mutant samples were analysed by LC-MS/MS yielding a large number of putative binding partners of WT or *Δ550* FOXN1. To focus on the most robust candidates and eliminate false positives we excluded from the analysis all proteins that 1) were detected in less than all three IP samples 2) corresponded to known contaminants (e.g albumins, keratins, histones, cytoplasmic proteins and ribosomal proteins) and 3) were proteins (according to Uniprot KB) known to localise to the cytoplasm.

To further define meaningful interactions we filtered our results based on the following assumptions. If the *Δ550* mutation does not interfere with the interaction of the *Δ550* protein with a protein partner, the protein amount of the putative partner will correlate with the amount of FOXN1 (wild type or mutant) across all samples. Therefore, in the WT samples the putative partner will be expected to have higher protein levels compared to the *Δ550* samples similar to the protein levels of FOXN1. All candidate proteins displaying these characteristics were considered for further analysis (Figure 4.10c). Alternatively, the *Δ550* FOXN1 molecule could exert its dominant negative function via an interaction of higher affinity with a protein partner that is typically bound by WT-FOXN1, thus sequestering it away from the WT molecule. In this scenario, the amount of the cofactor detected in the IP will inversely correlate with the amount of FOXN1 protein (Figure 4.10 d). Applying these criteria reduced the number of putative FOXN1 interacting partners to a total of 32 candidates, with 30 candidates positively (Figure 4.10c) and 2 inversely correlated with the concentration of FOXN1 (Figure 4.10d) (Table 4.2).

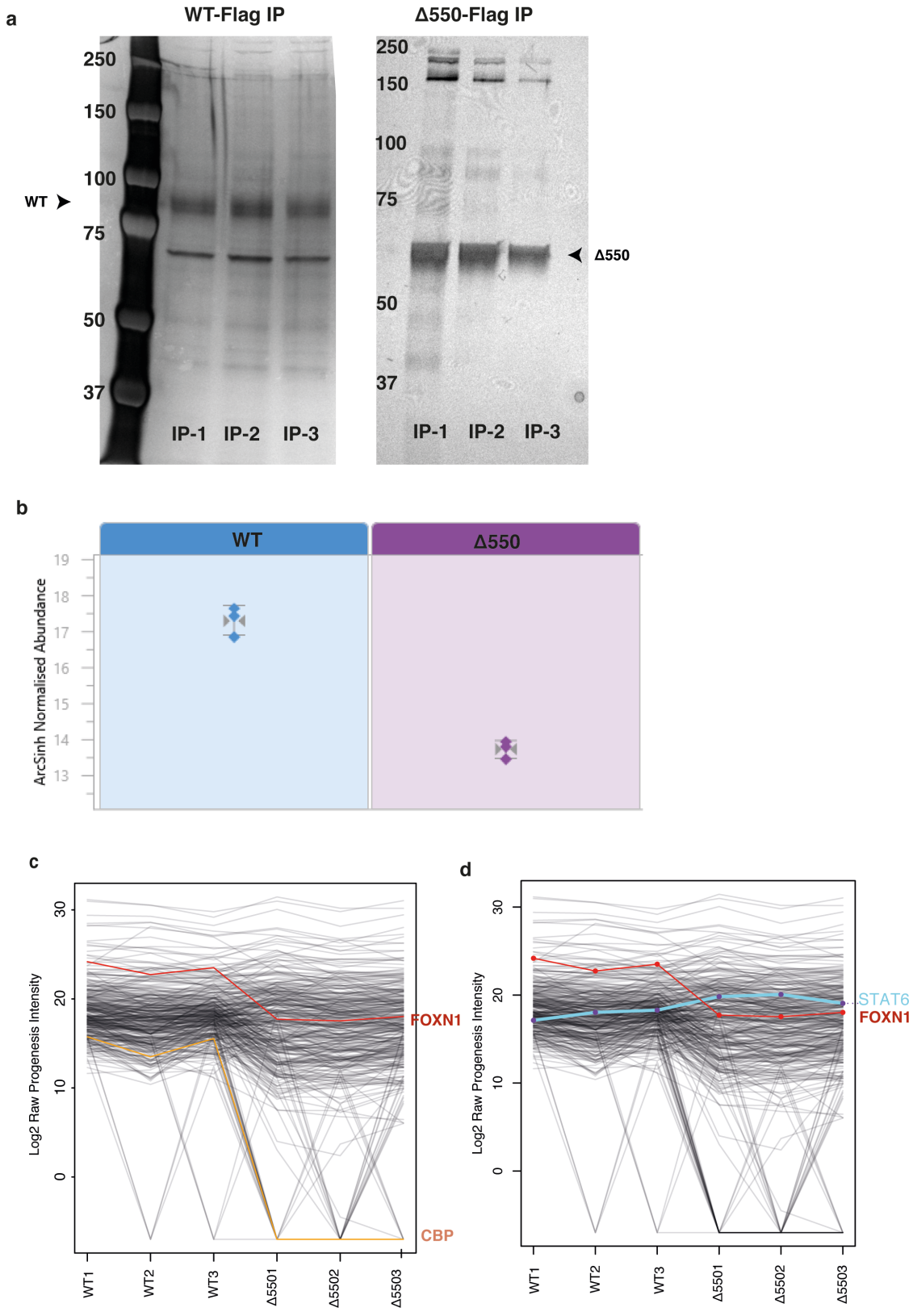


Figure 4.10 Identification of FOXN1 binding partners using MS a) IP of WT FOXN1 and *Δ550* FOXN1 appear to associate with multiple proteins other than FOXN1. Silver staining of FLAG pull downs in lysates from 4D6 cells transfected with either WT or Δ550 tagged with a FLAG b) Normalised abundance view of FOXN1 wild type or Δ550

protein. Each point corresponds to an individual sample. The data represent one independent experiment with three biological replicates per condition. The mean of the values is demarcated by the arrow, the standard deviation is marked by bars. The data were analysed by Progenesis QI software http://www.nonlinear.com/progenesis/qi-for-proteomics/ c) Normalised abundance of proteins found across three IPs of WT-FOXN1 (WT1-3) and three IPs of Δ550 FOXN1 (Δ5501-3). The red line identifies normalised FOXN1 abundance, whereas the orange line shows the normalised abundance of CBP d) Normalised abundance of proteins found across three IPs of WT-FOXN1 (WT1-3) and three IPs of Δ550 FOXN1 (Δ5501-3). The red line identifies normalised FOXN1 abundance, whereas the light blue line shows the normalised abundance of STAT6

The STRING protein-protein interaction database (database of known and predicted protein–protein interactions containing information from experimental data, computational predictions and public text collections https://string-db.org) was queried in order to construct a potential interaction network. With this approach we identified protein-protein interactions that belonged to three major cellular constituents i) mRNA splicing, ii) transcriptional co-activators iii) DNA binding proteins likely to be involved in FOXN1's interaction with DNA (Figure 4.11). None of these partners have been previously associated with FOXN1, which is most likely explained by the fact that thymic and skin epithelial expressing FOXN1 have never been investigated to establish protein-protein interactions

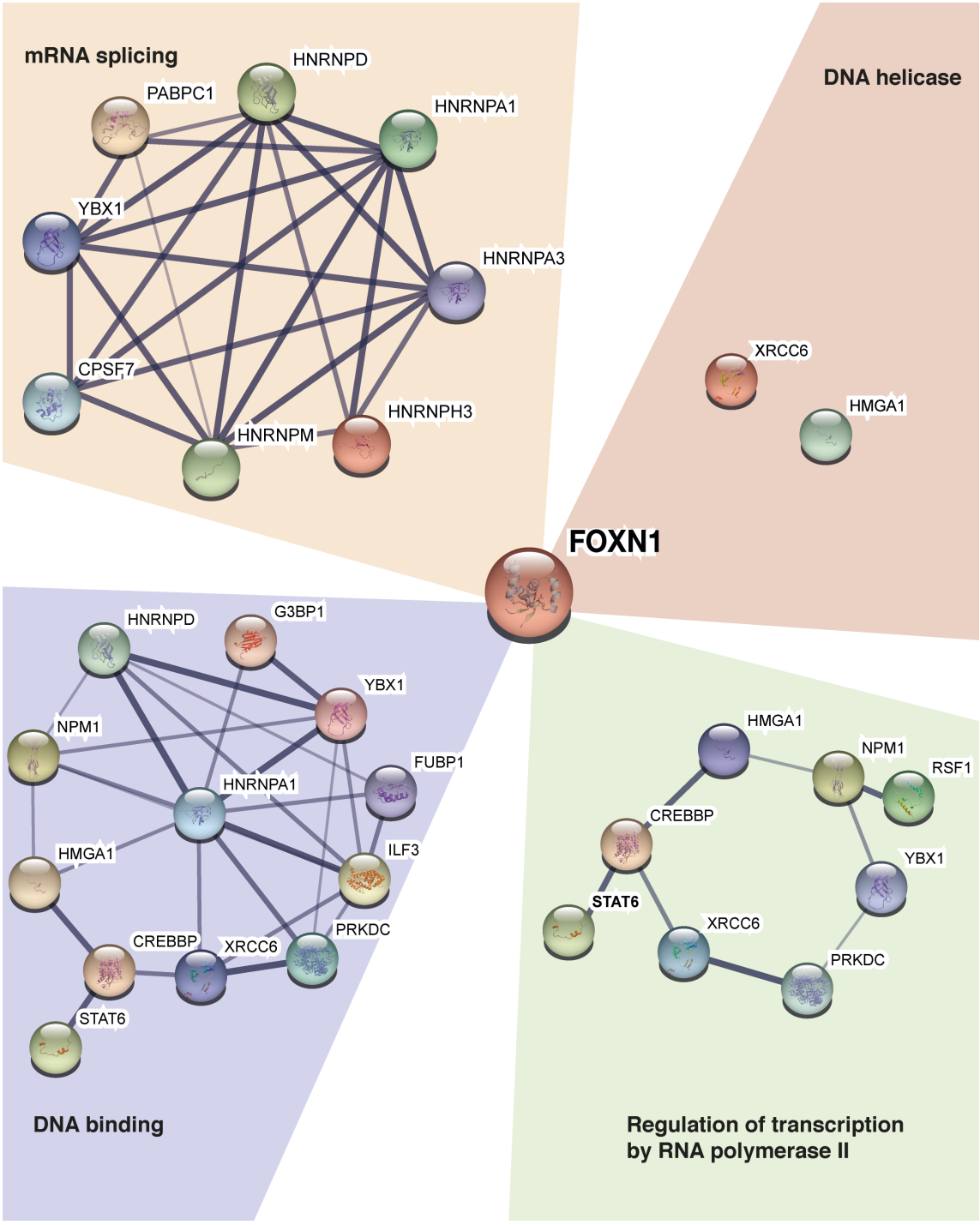


Figure 4.11 Interaction network of FOXN1 associated proteins as identified by IP and MS. The network was constructed using the STRING protein-protein interaction database. Lines represent previously reported interactions. Line thickness reflects the strength of data supporting an interaction.

Accession	Gene Name	Subcellular location [CC]	Gene ontology
P17096	HMGA1	Nucleous	DNA Binding [GO:0003677], negative regulation of transcription [GO:0045892]; positive regulation of transcription [GO:0045944];
P12956	XRCC6	Nucleous	DNA Binding [GO:0003677]; positive regulation of transcription [GO:0045944];
Q92793	CBP	Nucleous	acetyltransferase activity [GO:0016407]; RNA polymerase II transcription factor binding [GO:0001085]; transcription coactivator activity [GO:0003713]; transcription corepressor activity [GO:0003714]; transcription factor binding [GO:0008134]; DNA Binding [GO:0003677]
P06748	NPM	Nucleous	activating transcription factor binding [GO:0033613]; RNA binding [GO:0003723]; transcription coactivator activity [GO:0003713]; positive regulation of transcription by RNA polymerase II [GO:0045944];
Q14103	HNRPD	Nucleous, cytoplasm	mRNA splicing GO:0000398,
Q13283	G3BP1	Nucleous, cytoplasm	DNA Binding [GO:0003677]
P78527	PRKDC	Nucleous	DNA Binding [GO:0003677], positive regulation of transcription [GO:0045944];
Q7KZF4	SND1	Nucleous	RNA binding [GO:0003723]; transcription coregulator activity [GO:0003712]
Q8NC51	PAIRB	Nucleous	RNA binding [GO:0003723]
P68104	EF1A1	Nucleous	translation [GO:0006412];
P67809	YBX1	Nucleous, cytoplasm	mRNA splicing GO:0000398, negative regulation of transcription [GO:0000122]; transcription by RNA polymerase II [GO:0006366]
Q6AHZ1	Z518A	Nucleous	DNA Binding [GO:0003677]
Q12906	ILF3	Nucleous	DNA binding [GO:0003677];
P04908	H2A1B	Nucleous	DNA binding [GO:0003677];
O15353	FOXN1	Nucleous	DNA Binding [GO:0003677]
Q96AE4	FUBP1	Nucleous	positive regulation of gene expression [GO:0010628]; transcription by RNA polymerase II [GO:0006366], DNA Binding [GO:0003677]
P09651	ROA1	Nucleous	mRNA splicing GO:0000398
Q05639	EF1A2	Nucleous	translation [GO:0006412];
Q96T23	RSF1	Nucleous	negative regulation of transcription [GO:0045892]; positive regulation of transcription by RNA polymerase II [GO:0045944]; acetyltransferase activity [GO:0016407];
P43243	MATR3	Nucleous	RNA binding [GO:0003723]
P04792	HSPB1	Nucleous	RNA binding [GO:0003723]
O75150	RNF40	Nucleous	mRNA 3'-UTR binding [GO:0003730];
Q9NZI8	IF2B1	Nucleous	RNA binding [GO:0003723]
P11940	PABP1	Nucleous	mRNA splicing GO:0000398
P52272	HNRPM	Nucleous	mRNA splicing GO:0000398
P51991	ROA3	Nucleous	mRNA splicing GO:0000398
Q8N684	CPSF7	Nucleous	mRNA splicing GO:0000398
P48634	PRC2A	Nucleous	RNA binding [GO:0003723]
P31942	HNRH3	Nucleous	mRNA splicing GO:0000398
Q9H869	YYAP1	Nucleous	regulation of cell cycle [GO:0051726]
Q8IV63	VRK3	Nucleous	ATP binding [GO:0005524]; protein phosphatase binding [GO:0019903]; protein serine/threonine kinase activity [GO:0004674]
P42226	STAT6	Nucleous	DNA-binding transcription activator activity [GO:0001228]; [positive regulation of transcription [GO:0045944];

Table 4.3: List of putative FOXN1 binding partners. Uniprot KB was used to determine the subcellular localisation and the gene ontology (GO) of each protein. In bold are the two proteins that inversely correlate with the amount of FOXN1 detected in these cells (4.10d)

4.3.9 Validation of candidate FOXN1 interacting proteins using the EYFP^{FOXN1} reporter cell line

An interaction between FOXN1 and a given candidate protein identified by co-IP followed by mass spectrometry proteomics analysis does not necessarily imply its functional relevance. To verify that a specific interaction partner of FOXN1 assists its transcriptional function, loss of function studies were designed using CRISPR screen mediated deletions of individual candidate proteins in a suitable reporter cell line.

A human thymic epithelial cell line (designated EYFP$^{\beta5t}$FOXN1^{CMV} 4D6 cells) was next created that expressed a reporter to easily visualise FOXN1 transcriptional activity. To this end 4D6 cells were stably transduced to integrate a transgene composed i) of a CMV promoter driving the constitutive expression of FOXN1 and ii) of a sequence with a minimal β5t promoter controlling the expression of *EYFP* (see chapter 4.2.7). Under these conditions the constitutively expressed WT FOXN1 is expected to bind to the β5t promoter and drive the expression of *EYFP* (Figure 4.12a). When a functionally relevant FOXN1 partner is deleted the functionality of FOXN1 will be impaired and this is expected to result in a decrease in *EYFP* expression.

As a proof of principle EYFP$^{\beta5t}$FOXN1^{CMV} 4D6 reporter cells were transfected with WT or *Δ550* FOXN1 and EYFP expression was assessed by FACS. Transfection with increasing amounts of WT FOXN1 did not have an impact on the percentage of EYFP positive cells (Figure 4.12a). As the constitutive transgenic expression of WT FOXN1 was already saturating the β5t promoter regions upstream of the *EYFP* gene. In contrast, transfection with increasing amounts of *Δ550* FOXN1 mutant lead to a gradual reduction in the percentage of EYFP positive cells (Figure 4.12b). This result is in keeping with the dominant negative function of the mutant. Therefore, we

considered the EYFP$^{\beta5t}$FOXN1^{CMV} 4D6 reporter cells as a valid tool to test FOXN1 mediated transcription in the absence of specific proteins that serve as candidates of FOXN1 interactors.

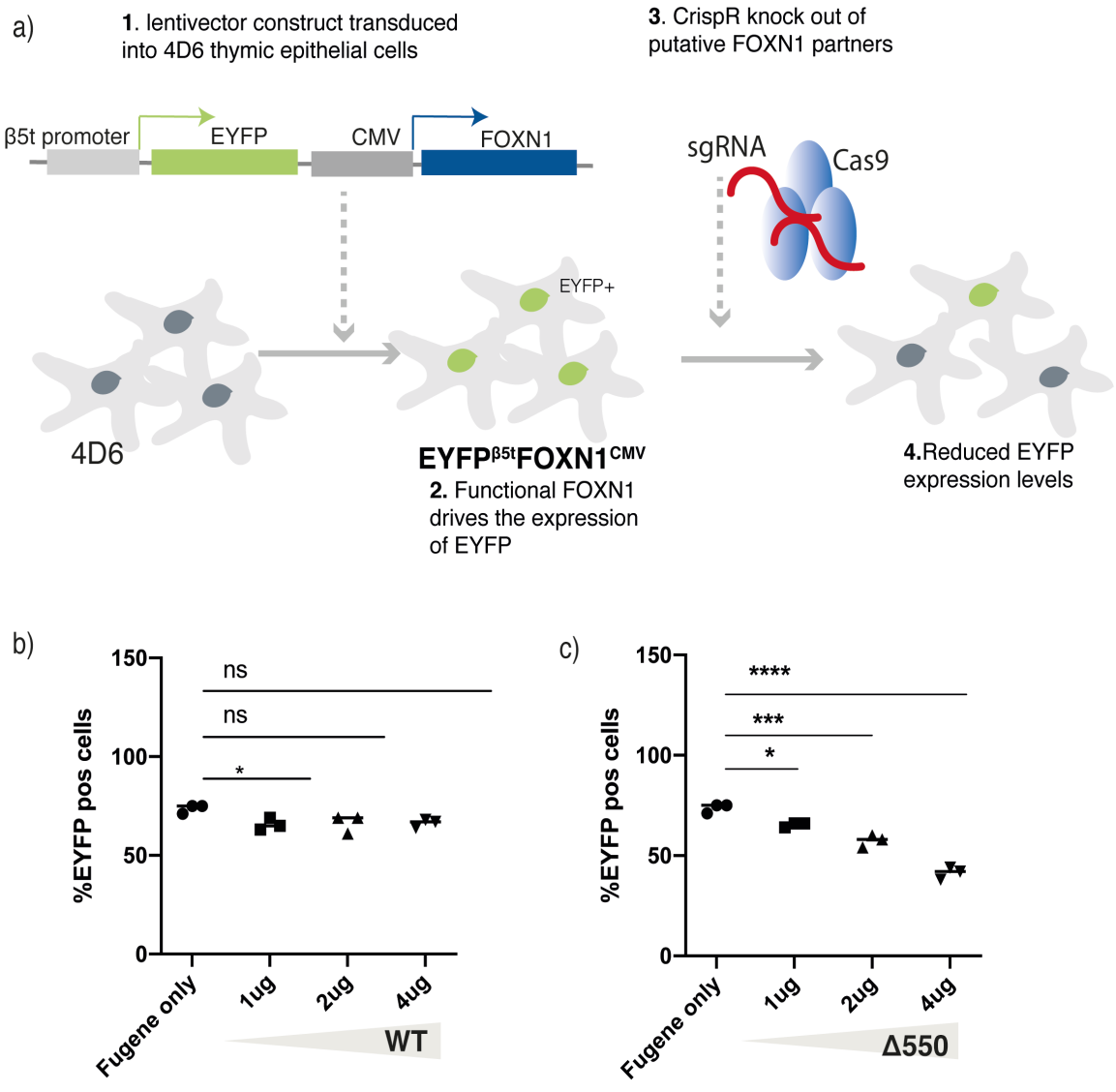


Figure 4.12 Generation of a suitable reporter cell line and validation of candidate FOXN1 interacting partners a) Schematic representation of the generation of the EYFP$^{\beta5t}$FOXN1^{CMV} reporter cell line (see also chapter 4.2.7) b) Transfection of EYFP$^{\beta5t}$FOXN1^{CMV} cells with increasing doses of WT-FOXN1 does not increase the percentage of EYFP positive cells c) Transfection of EYFP$^{\beta5t}$FOXN1^{CMV} cells with increasing doses of *Δ550* decreases the percentage of EYFP positive cells. The data shown is representative of one independent experiment with three technical replicates in each condition. Statistical comparison was done using one way ANOVA p*<0.036, p**=0.0002, p****<0.0001, ns>0.05

The Creb Binding Protein (CBP) was among the putative FOXN1 interacting partners identified by the MS analysis. CBP functions as a transcriptional coactivator for a variety of transcription factors including Jun, Fos[205], STAT proteins[206] and AIRE [207]. In parallel, this molecule also acts as an acetylotransferase of histones and transcription factors and in this way it regulates gene transcription[208]. CBP was the first protein found to interact with AIRE (AutoImmune REgulator), the master transcriptional facilitator of tissue restricted antigen expression in medullary TEC, a phenomenon that controls the negative selection of autoreactive T cells [12]. CBP colocalises with AIRE in nuclear bodies and via direct acetylation of AIRE's lysine residues controls both the size and number of these structures [209][12]. We therefore considered CBP as a promising FOXN1 interaction partner and decided to further probe its function in the EYFP$^{\beta 5t}$FOXN1^{CMV} reporter cell line.

YBX1 was another putative FOXN1 partner identified by the MS analysis. Indeed YBX1 (Y- box binding protein 1) was already predicted to bind to FOXN1 as a result of an in-silico analysis by Dr Alex Aliper and colleagues at Insilico medicine, a bioinformatics company collaborating with the Hollander lab. Of note, YBX1 does not have any known or apparent role in thymus biology. We therefore included this candidate in any further experiments

CrispR was used to delete the genes coding *CBP* and *YBX1* respectively (Figure 4.13). CrispR targeted loss of FOXN1 expression was used as a positive control whereas KO the loss of *CCR5* expression was used as a negative control since this chemokine receptor has no known function in TEC. The EYFP frequency was always calculated relative to cells transfected with the Cas9 vector only. The deletion of CBP resulted in a significant reduction in the frequency of EYFP positive cells, inferring that a loss of

CBP expression impaired FOXN1-mediated activation of EYFP transcription under the control of β5t specific promoter. The fact that the reduction in EYFP expression was comparable to cells in which FOXN1 was targeted shows that the functional consequences of a loss of CBP was significant. The experimental limitations of CRISPR gene targeting in a population of cells that have not been selected for such an event is a likely explanation accounting for the observation that some EYFP-positive cells remained even when FOXN1 was deleted.

The deletion of YBX1 had also an effect on the frequency of EYFP positive cells albeit to a lesser extent when compared to the loss of CBP expression (Figure 4.13). Nonetheless, a reduced frequency of EYFP positive cells was observed attending to a potential role of YBX1 in support of FOXN1 transcriptional control.

In conclusion, our data suggest that CBP is a functionally meaningful partner to FOXN1 as it disrupts, If not completely at least significantly its transcriptional function. Further validation using reciprocal co-IPs and imaging are however required to show FOXN1 and CBP's functional cooperativity and physical localisation, respectively. A similar approach is planned for the validation of other putative FOXN1 cofactors (presented on Table 4.2).

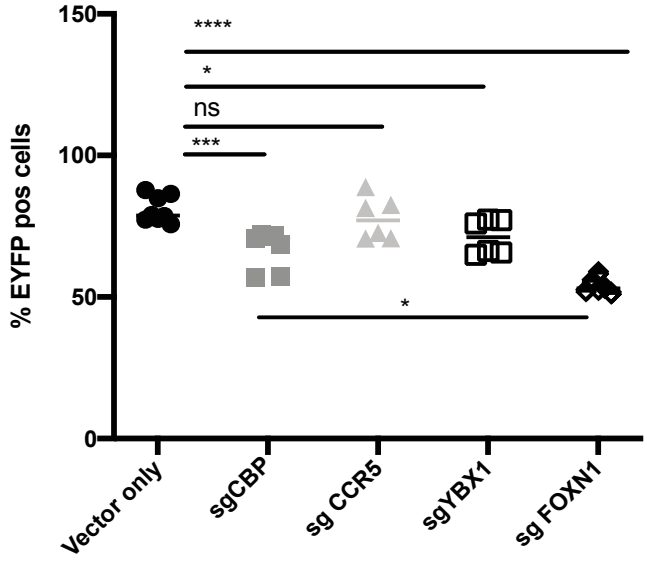


Figure 4.13 Verification of CBP and YBX1 as FOXN1 co-factors. The percentage of EYFP positive cells was compared between EYFP$^{\beta 5t}$FOXN1^{CMV} cells transfected with the indicated Cas9 expression vector used either as a negative control (recombinant for sgCCR5), as a positive control (recombinant for sgFOXN1) or as the experimental probe (recombinant for sgCBP or sg YBX1). Three independent experiments for vector only and sgCBP samples, 2 for sgCCR5, sgYBX1 and sgFOXN1 samples. Statistical analysis was performed using unpaired t-tests p*<0.036, p**=0.0002, p****<0.0001, ns>0.05

4.4 DISCUSSION

Transcription factors can form dimers or oligomers and in this way modulate DNA-binding specificity and affinity, the recruitment of different binding partners and eventually the transcription of target genes[194]. Indeed. there are multiple examples of forkhead family members that can form multimers[82], homodimers[83, 210], or heterodimers[82, 210]. Here we show, to our knowledge for the first time, that WT-FOXN1 can form homo-multimers in thymic epithelial cells but fails to do so in other epithelial cell types. The presence of the *Δ550* mutant disrupts the formation of WT homo-multimers, further attending to the mutant's dominant negative potential. It remains to be shown whether *Δ550* FOXN1 molecules can form homo-multimers on their own or even whether they can interact with the WT form.

Although *Δ550* FOXN1 disrupts the formation of WT-FOXN1 multimers, its presence does not completely abrogate WT's transcriptional activity as discussed in chapter 3. The combination of these two data sets forms the empirical basis for the hypothesis that WT-FOXN1 is able to regulate the transcription of its target genes both as a monomer and as a multimer. In fact, it has been shown for other TF that the formation of homodimeric, heterodimeric, or multimeric complexes can influence their DNA binding specificity [211]. For example, T box transcription factors can bind to DNA both as monomers or homodimers and, in each case, they display distinct binding specificities[212]. If this would be true for FOXN1, these macromolecular features could explain the factors possible dual nature as a trans-activator and a repressor, each individual function orchestrating distinct transcriptional programs at possibly different stages of development or in distinct TEC subpopulations. However, whether

FOXN1 exerts a dual function consequent to the function of higher ordered structure demands further testing. It also remains to be shown whether the formation of FOXN1 homo multimers is required for DNA binding or whether this structure is a consequence of DNA binding. This is not examined as part of this thesis. Chapter 5 examines in more detail the DNA binding properties of WT and *Δ550* FOXN1.

In the nucleus of thymic epithelial 4D6 cells WT-FOXN1 forms higher ordered structures that resemble nuclear bodies. Nuclear bodies are self-organised membraneless organelles that participate in nuclear organisation and promote the organised regulation of transcription[195, 197]. They function by concentrating a variety of reactive molecules and therefore facilitate their efficient interaction within a discrete microenvironment[195, 197]. Here we demonstrate that the newly identified WT-GFP nuclear bodies exhibit key properties of membrane-less organelles [195, 197]. WT-GFP molecules are dynamically recruited to these organelles and reconstitute them after photobleaching. Importantly, the diffusion within the nuclear bodies is significantly slower when compared to areas in the rest of the nucleoplasm underscoring biologically meaningful interactions among FOXN1 and other yet to be determined molecules.

Nuclear bodies participate in specific biological processes including RNA biosynthesis, DNA replication, and DNA repair[195, 197, 213]. One prominent type of nuclear bodies contains factors involved in pre-mRNA splicing, pre-rRNA processing and the biogenesis of RNA processing complexes [197, 213].The mass spectrometry analysis of WT-FOXN1 pull downs identified several putative interacting partners, some of which are involved in RNA processing as splicing factors and proteins involved in transcriptional activation. The supposed physical interactions between FOXN1 and

these molecules awaits further verification by reciprocal co-IPs and their colocalization to FOXN1 within nuclear bodies also needs to be shown. Finally, the function of individual candidates will need to be tested for example in the EYFP$^{\beta 5t}$FOXN1^{CMV} 4D6 reporter cell line that will allow to interrogate their cooperative function in FOXN1 controlled transcription.

One of the putative FOXN1 partners identified by the proteomics study was CBP. CBP is an acetylotransferase able to modify directly the function of multiple transcription factors via its catalytic function or indirectly by acetylating histones which will change the balance between repressive and permissive chromatin[208, 214]. CBP was the first protein found to interact with AIRE [207]. CBP mediated acetylation of AIRE's lysine residues has been proposed to inhibit AIRE's function[209, 215], while CBP mediated histone acetylation at AIRE-dependent loci has been suggested to promote gene expression. We were able to show that FOXN1 and CBP engage in a functional interaction, as the CRISPR deletion of CBP in EYFP$^{\beta 5t}$FOXN1^{CMV} 4D6 reporter cells significantly reduced FOXN1's transcriptional competence. However, the exact mechanism of this interaction remains to be elucidated.

Acetylation of lysines in intrinsically disordered regions (IDRs) found in proteins, apparently regulates the formation of membraneless organelles such as nuclear bodies [216]. FOXN1's C-terminus transcriptional activation domain contains IDRs[87] a characteristic of many transcriptional activation domains[217]. An attractive scenario could therefore be that CBP acetylates IDRS in the C-terminus of FOXN1 and in this way it controls the formation of nuclear bodies that in turn facilitate the function of FOXN1 as a master transcriptional regulator. This mechanistic model will need however to be tested.

In conclusion, this study provides a first description of the FOXN1 interactome. The likely physical association of FOXN1 with common transcriptional regulators, such as CBP, provides yet another example of how cells use common transcriptional complexes to mediate specific genetic responses to diverse cellular signals

CHAPTER 5

THE IMPACT OF THE *Δ550* MUTATION ON DNA BINDING

5.1 Introduction and Aims 140

5.2 Materials and Methods 141

5.2.1 Electrophoretic Mobility Shift Assay (EMSA) to assess the DNA binding affinity of purified wild type and mutant proteins. 141

5.2.2 Chromatin Immunoprecipitation (ChIP) followed by DNA-Sequencing 142

5.3 Results 145

5.3.1 Both the wild-type and the Δ550 FOXN1 mutant bind DNA with comparable affinity 145

5.3.2 Qualitative differences in the DNA binding of WT and Δ550 FOXN1 in 4D6 cells. 148

5.4 Discussion 153

5.1 INTRODUCTION and AIMS

All members of the forkhead family of transcription factors contain an evolutionary conserved DNA binding domain, known as the forkhead domain (FKH) [77]. In the FOXN1 protein, this sequence is centrally located between amino acids (aa) 270 and 367[218]. The FKH is flanked by the N-terminus which is involved in TEC differentiation and the C-terminus which contains the transcriptional activation domain (as discussed in detail previously in Chapter 3) [53-55].

The *Δ550* FOXN1 mutant has an intact DNA binding domain. It is therefore predicted to retain its ability to bind DNA. We hypothesised that in a heterozygous state the co-expression of WT and *Δ550* FOXN1 results in the mutant to occupy DNA spaces normally occupied by the WT protein and thus preventing their normal transcriptional regulation. The validity of this hypothesis was tested by two individual approaches; a) Electrophoretic Mobility Shift Assay (EMSA) and b) chromatin immunoprecipitation followed by DNA sequencing **(**ChIP-Seq). By employing EMSA we compared the binding affinity of purified WT and mutant proteins for an oligonucleotide containing a FOXN1 DNA binding motif previously characterised in mouse TECs studies [104]. Using ChIP-Seq we explored qualitative differences in the DNA binding properties between WT and mutant FOXN1 proteins in 4D6 TEC cells and further associated these differences to differential gene expression studies established with the same cells used for RNA-seq studies (discussed in chapter 3).

5.2 Materials and Methods

5.2.1 Electrophoretic Mobility Shift Assay (EMSA) to assess DNA binding affinity

Purification of wild-type and *Δ550* FOXN1 constructs.

WT and *Δ550* FOXN1 constructs were cloned into the pNIC28-Bsa4 vector for histidine (His) tagged overexpression in *E.coli*. For protein purification frozen cell pellets were thawed and resuspended in lysis buffer (50 mM HEPES pH 7.5, 500 mM NaCl, 5% glycerol, 10 mM imidazole, 0.5 mM Tris (2-carboxyethyl) phosphene (TCEP). Sonication was used to assist lysis and cell debris was removed by centrifugation. A Ni-IDA IMAC gravity flow column was used to purify the His-tagged proteins from the whole cell lysate. The purification tag was cleaved with the addition of 1:20 mass ratio of His-tagged TEV protease by overnight incubation in buffer containing 20 mM HEPES, pH 7.5, 500 mM NaCl, 5 % glycerol, 0.5 mM TCEP. To remove the TEC protease an IMAC column was used and a final protein purification was performed by size exclusion chromatography using a HiLoad 16/60 Superdex 200 column at 1 ml/min. Protein concentrations were determined by NanoDrop measurement at 280nm using the calculated molecular mass and extinction coefficients.

Electrophoretic Mobility shift assay

The DNA probe used in the assay was found within the promoter of the proteasome subunit alpha 7 (PSMA7), a high-confidence FOXN1 target [104]. The sequence was as follows: 5'GCAGCA**GACGC**AACAGAGCGA**GACGC**CAGGG3' (with FOXN1 consensus sites in bold). To prepare radiolabeled double-stranded DNA probes, forward strand oligonucleotides were incubated for 2 h at 37 °C with T4 polynucleotide kinase in the presence of [γ-^{32}P] ATP. Non-radiolabeled complementary oligonucleotides were

added in a 2-fold excess, the mixture was heated to 95 °C and subsequently cooled slowly at room temperature. A Bio-Rad P6 micro-biospin column was used to purify double-stranded DNA probes in 10 mM Tris pH 7.5, 50 mM NaCl. In EMSA experiments the radiolabeled DNA probe was used at a constant concentration (0.1 nM and increasing amounts of the different FOXN1 constructs were titrated (2-fold serial dilution; concentration range of 10 nM to 1400 nM) into the DNA binding reaction. The final reaction volume was 7 µl (5µl protein stock, + 2µl DNA probe) in buffer containing 50 mM Tris- HCl, pH 7.5, 25 mM NaCl, 50 mM L-arginine-HCl, pH 7.5, 0.5 mM EDTA, 0.1% Tween 20, 2 mM DTT, and 5% glycerol. Reactions were incubated for 30 min at RT before being loaded on to a 12% native polyacrylamide gel electrophoresis in Tris borate EDTA buffer. Gels were run on ice at 170 V for 70 min, visualized using phosphorimaging, and quantified by quantity one 1-D analysis software (Bio-Rad). A sigmoidal four-parameter logistic nonlinear regression model in PRISM (GraphPad) was used to calculate the Apparent dissociation constants. The above analysis was performed in collaboration with Joseph Newman (Structural Genomics Consortium, University of Oxford, ORCRB, Roosevelt Drive, Oxford, United Kingdom).

5.2.2 Chromatin Immunoprecipitation (ChIP) followed by DNA-Sequencing

Optimal conditions for chromatin shearing and fixation for 4D6 cells were determined using the Chromatin Shearing Optimization kit Low SDS (iDeal Kit for TFs) (Diagenode Cat. No. C01020013). To achieve chromatin fragments of 100-600bp, optimal fixation time for 2.5 x10^6cells was determined to 20 min followed by DNA shearing with 8 sonication cycles 30'' ON/30'' OFF at a Bioruptor Pico sonication device (Diagenode).

4D6 cells were transfected with either WT or *Δ550* mutant FOXN1 construct tagged with a FLAG and three biological replicates of each transfected cell population were collected for ChIP-Seq analyses. The chromatin immunoprecipitation was performed using the iDeal ChIP-seq kit for Transcription Factors (Cat. No. C01010054) as per manufacturer's recommendations. Briefly, 48 hours post transfection 2.5 x10^6cells were collected and subjected to protein-DNA crosslinking for 20 min. Cells were then lysed and chromatin was sheared for 8 sonication cycles (30'' ON/30'' OFF). Sheared chromatin was immunoprecipitated using M2 anti-FLAG antibody (F1804 Sigma) while parallel input samples from non-immunoprecipitated chromatin were prepared for each sample. DNA libraries for all 12 samples were prepared using the MicroPlex Library Preparation Kit (12 indexes;cat number C05010012) following the manufacturer's recommendations. Libraries were pooled and were sequenced at the Wellcome Trust Centre for Human Genetics, University of Oxford using 75 bp paired-end sequencing on the Illumina HiSeq4000 platform.

Data analysis was performed by Dr Adam Handel (Department of Paediatrics and Nuffield Department of Clinical Neurosciences, University of Oxford). Briefly, contaminating adaptor sequences were removed from fastq sequences using Trimmomatic (version 0.32). Reads were aligned against the human genome (GRCh38.EBVB95-8wt.ERCC) using STAR (version 2.5.3a). Peaks were called on deduplicated aligned sequences (paired ChIP and input samples) using MACS2 (version 2.0.10) with a relaxed P value setting of 0.1. Peaks from replicates were then pooled and analyzed using irreproducible discovery rate analysis (IDR < 0.05) (https://sites.google.com/site/anshulkundaje/projects/idr). Peaks were filtered against the ENCODE blacklist regions

(https://sites.google.com/site/anshulkundaje/projects/blacklists). *De novo* motif identification was performed using MEME-ChIP [219]

5.3 RESULTS

5.3.1 Both the wild-type and the *Δ550* FOXN1 mutant bind DNA with comparable affinity

The affinity of the interaction between a purified protein and a radiolabeled DNA probe can be measured by EMSA. The technique is based on the observation that protein-DNA complexes migrate slower on a gel compared to free DNA[220]. The affinity of the interaction can be calculated by incubating increasing concentrations of the protein of interest with a standard amount of the radiolabeled DNA and determining the concentration at which the protein-DNA complex begins to migrate slower compared to free-DNA probe.

EMSA was used to assess the binding affinity of different FOXN1 constructs to a DNA probe containing in a tandem arrangement two copies of the canonical *GACGC* FOXN1 binding motif. The sequence of the DNA probe is part of the promoter sequence of the proteasome subunit *PSMA7* gene (a high confidence FOXN1 target)[104]. We observed that the FKH on its own did not bind to DNA over a large range of protein concentrations tested (10 nM to 1400 nM) (Figure 5.1a+g). A meaningful protein-DNA interaction was also not detected when the normal N-terminus part was added 5' to the FKH (Figure 5.1 b+g). In contrast, the 3' addition of only the C-terminus to the FKH (Figure 5.1 c+g) stimulated binding to DNA with affinities similar to those of the full length FOXN1 (Figure 5.1 e+g). Truncation of the C-terminus at aa 457 (*Δ457*) decreased DNA binding affinity but did not completely disrupt it (Figure 5.1 d+g). We therefore conclude that the C-terminus is essential for the factor's DNA binding. The binding affinity of the *Δ550* FOXN1 mutant protein was similar to that of the WT, that

is both constructs bound to the DNA probe at a concentration of 90 nM (Figure 5.1 f+ g). This finding suggests that the *Δ550* FOXN1 mutant despite its shortened C-terminus and the presence of an aberrant sequence, can be expected to bind DNA with a comparable affinity. The current study is part of a manuscript that is under revision for publication [87].

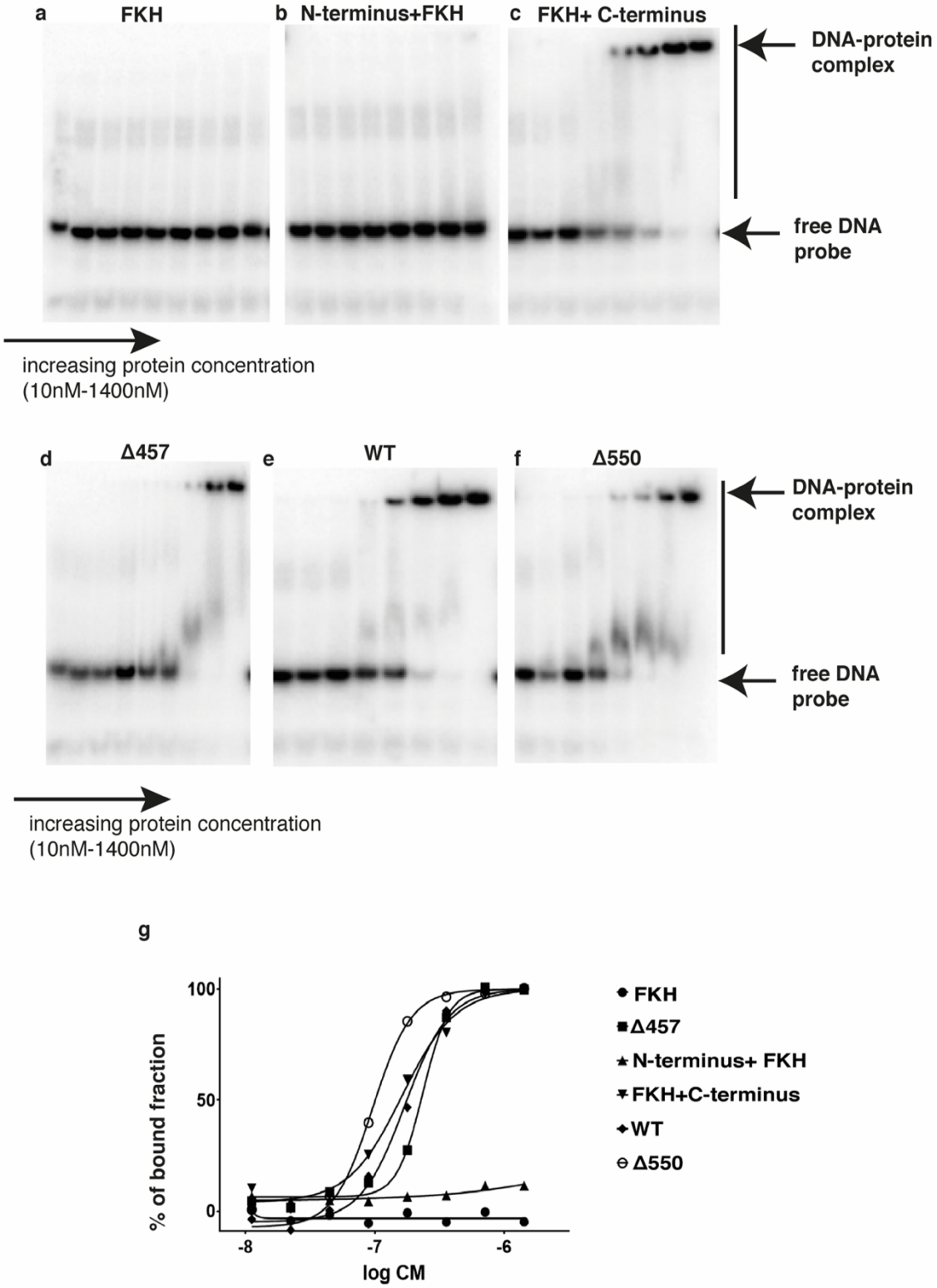


Figure 5.1 EMSA analysis to assess the DNA binding ability of different FOXN1 constructs. Representative EMSA showing increasing amounts of purified a) FKH aa 270-373 b) N-terminus plus FKH aa 1-373 c) FHK plus C-terminus aa 270-614 d) *Δ457* mutant aa 1-457 e) WT FOXN1 protein aa 1-614 f) *Δ550* mutant incubated with a radiolabelled DNA oligo containing a tandem FOXN1 binding motif g) Quantification of the bound fraction fitted to a standard binding isotherm for all FOXN1 mutant constructs. The graph is representative of three experimental replicates for WT and Δ550 constructs and one technical replicate for FKH, N-terminus plus FKH, FHK plus C-terminus, *Δ457 constructs.*

5.3.2 Qualitative differences in the DNA binding of WT and *Δ550* FOXN1 in 4D6 cells.

Identification of FOXN1 binding sites and motifs

Chromatin immunoprecipitation followed by sequencing (ChIP-seq) analysis allows the mapping of transcription factor's binding sites across an entire genome[221]. To directly identify differences in DNA binding sites between WT and *Δ550* mutant FOXN1, we performed a ChIP-seq analysis. To this end, 4D6 cells were transfected with vectors encoding either WT -FLAG or *Δ550*-FLAG FOXN1 molecules. Tagged FOXN1 protein was pulled down with an anti-FLAG monoclonal antibody, the associated chromatin was eluted from the protein DNA- complex and subsequently sequenced. The analyses of the WT and *Δ550* mutant FOXN1 samples revealed 10,273 and 16,426 ChIP-Seq peaks respectively, at an irreproducible discovery rate (IDR) of <0.05. There was a significant enrichment in overlap of the WT and *Δ550* FOXN1 peaks (122.1-fold, $p < 0.0001$) (Figure 5.2a). We found that 72.5% of the WT FOXN1 peaks were within 5 kb distance from the transcriptional start sites (TSSs), while for the *Δ550* mutant 52.6% of the peaks were located within the same distance (Figure 5.2b). These observations indicated that both WT and *Δ550 FOXN1* bind primarily to gene proximal regulatory regions.

Next, we applied motif analysis (MEME-ChIP)[219] to identify the DNA binding motif in the FOXN1 ChIP-seq peaks. The analysis was focused on sequences surrounding the summit (near the centre) of the ChIP-seq peaks. Using a non-supervised method, the consensus FOXN1-binding motif comprising of five nucleotides (*GACGC*) was identified as the top ranked candidate sequence on all WT FOXN1 ChIP-seq peaks (Figure 5.2c). In contrast this sequence ranked only as the second most frequent motif bound when analysing the *Δ550* mutant. Suggesting that this

mutant binds to DNA in a more promiscuous way. The *GACGC* motif was strongly enriched (2.24-fold) around the summit of both WT and *Δ550* FOXN1 ChIP-seq peaks when compared to surrounding sequences. It is of note that the identified FOXN1 core binding sequence is identical to the previously described FOXN1 binding motif in the mouse[104, 218] thus further validating our ChIP-seq analysis with human TEC 4D6 cells. In addition, this analysis demonstrates for the first time that human FOXN1 protein recognises the same consensus DNA binding sequence as the mouse FOXN1. Taken together, we have successfully identified the FOXN1 core DNA binding region near TSSs and characterised the core binding motif for both WT and *Δ550* FOXN1.

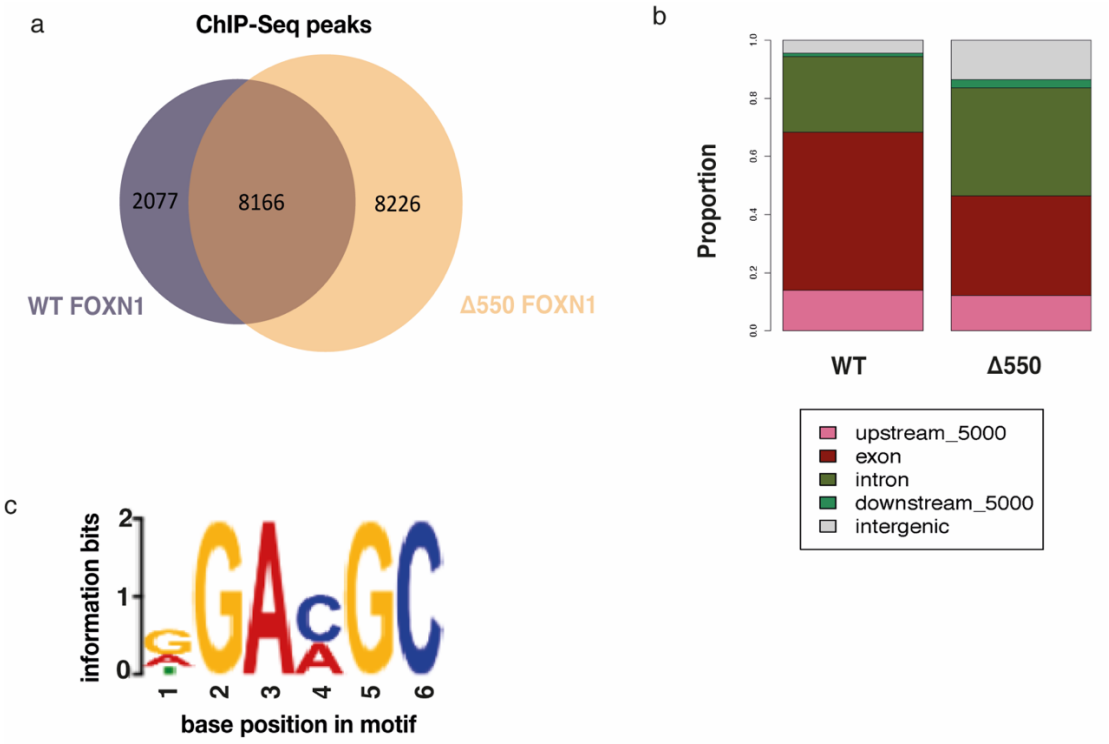


Figure 5.2 Qualitative differences in DNA binding between WT FOXN1 and *Δ550* mutant. a) Venn diagram showing the Intersection of the number of ChIP-Seq peaks between WT FOXN1 and *Δ550* mutant FOXN1 b) Proportion of WT and Δ550 FOXN1 ChIP-seq peaks falling in different RefSeq meta-gene regions as indicated c) Weblogo of MEME-derived FOXN1-binding site motif for TSS-associated peaks (–5 kb before and 100 bp after TSS), E = 1,7e-362 for the WT peaks and E=2,5e-258 for the *Δ550* mutant peaks.

Identification of WT and *Δ550* mutant regulated genes

Transcription factor binding does not necessarily imply gene regulation. To understand how FOXN1 DNA binding regulates the transcription of nearby genes, the FOXN1 ChIP-seq data were integrated with RNA-Seq data obtained from 4D6 cells transfected to express WT and *Δ550* FOXN1 (described in chapter 3, section 3.3.7). We found that only genes that were differentially regulated by the WT FOXN1, relative to an empty vector, were enriched for the FOXN1 ChIP-seq signal (Figure 5.3a). There was no significant enrichment of WT FOXN1 peaks in genes differentially regulated by the *Δ550* mutant (Figure 5.3b). FOXN1-binding sites of the *Δ550* mutant were enriched for genes shown to be upregulated by WT FOXN1 (Figure 5.3c) while there was no significant enrichment of *Δ550* peaks in genes found the be differentially regulated by *Δ550* FOXN1 (Figure 5.3d).

A recent study by Zuklys et al [104] combined ChIP-Seq and RNA-seq analysis of primary mouse TECs, expressing a FLAG-tagged version of FOXN1 and directly identified 413 high confidence FOXN1 targets[104]. In our study, human WT FOXN1 and *Δ550* FOXN1, in TEC 4D6 cells, were found to bind upstream of 53.2% (220/413) and 53.9% (223/413) of these high confidence targets respectively. Although, these were not necessarily identical as only 43% (178/413) were the same between WT and *Δ550*. Collectively, our data suggests that although the mutant is transcriptionally inert it can still occupy regulatory regions of genes normally regulated by the WT FOXN1 with the same affinity. Therefore, under heterozygous conditions expressing both the WT and the *Δ550* FOXN1, as is the case of the athymic *Δ550* patient (chapter 2), the product of the mutant allele could compete with the WT FOXN1 for DNA binding.

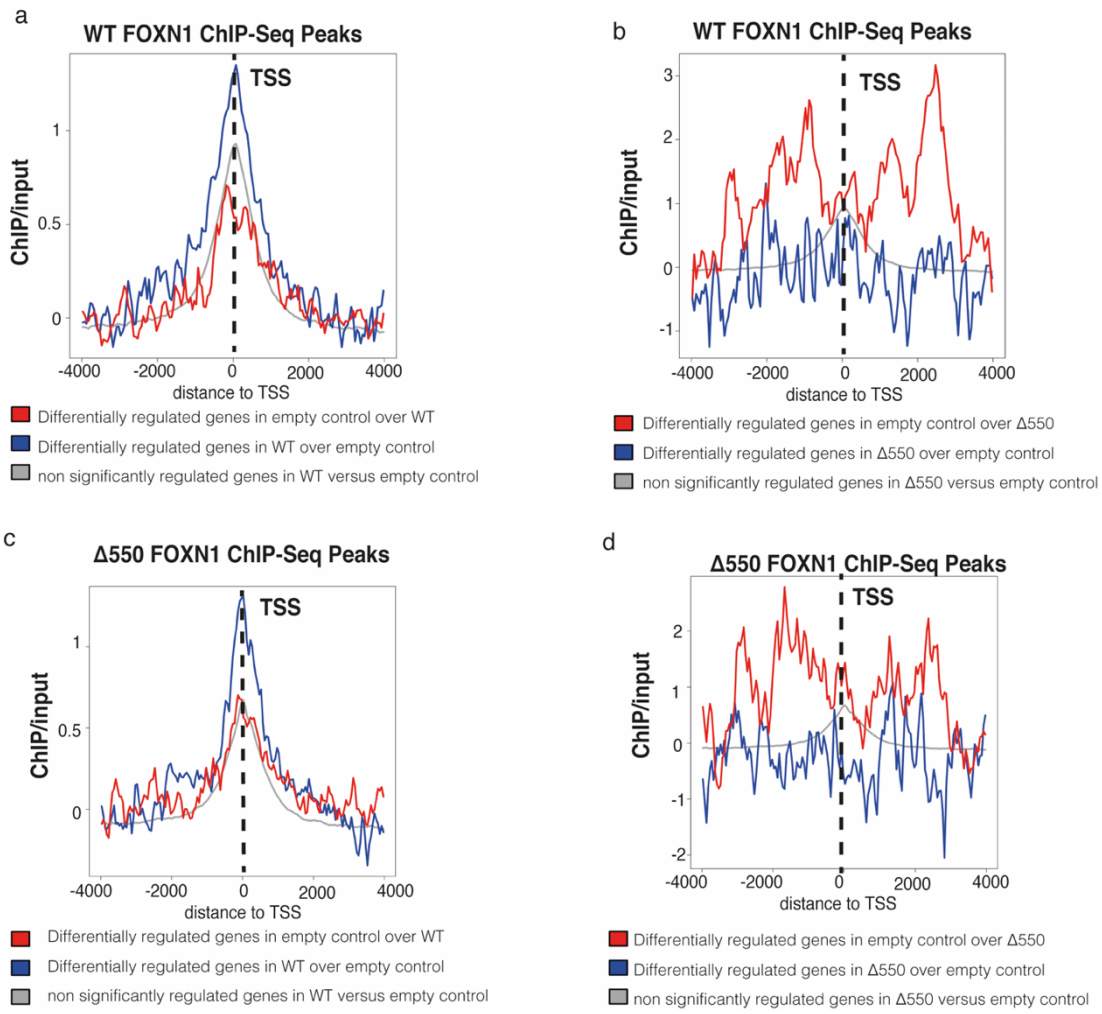


Figure 5.3 WT and Δ550 DNA binding and regulation of gene expression, a) enrichment of WT FOXN1 ChIP-Seq signal over input in 4 kb regions flanking the TSS for genes differentially regulated by WT FOXN1 (vs. empty control) b) enrichment of WT ChIP-Seq signal over input in 4 kb regions flanking the TSS for genes differentially regulated by *Δ550* FOXN1 (vs. empty control) c) enrichment of *Δ550* ChIP-Seq signal over input in 4 kb regions flanking the TSS for genes differentially regulated by WT FOXN1 (vs. empty control) d) enrichment of *Δ550* ChIP-Seq signal over input in 4 kb regions flanking the TSS for genes differentially regulated by *Δ550* FOXN1 (vs. empty control).

5.4 DISCUSSION

This chapter discusses the DNA binding specificities of WT FOXN1 and *Δ550* mutant proteins. We have previously resolved the crystal structure of the DNA binding domain of human FOXN1[87]. There we could demonstrate that the third α' helix of the forkhead domain comes into direct contact with the canonical *GACGC* DNA binding motif positioned in the DNA's major groove [87]. A single amino acid substitution within this region both in the human and mouse proteins results in the "NUDE" phenotype, highlighting the importance of this interaction[46, 183]. In this chapter, we show that the forkhead domain of FOXN1 either alone or in the presence of the N-terminus cannot bind to DNA. In contrast, the C-terminus domain is essential for facilitating protein-DNA interaction. The *Δ550* mutant has an intact DNA binding domain followed by a C-terminus that lacks 98 amino acids and contains an aberrant protein sequence in comparison to the WT sequence. However, it is still able to bind to the canonical *GACGC* binding motif with an affinity that is comparable to that of the WT protein.

In 4D6 TEC cells both WT and *Δ550* proteins recognise the same *GACGC* consensus DNA binding motif. This FOXN1 core binding sequence is identical to the previously described motif found in the mouse studies[104, 218]. Whether WT FOXN1 accesses this core motif via direct DNA binding or via nucleosome binding is unknown. The latter is a property of pioneer transcription factors, that have the ability to bind DNA packed with nucleosome and facilitate their displacement[222]. FOXA and FOXD3, members of the forkhead family of transcription factors have been described as pioneer factors

[89, 90, 185]. However, it remains to be determined whether FOXN1 also acts in this capacity and how the *Δ550* mutation may interfere.

To determine whether FOXN1's DNA binding also affects transcription, we integrated the ChIP-Seq and the RNA-Seq data obtained from 4D6 TEC cells transfected to overexpress WT or *Δ550* FOXN1. This analysis revealed that the mutant protein occupies regulatory regions of genes normally bound and regulated by WT FOXN1. Based on these findings we conclude that a concomitant expression of the WT FOXN1 and the *Δ550* mutant will result in a situation of competitive DNA binding. Given that the mutant is transcriptionally inert, co-expression of these two FOXN1 forms will compromise the regulation of normal target gene transcription.

In mouse primary TEC, FOXN1 directly binds to and regulates the transcription of 413 target genes[104]. The *in-vitro* ChIP-Seq assay described in this chapter, using nuclear lysates from the human TEC 4D6 cell line transfected with FLAG-tagged WT or *Δ550* FOXN1, identified FOXN1 ChIP-seq peaks in the TSS of about 50% of the high confidence FOXN1 targets previously described in the mouse primary TEC[104]. The absence of human FOXN1 binding upstream of the remaining high confidence FOXN1 targets could be attributed to differences in the chromatin accessibility profile between mouse primary TECs and the human 4D6 TEC cell line. Alternatively, distal promoters or enhancers may also account for this difference as they play a role in the regulation of gene expression when brought close in 3-D space by DNA bending. This situation is not captured by the conventional ChIP-Seq method used in the above studies. Therefore, to access the full breadth of FOXN1 gene regulation, analysis of the 3-D mechanisms of transcriptional regulation using chromosome

conformation capture assays would be required[223]. It also remains to be elucidated whether FOXN1 can also control the transcription of other genes indirectly via the interaction with other DNA binding proteins.

CHAPTER 6

THE IMPACT OF THE *Δ505* MUTATION ON TEC & T CELL DEVELOPMENT

6.1 Introduction-Aims 158

6.2 Materials and Methods 159

6.2.1 Mouse handling 159

6.2.2 Generation of FOXN1$^{WT/\Delta505}$ heterozygous mice using CRISPR/Cas9 159

6.2.3 Genotyping of FOXN1$^{WT/\Delta505}$ mice 160

6.2.4 Thymic epithelial cell isolation 163

6.2.5 Isolation of thymocytes 165

6.2.6 Antibody staining 166

6.2.7 FACS analysis and sorting 166

6.3 Results 168

6.3.1 The equivalent of the human *Δ550* mutation in the mouse Foxn1 gene 168

6.3.2 The impact of the *Δ505* mutation on TEC development 171

6.3.3 The impact of the *Δ505* mutation on thymocyte development 178

6.4 Discussion 182

6.1 INTRODUCTION

Functional FOXN1 is required for regular thymus organo-senescence and maintenance. The progressively reduced detection of *Foxn1* transcripts correlates with the organ's age-related involution. Patients heterozygous for the *Δ550* FOXN1 mutation were athymic at the time of diagnosis but must have had some thymopoiesis prior to that date as a restricted frequency of T cells could be detected in the blood. The patient's T Cell Receptor (TCR) repertoire was restricted but sufficiently diverse to avert life-threatening infections. Hence, and as discussed in chapter 2, clinical and haematological evidence argued that patients heterozygous for the *Δ550* FOXN1 mutation must have had initially generated functional thymic tissue which prematurely involuted by the time these patients were brought to medical attention. We therefore hypothesise that the *Δ550* FOXN1 mutation ablates normal FOXN1 function in a developmental specific fashion leading to premature thymic atrophy.

To test this hypothesis and to probe the in vivo consequences of the *Δ550* FOXN1 mutation on thymus organogenesis we created and analysed a novel mouse model. This mouse model bears a comparable single nucleotide loss in the mouse *Foxn1* sequence resulting in a mutant *Foxn1* designated *Δ505 Foxn1.*

A colony of mice heterozygous for the *Δ505 Foxn1* mutation has been established in the past few months and its immunological analysis is ongoing. Therefore, data presented in Chapter 6 represents a first series of phenotypic analysis which will be confirmed and extended over time. A complete in-depth investigation of this mouse model is therefore beyond the scope of this doctoral thesis.

6.2 MATERIALS AND METHODS

The generation of the mouse Δ505 construct was done as described in chapter 3.2.3. Luciferase assays, qRT-PCR analysis and Western blot (WB) were performed as described in chapter 3.2.

6.2.1 Mouse handling

All animal work was conducted in accordance with UK Home Office regulations and all procedures were performed as stated in the relevant project license. Mouse colonies were maintained at the University of Oxford Biomedical Science facilities. Schedule 1 killing was used for mouse culling. Age and gender matched wild type mice (denoted as WT) were used in all experiments as a reference for genetically modified animals.

6.2.2 Generation of FOXN1$^{WT/\Delta505}$ heterozygous mice using CRISPR/Cas9

Mice heterozygous for a *Foxn1* allele with a single nucleotide loss at position 1470 (designated FOXN1$^{WT/\Delta505}$) were generated in collaboration with Philip Hublitz (WIMM Genome Engineering Facility, MRC Weatherall Institute of Molecular Medicine, Radcliffe Department of Medicine, University of Oxford), using the CRISPR/Cas9 technology. In detail, murine JM8.1 C57B/6 ES cells were transfected with a plasmid construct that allowed expression of a Puromycin resistance gene, the Cas9 endonuclease and a single guide RNA (sgRNA) targeting the region in which the base pair change was expected to take place. The single stranded donor oligonucleotide (ssODN) for homology directed repair was also co-transfected to allow homologous integration of the desired genetic change. The ssODN was complementary to exon 8

of the mouse *Foxn1* locus with a single base pair deletion of an Adenine at cDNA position 1370. It also contained a *de novo* restriction enzyme site (PvuII) that was inserted in the sequence without changing the codon usage. Mouse embryoninc stem cell (mESC) clones that had incorporated the correct genetic change as confirmed by PCR and digestion screen, and ultimately verified by cloning and Sanger-sequencing. Successfully targeted embryonic stem cells (ESC) were injected into the blastocysts of albino C57BL/6BrdCrHsd-Tyrc mice. Resultant chimeric animals were selected by the presence of black coat color and confirmed by genotyping. Male chimeras with a reasonably high percentage of chimerism were mated with albino C57BL/6BrdCrHsd-Tyrc female mice to establish germline transmission. Successful integration of the mutant allele was ultimately verified by genotyping. Heterozygous *Δ505* mice were mated with C57BL/6J WT black mice to expand the colony. C57BL/6J black inbred wild-type mice and C57BL/6BrdCrHsd-Tyrc albino wild-type mice, which have a mutation in the tyrosinase gene, were obtained from the in-house colony maintained by the Transgenic Service of the WIMM and of the University of Oxford.

6.2.3 Genotyping of FOXN1$^{WT/\Delta505}$ mice

Tissue samples from ear clips taken from mice older that 10 days, were lysed overnight in 600 µl lysis buffer [Tris 100 mM (Merck), Ethylenediaminetetraacetic acid (EDTA) (Sigma), 5 mM Sodium Dodecyl Sulfate (SDS) (Sigma), 0.2% Sodium Chloride (NaCl) (VWR), 200 mM Proteinase K 100 µg/ml (Roche)] at 55°C. Remaining debris was pelleted by centrifugation and discarded. Genomic DNA was precipitated with 600 µl isopropanol (VWR) and washed with 500 µl 70% ethanol (VWR). The supernatant was discarded and the DNA pellet was left to dry for 30min to 1h before being resuspended

in 30 µl TE buffer. Genomic DNA was amplified by polymerase chain reaction (PCR) in a thermocycler (Applied Biosystems) under the conditions listed below (Table 6.1). One µl of DNA was used in each 25 µl reaction mix containing 200 µM deoxynucleotides (dNTPs) (Sigma), 0.5 µM each of the relevant forward (FP: 5'aaactgggctctccgctgctg3') and reverse (RP:5'agtagagtatcgtgcatggtcctgg3') primers, 1X Taq buffer and 0.02 units/µl Taq polymerase (Sigma). A temperature of 64°C was chosen as the optimal annealing temperature (Tm) after testing a temperature gradient (Figure 6.1a).

Amplification step	Temperature	Duration	Number of cycles
Initial Denaturation	95°C	3 min	1
Cycles of template denaturation, primer annealing and extension	95°C	30s	x35 cycles
	64°C	30s	
	72°C	25s	
Final extension	72°C	5 min	1
hold	4°C	hold	

Table 6.1: Reaction conditions for PCR amplification

PCR amplicons were digested using PvuII (NEB) restriction enzyme at 37°C for 1 hour using 5 units of enzyme per PCR reactions and 1x Cut Smart buffer (NEB). Digested amplicons were run on an agarose gel.

Agarose gels were prepared by dissolving UltraPure Agarose (Invitrogen) in 1X Tris-Borate-EDTA (TBE) buffer (Sigma) and subsequently adding 1:20000 GelRed dye (Biotium). The concentration of agarose used was dependent on the expected PCR product size. 10 µl of amplified PCR product for each genotyping sample was mixed 6:2 with 6X gel loading dye (Thermo Fisher Scientific), loaded into wells of the gel and run at 100V. The 1 kb Plus DNA ladder (NEB) was used as a marker to determine the size of the PCR product. Gels were visualised using the Gel Doc XR+ system (Bio-Rad). The undigested PCR amplicon (uncut) was detected at 389bp size (Figure 6.1.b). PvuII

digested amplicons from FOXN1$^{WT/WT}$ mice generated two bands of 389bp and 70bp size respectively, whereas PvuII digested amplicons from FOXN1$^{WT/\Delta505}$ heterozygous mice generated two additional bands of 213 and 97bp sizes respectively (Figure 6.1.b).

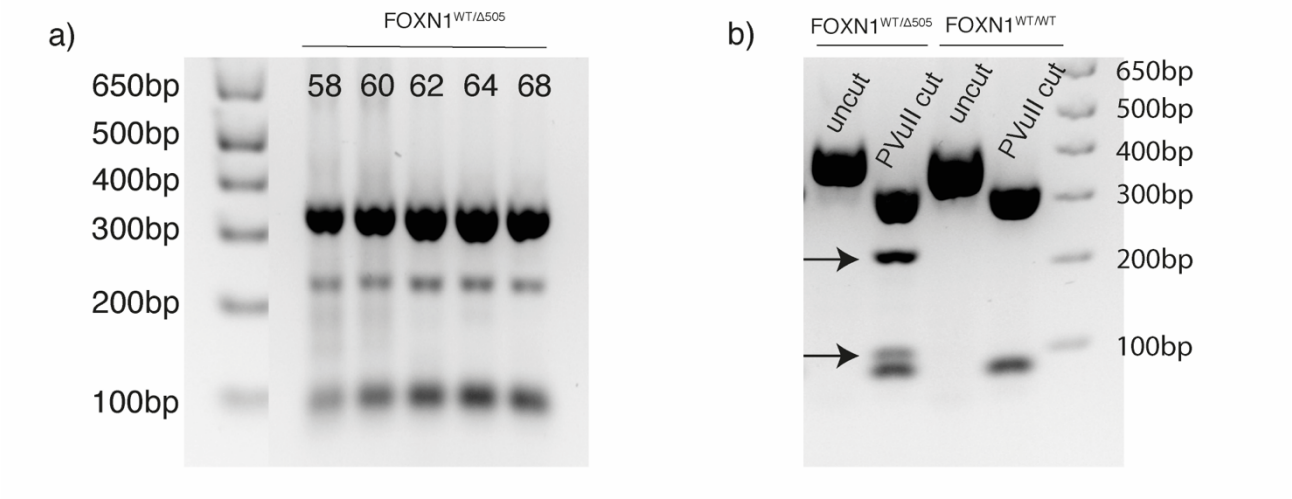


Figure 6.1. Genotyping of FOXN1$^{WT/\Delta505}$ heterozygous mice a) A temperature of 64°C was chosen as the optimal annealing temperature (Tm) for the genotyping PCR reaction. Range of different Tms tested for amplification of DNA extracted from FOXN1$^{WT/\Delta505}$ mice. PCR amplification was followed by PvuII digestion. b) Examples of FOXN1$^{WT/\Delta505}$ and FOXN1$^{WT/WT}$ genotypes.

6.2.4 Thymic epithelial cell isolation from FOXN1$^{WT/\Delta 505}$ mice

Isolated thymi were cleaned of residual fat, broken blood vessels and connective tissue. The tissue was then subjected to a sequential enzymatic digestion by incubation at 37°C waterbath in Liberase digestion buffer (PBS Gibco 1X, Liberase Roche 2.5 mg/ml, DNase Roche 10 mg/ml). Briefly, 1.5 ml of digestion buffer were added to each sample and thymi were gently disrupted by pipetting. The mixture was incubated for 10 min, after which the supernatant was collected. This step was then repeated 2 more times, first in 1 ml and then in 0.8ml of fresh digestion buffer.

The supernatant was collected into a 50 ml Falcon tube (Corning) containing 40 ml of cold FACS buffer [Phosphate-Buffered Saline (PBS) Gibco 1X, Fetal Calf Serum (FCS) Sigma 2%]. After centrifugation (1500rpm for 4 minutes) the resulting cell pellet was resuspended in 5ml of FACS buffer to achieve a single cell suspension. Adult TECs were incubated with anti-CD45 beads (Miltenyi Biotec) at a concentration of 5 x 10^6 µl per 10 x 10^6 cells for 15 min at 4°C. Cells were washed with FACS buffer and filtered through a 30 µm filter (Millipore). The concentration of cells was adjusted to 100 x 10^6 cells/ml in FACS buffer and samples were depleted based on CD45 expression using the “depleteS” program on the AutoMACS separator (Miltenyi Biotec). CD45 depleted fractions were stained for FACS analysis. The gating strategy for the assessment of the TEC phenotype is shown in Figure 6.2. Gates for Gp2 and Tspan8 were adjusted based on an isotype control for each of the antibodies. Details of antibodies used for the FACS assisted analysis and sorting of TECs are listed in Table 6.2.

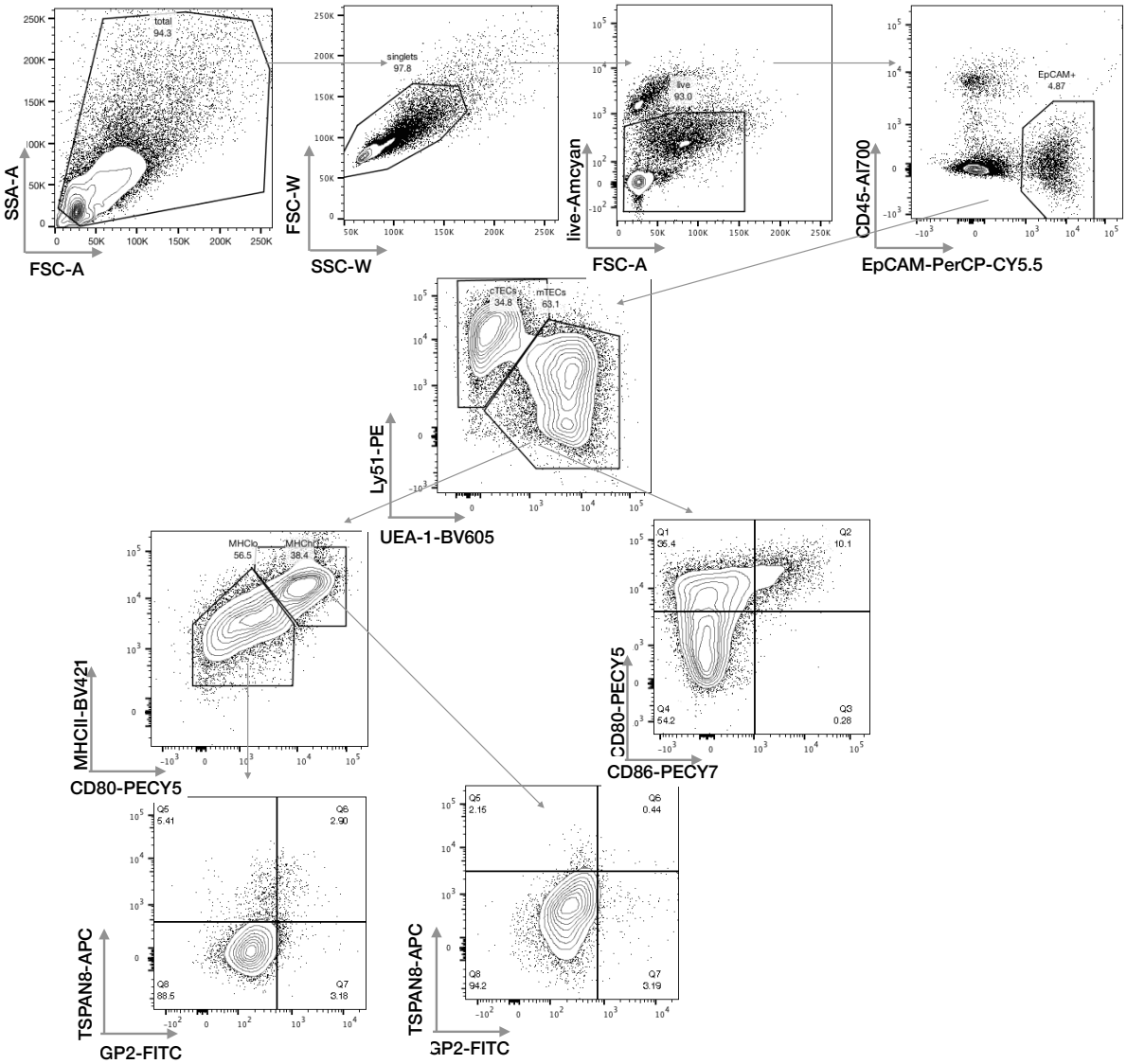


Figure 6.2 Gating strategy for the characterization of TEC subpopulations. Cells were distinguished by their size (as defined by Forward SCatter (FSC)/Side SCatter (SSC) parameters). Doublets were discriminated by gating according to Side SCatter-Width (SSC-W) / Forward Scatter- Area (FSC-A) and additional gating was performed to discriminate dead cells (Live/dead aqua stain positive). CD45-Epcam^{+} cells were selected (total TECs). TECs were then differentiated as cTECs and mTECs by Ly51 and UEA-1 expression respectively. MTECs were further gated using the markers CD80 and MHCII to determine two dinstinct maturational stages, mTEC^{hi} (CD80^{hi}MHCII^{hi}) and mTEC^{lo} (CD80^{lo}MHCII^{lo}). Alternatively, mTECs were further gated using the markers CD80 and CD86 to define three maturational stages CD80^{neg}CD86^{neg}, CD80^{pos}CD86^{neg}, CD80^{high}CD86^{pos}. MTEC^{hi} and MTEC^{lo} were also separately assessed for the expression of the tissue restricted antigens (TRAs) TSPAN8 and GP2. The example shown above is representative for the gating strategy and analysis that has been carried out with a 16-week-old FOXN1$^{WT/WT}$ mouse.

6.2.5 Isolation of thymocytes

Thymocytes were obtained by gentle disruption of thymic lobes between 2 frosted glass slides (Thermo Scientific). Cells were filtered through a 70 µm filter (Millipore) and washed with ice-cold FACs buffer. Samples were stained with antibodies using standard conditions and then subjected to FACS assisted phenotyping and sorting (Table 6.2). The gating strategy for the assessment of different thymocte developmental stages is shown in Figure 6.3.

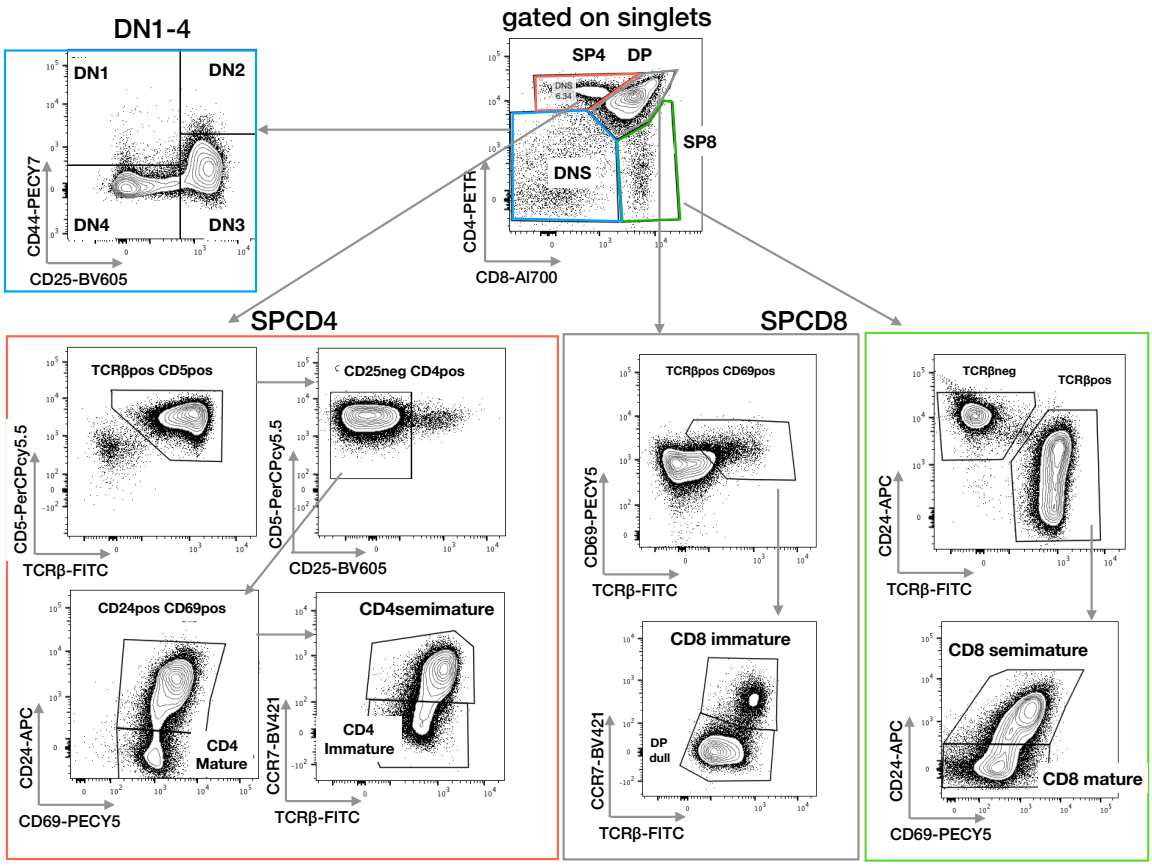


Figure 6.3 Gating strategy for the assessment of the different thymocyte developmental stages. Cells were distinguished by their size (as defined by their FSC/SSC). Doublets were discriminated by gating according to SSC-W/FSC-A. T cells were then distinguished based on the CD4 and CD8 expression. The stages of double negatives or DNs ($CD4^{neg}CD8^{neg}$) were defined by CD44 and CD25 expression. The single positive CD4 (SPCD4) were further gated as $TCR\beta^{pos}$ $CD5^{pos}CD25^{neg}$ and were divided into immature ($TCR\beta^{pos}CCR7^{neg}$), semimature ($TCR\beta^{pos}CCR7^{pos}$) and mature populations($CD69^{pos}CD24^{neg}$). CD8 immature cells were defined as $CD4^{pos}$ $CD8^{pos}$ $TCR\beta^{pos}$ $CD69^{pos}$ $CCR7^{pos}$. CD8 semimmature cells were defined as $CD8^{pos}$ $TCR\beta^{pos}$ $CD24^{lo}CD69^{pos}$. CD8 mature cells were defined as $CD8^{pos}$ $TCR\beta^{pos}$ $CD24^{neg}CD69^{neg}$. The representative example shown above is from a 16-week-old $FOXN1^{WT/WT}$mouse.

6.2.6 Antibody staining

Antibodies listed in Table 6.2 were used for FACs phenotypic analysis and FACs sorting.

Antibody	Clone	Isotype	Conjugate	Source
CCR7	4B12	Rat LOU/M IgG2a	BV421	BD Biosciences
CD24	M1/69	Rat IgG2b, κ	APC	BioLegend
CD25	PC61.5	Rat IgG1, l	BV605	eBioscience
CD4	RM4-5	Rat IgG2a, κ	PE Texas Red	BioLegend
CD44	IM7	Rat IgG2b, κ	PE Cy7	eBioscience
CD45	30-F11	Rat IgG2b, κ	Alexa Fluor 700	BioLegend
CD5	53-7.3	Rat IgG2a, κ	PerCP, Cy5.5	BioLegend
CD69	H1.2F3	Armenian Hamster IgG	PE Cy5	BioLegend
CD80	16-10A1	Armenian Hamster IgG	PE Cy5	BioLegend
CD86	GL-1	Rat IgG2a, κ	PE Cy7	BioLegend
CD8a	53-6.7	Rat IgG2a, κ	Alexa Fluor 700	BioLegend
EPCAM,	G8.8	Rat IgG2a, κ	PerCP Cy5.5	BioLegend
Ly51	6C3	Rat IgG2a, κ	PE	BioLegend
MHC-II	28-14-8	Mouse IgG2a, κ	BV421	eBioscience
Streptavidin	-	-	BV605	BioLegend
TCRβ	H57-597	Rat IgG2b, κ	FITC	eBioscience
Gp2	2F11-C3	Mouse IgG1 κ	FITC	MBL
Tspan8	657909	Rat IgG_{2B}	APC	R&D Systems

Table 6.2 list of antibodies used for the FACs phenotypic analysis and FACs cell sorting

The UEA-1 lectin (Vector Laboratories) was used pure, followed by anit-UEA1 biotin staining with secondary streptavidin-BV605. For live dead discrimination Live/Dead Fixable Aqua stain kit (Thermo Fisher Scientific) was used. The Live/Dead Aqua stain was conducted for 30 min at 4°C in the dark, where 1 µl of the stain was added to up

to 20 x10^6 cells in 1 ml of PBS. Extracellular antibody stainings were conducted for 20 min at 4°C in the dark. CCR7 staining was performed at 37°C water-bath for 30min. Working concentrations of antibodies used were calculated by antibody titration and ranged between 0.25-1.5 µg/100 µl (of up to 20 x10^6 cells).

6.2.7 FACS analysis and sorting

For FACs assisted phenotype analysis and cell sorting the BD FACS Aria III (BD Biosciences) was used. Samples were resuspended in between 0.2 to 1 ml of FACS buffer depending on cellularity, filtered with 0.70µm filters and gently vortexed before loading onto the machine. Cells were sorted into DNAse RNAse free eppendorf tubes (Axygen) coated with FCS. Sorting was conducted using the 4- way purity mask, with a routine purity of ≥99%. Flow cytometry analysis was performed with FlowJo software (Tree Star, Olten, Switzerland).

6.3 RESULTS

6.3.1 The equivalent of the human *Δ550* mutation in the mouse *Foxn1* gene

Prior to generating a mouse model mimicking the heterozygous *Δ550* patient we wanted to confirm whether a mutation in mice equivalent to that in humans will also create a dominant negative *Foxn1* variant. The human and mouse *FOXN1* genes have an 86% sequence homology. As detailed earlier a single base pair deletion of an adenine at cDNA position 1370 of the human *FOXN1* gene, results in a frameshift and a consequent premature truncation of the c-terminus of the protein at amino acid (aa) 550. In contrast, the deletion of the same base pair in the mouse homologue leads to stop at aa 505 (Figure 6.4a). The mouse mutation was therefore named *Δ505*. The mutant mouse *Δ505* sequence was generated using site directed mutagenesis. Its molecular characteristics and the potential to act as a dominant negative mutant were compared to those of the human *Δ550* FOXN1.

When overexpressed in the mouse TEC1.2 cell line, transcripts for mouse *Δ505* were increased and protein levels decreased in comparison to mouse WT FOXN1 (Figure 6.4 b and c). This finding was identical to what was observed for human *Δ550* FOXN1 when expressed in human 4D6 cell line. As assessed by luciferase assay mouse *Δ505* FOXN1 was transcriptionally inactive (Figure 6.4d). When co-expressed with mouse WT FOXN1, the Δ505 variant exerted a dominant negative effect on the transcriptional activity of the WT protein (Figure 6.4 e).

Taken together, the mouse *Δ505 FOXN1* mutant acts as a dominant negative molecule suppressing WT-FOXN1 mediated transcription similar to the human *Δ550* variant. To study in-depth and in-vivo the consequences of a heterozygous *Δ505* allele on both

the development and function of TEC and T cells, we generated a mouse model heterozygous for the *Δ505* FOXN1 allele (FOXN1$^{WT/\Delta505}$) employing the CRISPR/Cas9 genome editing.

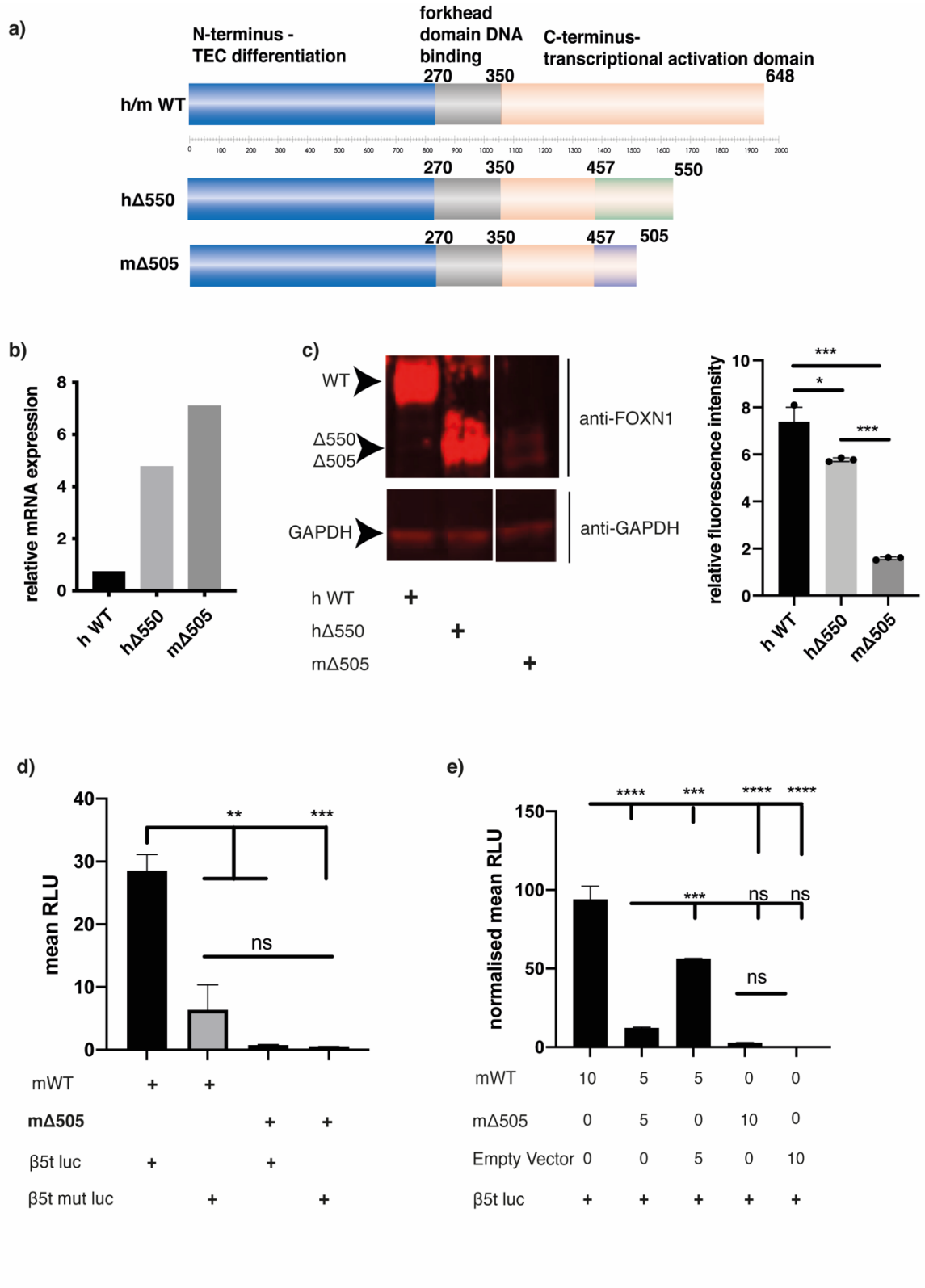


Figure 6.4 The molecular characteristics of the mouse Δ505 FOXN1 mutant (mΔ505) a) Schematic representation of human and mouse WT, human Δ550 (hΔ550) and mΔ505 FOXN1 proteins, in green and purple colours are the frameshifted regions that have arisen secondarily to the mutation. Numbered bar represents base pairs b) Transfection of mouse TEC1.2 cells with mΔ505 results in higher Foxn1 relative mRNA expression levels compared to the human WT FOXN1 (hWT) or the human Δ550 FOXN1 (hΔ550). The qRT-PCR analysis was performed 48hours post transfection, the data shown represent the mean of three technical replicates of a single experiment c) mΔ505 FOXN1 protein expression levels are decreased when compared to h.WT or h.Δ550 FOXN1 levels. Western blot analysis of HEK293 cells transfected to express h.WT, h.Δ550 both h.WT and h.Δ550 or mΔ505 constructs. Detection of the protein using an anti-FOXN1. GAPDH was used as loading control. The data shown is from a single experiment. Statistical comparison was done using unpaired t-test with correction for multiple comparisons *p<0.05, ***p<0.001 d) In-vitro expressed mΔ505 FOXN1 exerts a dominant negative effect on mouse WT FOXN1 (mWT). Luciferase assay on TEC1.2 mouse cells transfected with recombinant expressing plasmids as indicated. Co-transfection of mWT with an empty vector was used as a control. The data shown is representative of three independent experiments. RLU=relative light units, Statistical comparison was done using unpaired t-test with correction for multiple comparisons *p<0.05,**p<0.01, ***p<0.001, ****p<0.0001.

6.3.2 The impact of the *Δ505* mutation on TEC development

To assess whether the *Δ505* mutation results in premature tissue degeneration we focused our initial analysis on FOXN1$^{WT/\Delta505}$ mice aged 13-16weeks. At this age mice show already some of the hallmarks of thymic senescence, as marked by a decline in TEC and T-cell cellularity[224].

At 16weeks of age male mice heterozygous for the *Δ505* mutation (FOXN1$^{WT/\Delta505}$) had a regular coat but a significantly smaller thymus when compared to their WT littermates (FOXN1$^{WT/WT}$) (Figure 6.5 a). The size decrease correlated with an approximately 30% reduction in the total number of TECs (189,1±31.53 vs 137.4± 15.65) (Figure 6.5 b). The frequency of TEC (CD45^{-}EpCAM^{+}) among thymic cells, was unaffected by the mutation (Figure 6.5 c). However, the ratio of cTEC to mTEC was impaired with a reduced frequency of mTECs (58.92 % ± 6.4 vs 40.96 % ± 10.06) and a corresponding increase in cTECs (37.7 % ± 6.460 vs 55.70 % ± 11.34) in mice heterozygous for the mutant allele (Figure 6.5 d).

Although MHCII is not a direct FOXN1 target[104], its gene expression is considered, based on circumstantial evidence, to be influenced by the transcriptional activity of FOXN1[91]. MTECs from FOXN1$^{WT/\Delta505}$ mice expressed on their surface on average 44% less MHCII compared to WT animals, as measured by the geometric mean fluorescence intensity (gMFI) (Figure 6.5 e). In contrast, the levels of MHCII expression on cTEC was unaffected by the expression of the *Δ505 Foxn1* mutant (Figure 6.5e). Interestingly, *foxn1* expression levels in sorted cTEC were higher in FOXN1$^{WT/\Delta505}$ compared to WT mice (Figure 6.5 f), consistent with the findings of *in-vitro* expressed transcripts for each variant (Chapter 6.3.1 and Chapter 3 for Δ550).

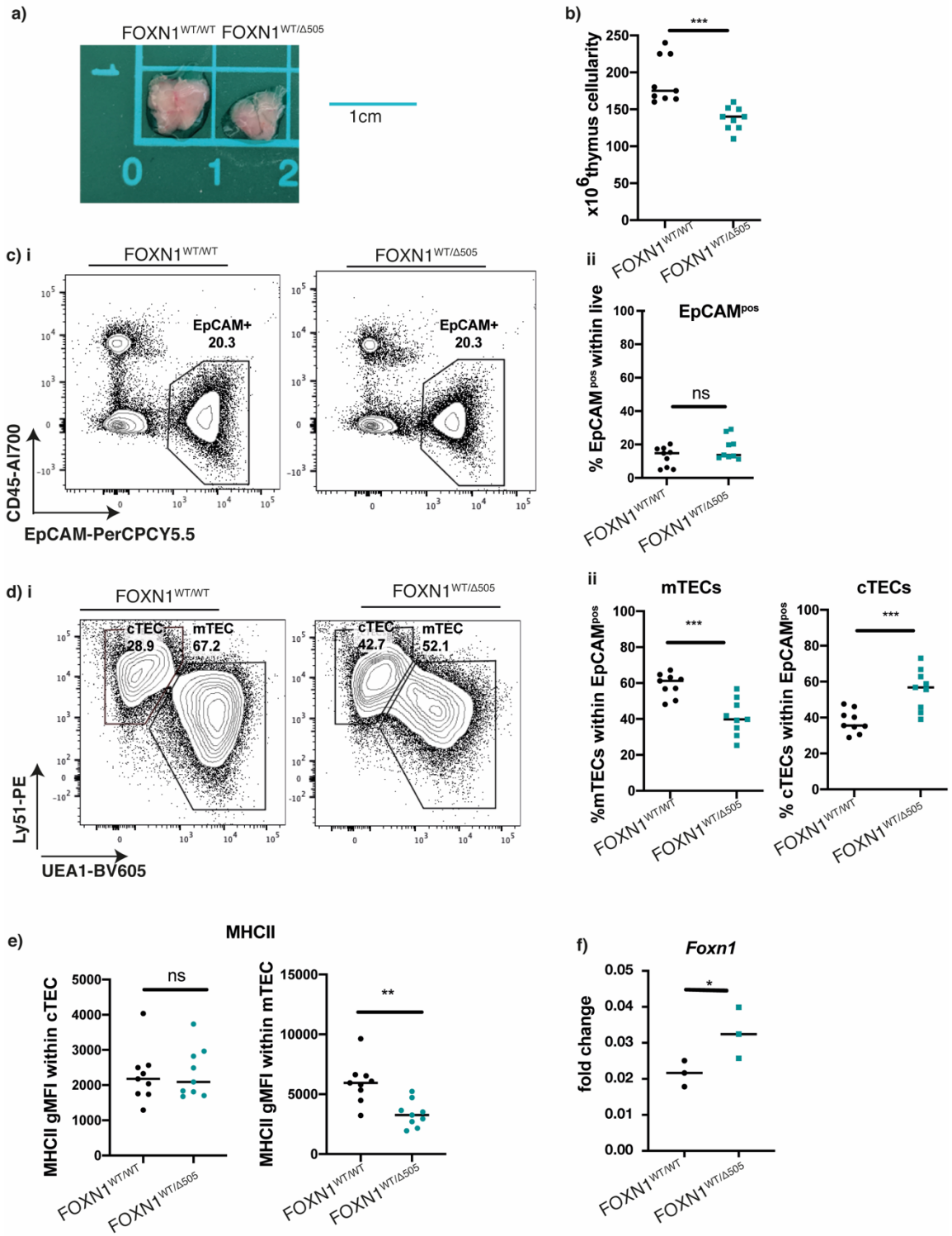


Figure 6.5 Thymic phenotype of FOXN1$^{WT/\Delta505}$mice a) representative images of thymic lobes isolated from FOXN1$^{WT/WT}$ and FOXN1$^{WT/\Delta505}$ mice b) total TEC cellularity c) i. Representative FACS plots of total EpCAM^{pos} ii. scatter plot with the frequency of EpCAM^{pos} TEC within live cells d) i. Representative FACS plots identifying mTEC and cTEC and ii. scatter plots with their frequencies within EpCAM^{pos} cells e) MHCII cell surface expression levels on cTEC (right) and mTEC (left) as determined by gMFI. The data shown are pooled from three independent experiments with a total of 9 16-week-old male mice for each of the mouse strains. f) qPCR analysis of *foxn1* expression levels in sorted primary cTEC from 3 FOXN1$^{WT/WT}$ and 3 FOXN1$^{WT/\Delta505}$ mice. Statistical comparison was done using two tailed unpaired t-test *p<0.05,**p<0.01, ***p<0.001

The analysis of specific TEC subpopulations revealed that, FOXN1$^{WT/\Delta505}$mice had fewer mature mTEC^{hi} (MHC^{hi}CD80^{+}) (32.04 % ± 7.746 vs 17.26 % ± 4.703) (Figure 6.6 a). The stepwise and differential upregulation of MHCII, CD80 and CD86 on mTEC, defines three sequential maturational stages: MHCII^{low}CD80^{lo}CD86^{neg} → MHCII^{high}CD80^{pos}CD86^{neg} → MHCII^{high}CD80^{high}CD86^{pos}. The frequency of mature (i.e MHCII^{high}) CD80^{pos}CD86^{neg} and CD80^{high}CD86^{pos} mTECs was significantly reduced in the FOXN1$^{WT/\Delta505}$mice (CD80^{pos}CD86^{neg}: 31.46%± 5.750 vs 16.03±3.859, CD80^{high}CD86^{pos}: 8.707% ± 3.323 vs 2.989 ± 0.7193) (Figure 6.6 b). The transitional capacity of cells from one stage to the next was therefore calculated by dividing the frequencies of cells with a specific developmental phenotype by the combined total of cells in said population and its immediate precursor population. Based on these calculations, there was a partial block in the transition of MHCII^{low} CD80^{lo}CD86^{neg} to the MHCII^{high} CD80^{pos}CD86^{neg} mTECs in the FOXN1$^{WT/\Delta505}$mice when compared to controls (Figure 6.6c).

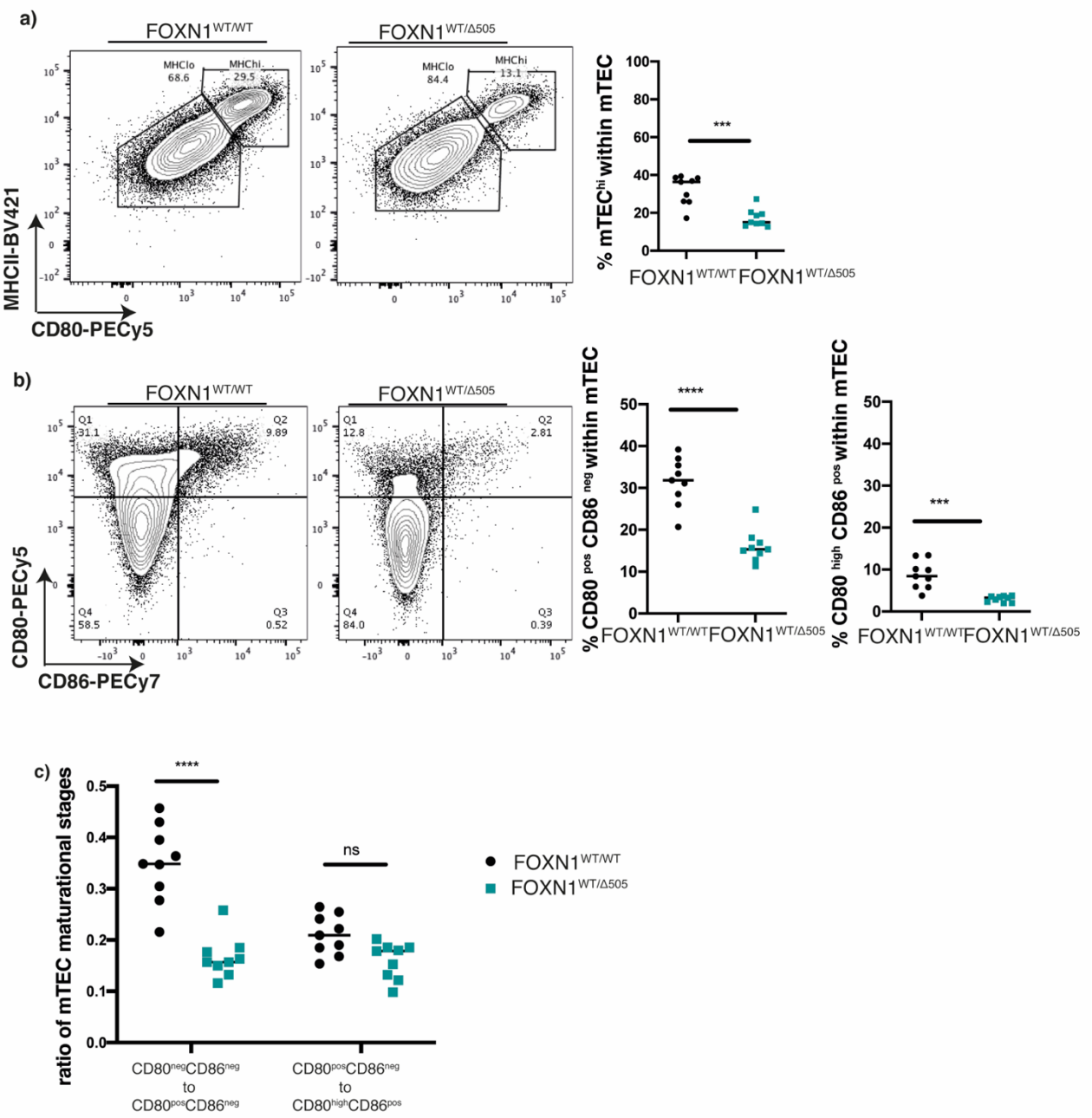


Figure 6.6 Partial differentiation block in mTEC maturation in FOXN1$^{WT/\Delta505}$mice a) left: Representative FACS plots of mTEC maturation based on the expression of MHCII and CD80, right: scatter plot with the frequency of mTEC^{hi} cells within mTEC b) left: representative FACS plots of mTEC maturation based on CD80 and CD86 marker expression, right: scatter plot with the frequency of CD80^{pos} CD86^{neg} and CD80^{high} CD86^{pos} cells within mTEC c) Transitional capacity along mTEC maturational trajectory as defined by CD80 and CD86 expression The data shown are pooled from three independent experiments with a total of 9 16-week-old male mice for each of the mouse strains. Statistical comparison was done using two tailed unpaired t-test *p<0.05,**p<0.01, ***p<0.001, ****p<0.0001

The functionality of mTECs, as measured by their ability to promote expression of tissue restricted antigens (TRA) was also partially compromised. There was a significant reduction in the expression of the tissue restricted, AIRE regulated antigen, Tspan8 by both $mTEC^{hi}$ (figure 6.7a) and $mTEC^{lo}$ (figure 6.7b) subpopulations. While the expression of the AIRE regulated GP2 antigen was slightly reduced only in the $mTEC^{lo}$ (figure 6.7b) subpopulation in mice heterozygous for the Δ505 allele. This finding may suggest that FOXN1 is also, but most likely indirectly, involved in promiscuous gene expression of some but not all loci encoding TRAs. This is in keeping with transcriptional activity of mature TEC rendered FOXN1 deficient [104].

In conclusion, 16-week-old male $FOXN1^{WT/\Delta505}$ mice, display a partial differentiation block in mTEC maturation which was correlated with their ability to effect TRA expression.

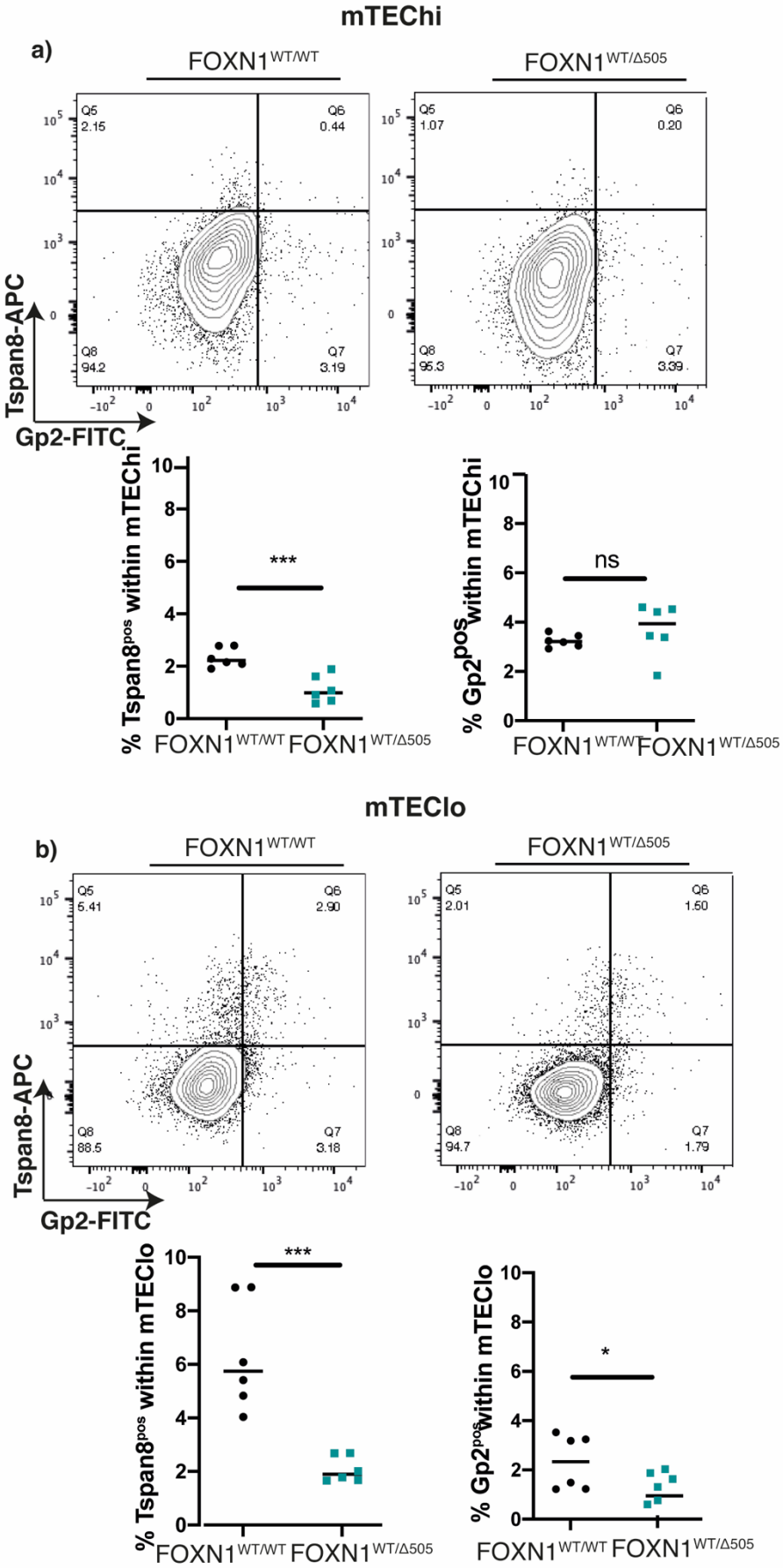

mTEChi
a)
FOXN1WT/WT
FOXN1WT/Δ505
Q5 2.15
Q6 0.44
Q8 94.2
Q7 3.19
Q5 1.07
Q6 0.20
Q8 95.3
Q7 3.39
Tspan8-APC
Gp2-FITC
% Tspan8pos within mTEChi
***
% Gp2pos within mTEChi
ns
FOXN1WT/WT FOXN1WT/Δ505
mTEClo
b)
FOXN1WT/WT
FOXN1WT/Δ505
Q5 5.41
Q6 2.90
Q8 88.5
Q7 3.18
Q5 2.01
Q6 1.50
Q8 94.7
Q7 1.79
Tspan8-APC
Gp2-FITC
% Tspan8pos within mTEClo
***
% Gp2pos within mTEClo
*
FOXN1WT/WT FOXN1WT/Δ505

Figure 6.7 TRA expression by mTEC in FOXN1$^{WT/\Delta 505}$ mice a)top: representative FACS plots with expression of Tspan8 and GP2 AIRE-regulated tissue restricted antigens by mTEC^{hi}, bottom: frequency of mTEC^{hi} expressing Tspan8 or GP2. b) top: representative FACS plots with expression of Tspan8 and GP2 AIRE-regulated tissue restricted antigens by mTEC^{lo}, bottom: frequency of mTEC^{lo} expressing Tspan8 or GP2. The data shown are pooled from two independent experiments with a total of 6 16-week-old male mice for each of the mouse strains. Statistical comparison was done using two tailed unpaired t-test *p<0.05,**p<0.01, ***p<0.001

6.3.3 The impact of the *Δ505* mutation on thymocyte development

We next tested whether the changes in mTEC differentiation and cellularity in FOXN1$^{WT/\Delta505}$mice affected T cell development. Consistent with the decrease in the numbers of TECs, thymocyte numbers were also reduced in *Δ505 Foxn1* heterozygous mice (Figure 6.8 a). However, the frequencies of single positive CD4 (SPCD4) or the single positive CD8 (SPCD8) (Figure 6.8 b) thymocytes remained unaffected. Similarly, the frequency of all double negative stages (DN1-4) were unchanged between FOXN1$^{WT/\Delta505}$mice and WT mice (Figure 6.8 c).

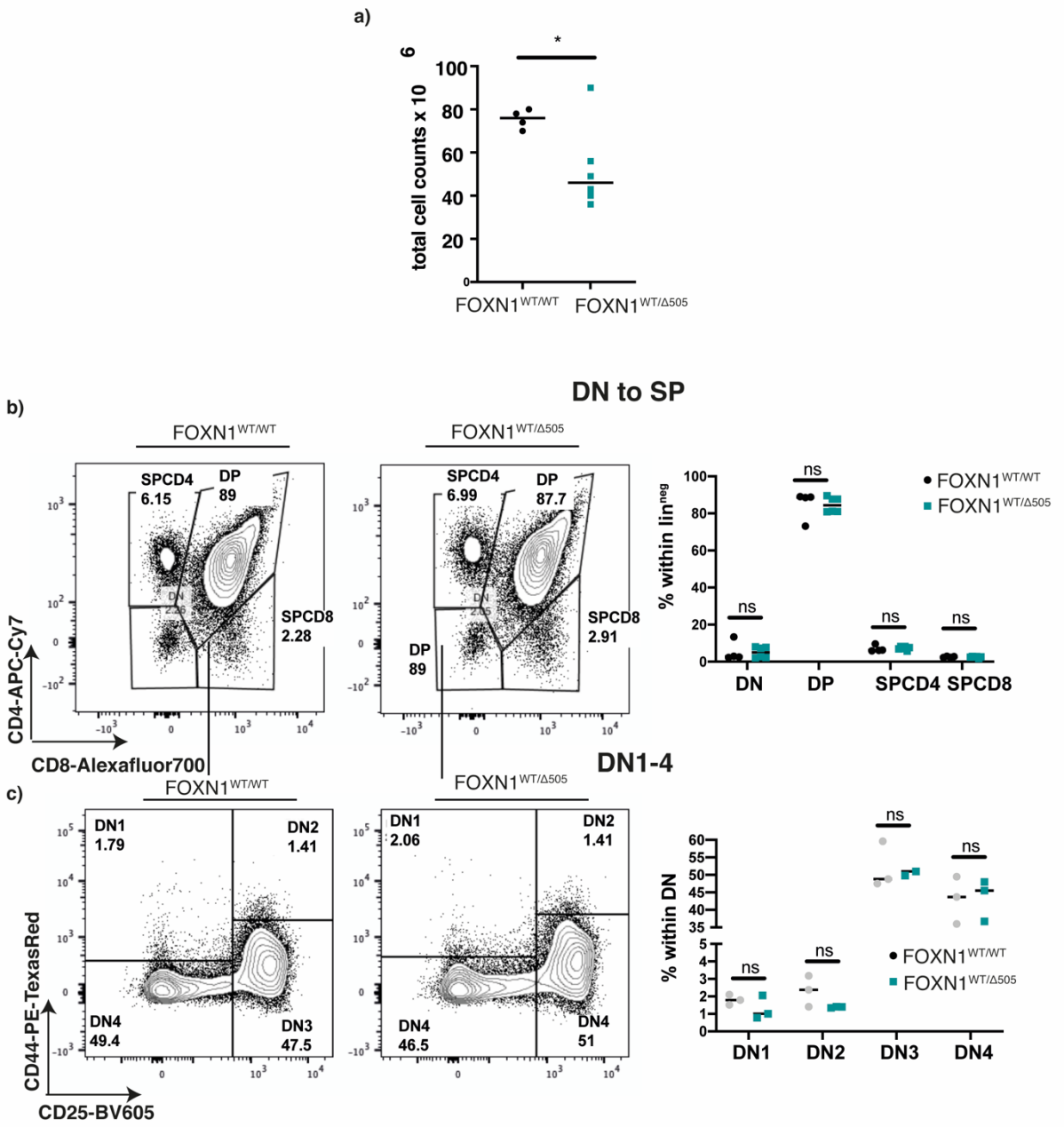
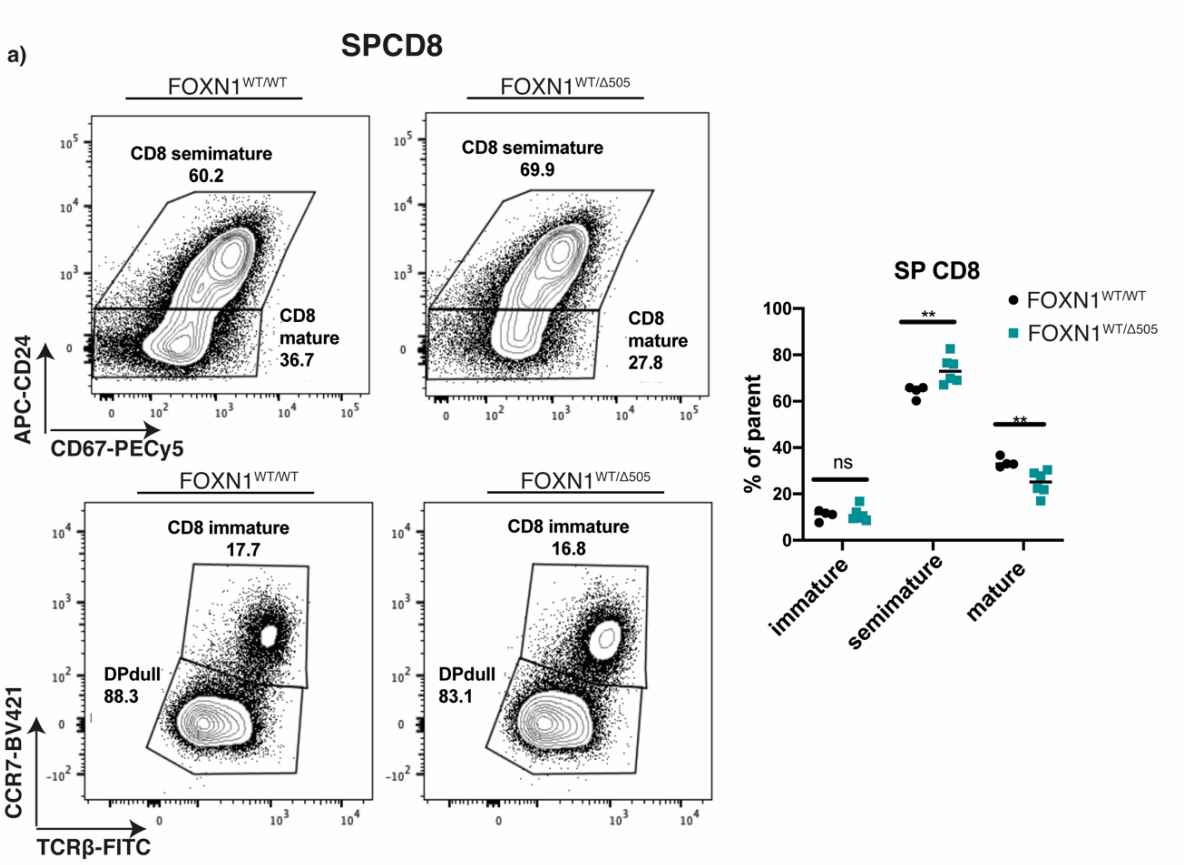


Figure 6.8 Thymocyte differentiation in FOXN1$^{WT/\Delta505}$mice a) total thymocyte cellularity after whole tissue disassociation b) Representative FACS plots (left) and scatter plot with the frequency (right) of the indicated thymocyte subpopulations c) Representative FACS plots (left) and scatter plot with the frequency (right) of the four DN stages. Data shown in graphs are pooled from two independent experiments using female mice at 13 weeks of age [WT (FOXN1$^{WT/WT}$): n=3, heterozygous Δ505 (FOXN1$^{WT/\Delta505}$): n=3] and male mice at 16weeks of age [WT (FOXN1$^{WT/WT}$): n=1; heterozygous Δ505 (FOXN1$^{WT/\Delta505}$): n=3]. Statistical comparison was done unpaired t-test with correction for multiple comparisons *p<0.05,**p<0.01, ***p<0.001, ****p<0.0001

Within the population of SPCD8 there was a significant decrease in the frequency of phenotypically mature cells (Figure 6.9a) suggesting a partial developmental block at an earlier stage. In contrast, the post selection maturation of SPCD4 cells was not compromised (Figure 6.9b). Already planned analysis will interrogate how changes in mTEC maturation and cellularity may affect, β-selection, positive and negative selection of thymocytes in *Δ505 Foxn1* heterozygous mice.

The data shown in chapter 6.3.3 are pooled from two independent experiments, one with female mice at 13 weeks of age and one with male mice at 16 weeks of age. Thymus size and the rate of thymic involution is -in addition to age- influenced by gender[127, 225]. These gender differences are mostly attributed to the presence of androgen receptors on both TEC and thymocytes.[226] To eliminate data variability due to gender differences future analysis will examine separately female and male FOXN1$^{WT/\Delta505}$mice.



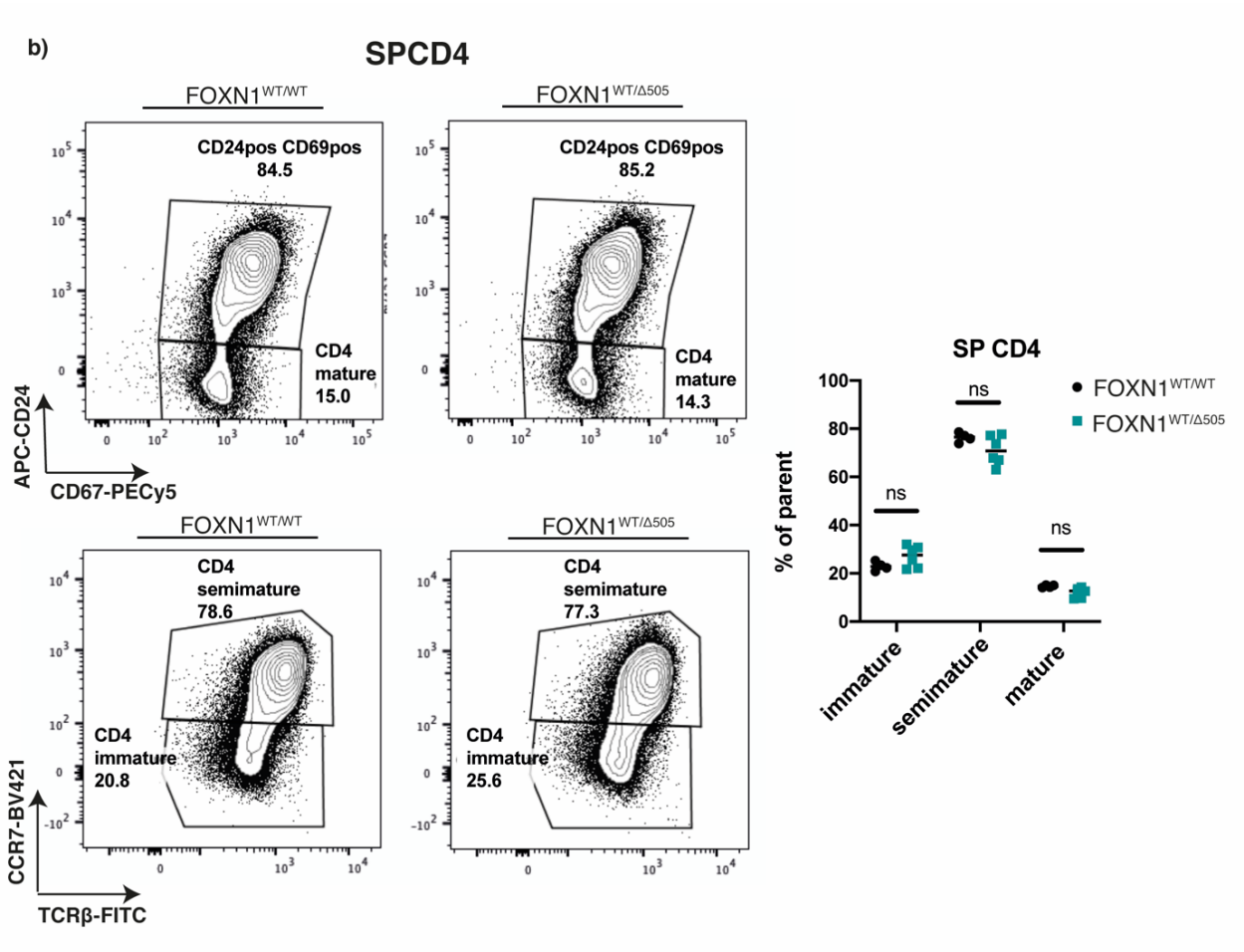


Figure 6.9 Partial maturation block in SPCD8 thymocyte maturation in FOXN1$^{WT/\Delta505}$mice a) top: representative FACS plots of SPCD8 maturation, bottom: scatter plot with their frequencies b) top: representative FACS plots of SPCD4 maturation, bottom: scatter plot with their frequencies. Data shown in graphs are pooled from two independent experiments using female mice at 13 weeks of age [WT (FOXN1$^{WT/WT}$): n=3, heterozygous Δ505 (FOXN1$^{WT/\Delta505}$): n=3] and male mice at 16weeks of age [WT (FOXN1$^{WT/WT}$): n=1; heterozygous Δ505 (FOXN1$^{WT/\Delta505}$): n=3]. Statistical comparison was done using unpaired t-test with correction for multiple comparisons *p<0.05,**p<0.01, ***p<0.001, ****p<0.0001

6.4 DISCUSSION

Human thymus function, as measured by naïve T cell output, reaches its peak during embryonic and early postnatal life[125, 227, 228]. However, after puberty the thymus undergoes a physiological age-related process of involution which is characterised by a loss of tissue architecture and a decline in T cell output [125, 227, 228] This tissue senescence is considered to be primarily caused by changes in TEC biology and numbers [103, 126, 127]. Indeed, thymic epithelial cellularity dramatically declines in humans as early as after the first year of life and the numbers decline dramatically and are replaced over time by fibroblasts and adipocytes[128-130]. FOXN1, has a critical role in this process as its expression progressively declines over time, a feature considered as one of the hallmarks of thymic involution [106, 132]. However, the forced (i.e transgenic) expression of FOXN1 attenuates this process [133].

The FOXN1$^{WT/\Delta 505}$ mice exhibit a reduction in thymus size compared to their WT littermates which correlates with diminished TEC and T cell numbers. A reduction in the frequency of mature mTEC and a decrease in their MHCII expression levels is observed. Their function as measured by the cells ability to promote the expression of the AIRE regulated TRA, Tspan8 was also compromised. In contrast, the frequency of cTEC was increased in mice heterozygous for the *Δ505 Foxn1* allele, while their MHCII levels were unchanged. Interestingly, similar phenotype of reduced mTEC numbers with a corresponding increase in cTEC, was observed in a mouse model exhibiting accelerated thymic involution[110]. In these animals *Foxn1* expression is disrupted due to the insertion of a *LacZ* gene in the 3′-untranslated region of the *Foxn1* locus, resulting in a 60% reduction of normal *Foxn1* mRNA levels. To fully characterise the

mice heterozygous for the *Δ505* allele, further analyses of the tissue architecture, the TEC phenotype during different developmental stages and the transcriptome of TEC subpopulations is planned.

The *Δ505* mutation appears to primarily affect the mTEC^{hi} compartment in the mutant mice. Different FOXN1 dose requirements for different TEC subsets have been inferred by a couple of studies [3, 9, 13, 16-18] which correlated with the observation that distinct TEC subsets express different levels of FOXN1[103, 105]. Adult mTECs express lower levels of FOXN1 compared to cTECs while mTEC^{hi} express higher levels when compared to mTEC^{lo}. [91, 106, 107]. A single study has shown that adult mTEC when compared to cTEC, are more sensitive to the loss of FOXN1, because its postnatal deletion results in dramatic tissue atrophy primarily affecting the medulla and its epithelial[110]. This finding has not been verified by other studies and it remains to be shown whether it is also true for this current study. It also remains to be detailed how *Δ505 Foxn1* heterozygosity affects TEC progenitors or other TEC subsets like nurse cells, a fraction of cTECs involved in thymocyte selection[229].

SPCD8 maturation was also partially blocked in FOXN1$^{WT/\Delta505}$ mice with a reduction in mature SPCD8s. In contrast, the maturation of SPCD4, DN and DP thymocyte subsets was comparable for FOXN1$^{WT/\Delta505}$ and FOXN1$^{WT/WT}$ mice. A possible link between the reduction of mature mTEC and the partial differentiation block in SPCD8s cannot be inferred from the literature as there are no studies suggesting a preferential role of mTEC^{hi} in SPCD8 maturation. However, one study with mice expressing less than 50% of the normal *Foxn1* levels, has made a similar observation of fewer mature mTECs (MHC-II^{hi} CD80^{+} CD86^{+}) and a partial maturational block at the SPCD8 thymocyte stage

[104]. A more extensive study on thymocyte subsets and their selection in FOXN1$^{WT/\Delta505}$ mice is therefore planned for the near future.

Interestingly FOXN1$^{WT/\Delta505}$ mice have on inspection a normal coat and lack any indications of a skin phenotype. This is consistent with previous studies using a series of *Foxn1* hypomorphic alleles[91, 103]. These studies show that although low levels of *Foxn1* severely affect the thymus, they are still sufficient to generate a normal coat. Only the complete loss of functional FOXN1, as is the case in the NUDE mice, impairs hair development. However, subtle changes in keratinocyte development and function have not yet been addressed in studies investigating mice with reduced wild type FOXN1 expression levels.

Finally, the comparison of the phenotype of the FOXN1$^{WT/\Delta505}$ mice to the heterozygous nude mice (FOXN1$^{-/WT}$) would be critical to further test *Δ505 Foxn1's* dominant negative role *in-vivo*. In adult FOXN1$^{-/WT}$ mice the only functional *Foxn1* allele leads to a 50% reduction in the normal *Foxn1* levels. Δ505 *Foxn1* could exert its dominant negative effect *in-vivo* by further reducing the levels of functional FOXN1 to below 50%. Further analysis is necessary in order to test the above hypothesis.

CHAPTER 7

DISCUSSION

7.1 Summary-Proposed mechanism 186

7.2 Future work 192

7.3 Conclusion 196

SUMMARY-PROPOSED MECHANISM

In this study we present evidence that the *Δ550* FOXN1 mutation, found in heterozygous patients with absent thymus and peripheral T cell lymphopenia, is a dominant negative mutant.

To date 11 individuals homozygous for three distinct loss of function mutations in the human *FOXN1* gene have been reported. These patients uniformly present with a form of severe combined immunodeficiency known as NUDE SCID [45, 46, 58, 65, 66]. The mutations that cause this severe pathology are located either in the N-terminus or the forkhead DNA binding domain of the FOXN1 protein and result in a loss of transcriptional function[45, 46, 58, 65, 66]. Individuals heterozygous for these mutations demonstrate normal peripheral T cell numbers in adulthood, albeit a slightly reduced CD8 T cell counts have been noted however do no cause an increase susceptibility to infections [67].

A recent study described 21 adult and paediatric patients with a total of 12 heterozygous *FOXN1* variants located in the C-terminus of the *FOXN1* gene [67]. The majority of these mutations, are single base pair deletions and are predicted to generate a truncated FOXN1 protein of the same length as the *Δ550* FOXN1 mutant. Patients with these mutations have T-cell lymphopenia primarily affecting the CD8 compartment [67]. These individuals were either healthy or demonstrated pathologies among which the upper respiratory track infections were the most common, while a few of them had recurrent severe infections[67]. The location of the mutation did not corelate with the presence or absence of thymic tissue as patients with the same single base pair deletion at protein position 437 could either be athymic or thymic [67]. The authors of this study claim that most of these *FOXN1* variants are

loss of function mutants as the phenotype of the heterozygous patients resembles that of mice heterozygous for a loss of function *Foxn1* allele (NUDE allele) [67]. However, the precise molecular mechanism of these reported mutations was not analysed in any detail and the possibility that some of these variants may act as dominant negative mutants was not excluded.

In this study we showed that the *Δ550* FOXN1 mutant acts *in-vitro* as a dominant negative molecule. Although on its own is transcriptionally inactive when co-expressed with its wild type counterpart in 4D6 thymic epithelial cells, the *Δ550* impairs the transcriptional activity of the WT as shown both by RNA sequencing and a luciferase assay. When $EYFP^{\beta 5t}FOXN1^{CMV}$ 4D6 reporter cells, where EYFP expression correlates with FOXN1's functionality, were transfected with increasing amounts of *Δ550* FOXN1 mutant there was a gradual reduction in the percentage of EYFP positive cells. Finally, the presence of the *Δ550* FOXN1 mutant disrupted the formation of WT FOXN1 homo dimers and WT-FOXN1 nuclear bodies further corroborating its role as a dominant negative mutant.

The *Δ505* FOXN1 variant, the mouse counterpart of the human *Δ550* mutant, also acts as a dominant negative mutant *in-vitro,* as shown by luciferase. *In-vivo* adult male mice heterozygous for the *Δ505* mutant allele exhibit a milder phenotype compared to the *Δ550* patients. These animals have a smaller thymus with increased frequency of cTEC and a partial maturation block in their mTEC differentiation. The functionality of mTEC, as assessed by their ability to promote TRA expression, was also impaired. Correlating with these changes there was a maturational block at later stages of CD8 T cell lineage development resulting in fewer SPCD8 T cells. In contrast, mice heterozygous for a loss of function *FOXN1* allele ($FOXN1^{WT/-}$) exhibit a similar phenotype during their first

week of life however at about 5 weeks of age their TEC phenotype resolves and resembles that of wild type mice[67]. To exclude the possibility that the phenotype observed in the FOXN1$^{WT/\Delta505}$ mice is not the consequence of a *Δ505* FOXN1 haplo-insufficiency but rather the result of a dominant negative interference with the wild type molecule *in-vivo*, a comparison of the TEC and T cell phenotype of the FOXN1$^{WT/\Delta505}$ with FOXN1$^{WT/-}$ mice at 16 weeks of age is required.

The work presented here also provides a detailed understanding of the molecular mechanism of FOXN1 function (Figure 7.1). Under physiological conditions, WT-FOXN1 forms homodimers in the nucleus of 4D6 thymic epithelial cells. Several of these homo-dimeric complexes come together to form microscopically visible higher ordered structures. These structures resemble nuclear bodies and exhibit key properties of membrane-less organelles [195, 197]. WT-GFP molecules are dynamically recruited to these organelles and appear to be continuously replaced as demonstrated by an efficient reconstitution after photobleaching. This latter property of the nuclear bodies distinguishes them from protein aggregates (e.g. amyloid plagues) that appear in the nucleus in the context of certain pathologies [195]. Importantly, the diffusion within the WT-GFP nuclear bodies is significantly slower when compared to areas in the rest of the nucleoplasm underscoring biologically meaningful interactions of FOXN1 with other yet to be defined molecules.

The proteomics study demonstrated that the acetylotransferase CBP is one of several putative FOXN1 partners. CBP's functional interaction with FOXN1 was shown using the EYFP$^{\beta5t}$FOXN1^{CMV} 4D6 reporter cells, as the deletion of CBP using CRISPR/cas9 significantly reduced the cells' competence for FOXN1 controlled transcription. However, the precise mechanism by which this occurs remains to be elucidated.

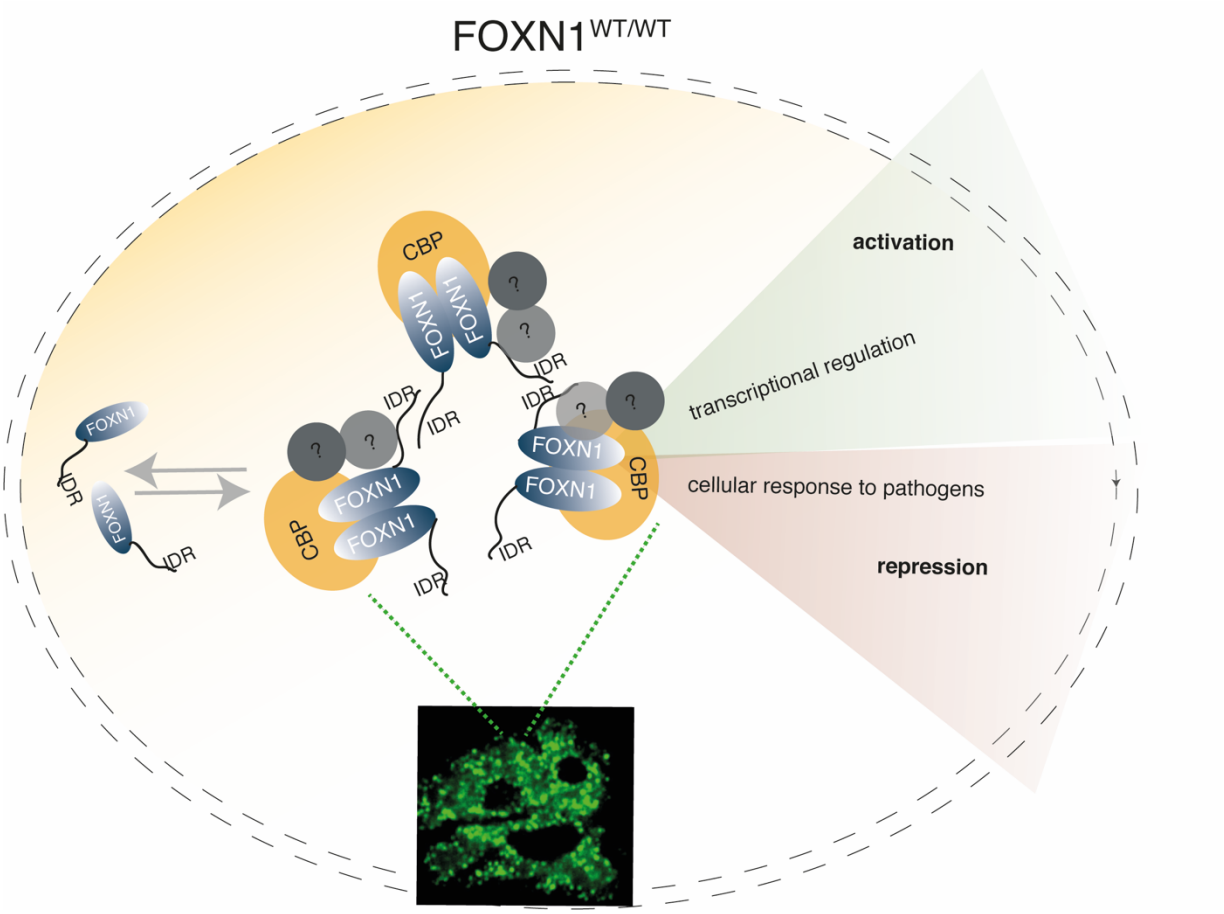


Figure 7.1: A proposed mechanism for WT-FOXN1 function. In the nucleus of thymic epithelial 4D6 cells, wild type FOXN1 molecules form homodimers. Several of these homodimers create higher ordered structures, resembling nuclear bodies. WT-GFP molecules are dynamically recruited to these membraneless organelles. Other proteins, including CBP, are predicted to be part of these structures. Ultimately the formation of the WT FOXN1 complexes is required for its function as a transcriptional regulator. IDR: intrinsically disordered region

How the *Δ550* FOXN1 mutant exerts its dominant negative effect on wild type FOXN1 was also investigated (Figure 7.2). The *Δ550* FOXN1 mutant is transcriptionally inactive due to the loss of the C-terminal tail containing part of the transcriptional activation domain. However, the forkhead domain, allowing for DNA binding, is still intact allowing the *Δ550* mutant to bind to the canonical FOXN1 binding motif upstream of genes normally regulated by the WT FOXN1. Our proteomics study also showed that the *Δ550* FOXN1 mutant can still interact with CBP. We therefore hypothesised that

the *Δ550* mutant either as a homo-dimer (Figure 7.2a) or monomer (Figure 7.2b) could form non-functional complexes with CBP and possible other FOXN1 co-factors that are present in the nucleus in limiting amounts and thus sequestering binding partners away from the WT FOXN1(Figure 7.2c). Importantly complexes with non-functional *Δ550* FOXN1 still bind the relevant DNA motifs thus displacing WT FOXN1 lacking co-factor binding. As a result, transcription is largely blocked. Some WT FOXN1 molecules would however still be able to form a limited number of functional complexes that may account for some limited transcriptional activity (Figure 7.2d).

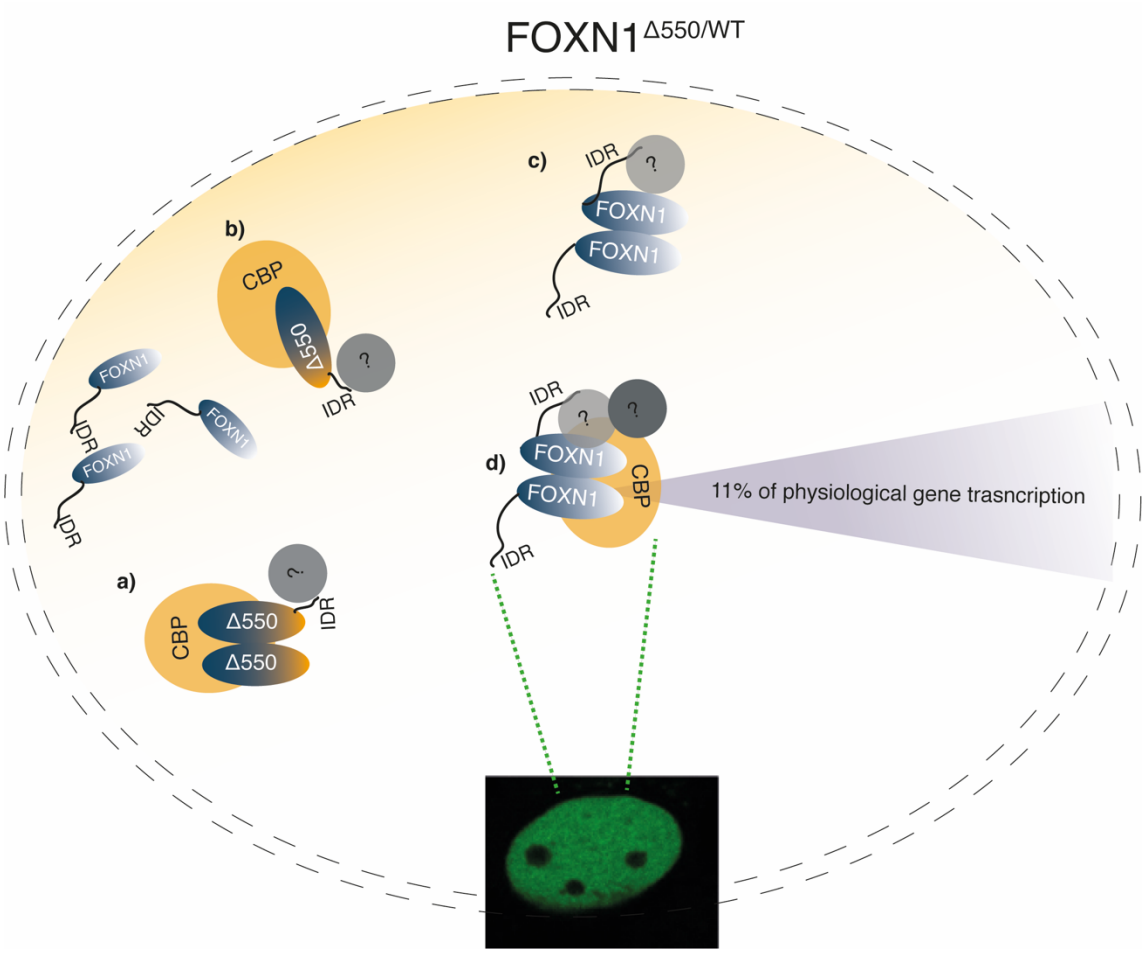


Figure 7.2: A proposed mechanism for the function of the dominant negative *Δ550*-FOXN1 mutant. *Δ550* FOXN1 mutant forms non-functional homo-dimers (a) or monomers (b) in complex with CBP and possible other FOXN1 co-factors, thus recruiting these partners away from WT FOXN1 (c). The non-functional *Δ550* FOXN1 complex is still able to occupy canonical DNA binding motifs normally occupied by WT FOXN1 but it is transcriptionally inactive. However, some complexes containing WT FOXN1 molecules still form thus accounting for a limited transcriptional activity (d). IDR: intrinsically disordered region

FUTURE WORK

The role and unique importance of FOXN1 as a master regulator of the transcriptional network that determines TEC identity has been previously established [44, 91, 104, 136, 137, 139]. Our *in-vitro* study recapitulates these findings, by showing that FOXN1 can act both as a repressor and an activator in 4D6 thymic epithelial cells. Several aspects related to FOXN1 biology remain unexplored. For example, whether FOXN1 preferentially acts as a transcriptional repressor or activator at different stages of thymus organogenesis remains to be determined, as has been shown for, Foxd3 and FOXA1, two other members of the forkhead family [185, 230]. At initial stages of neuro crest development Foxd3 (forkhead box protein D3), can act both as a transcriptional activator and a repressor, however over time there is a gradual shift towards a repressive activity[185].

A series of studies have associated FOXN1 with the expression of individual genes linked to TEC function, like *DLL4, β5t* and *CD83* [91, 104, 136, 137]. One study in particular identified a set of 450 high confidence FOXN1 targets in primary TEC from one-week old mice[104]. How this pool of FOXN1 regulated genes changes over development to define TEC identity and facilitate TEC function has not been examined. Little is also known about the mechanisms that govern the FOXN1-DNA interaction throughout different stages of thymus development. The FOXN1 core binding sequence *GACGC*, has been previously described [104, 218] and confirmed in the present study. However, studies on transcription factor-DNA binding interactions have pointed towards additional layers of complexity, beyond the DNA recognition motif, that modulate this interaction[211]. Our previous study has shown that the presence of methylation on the CpG nucleotides in the *GACGC* FOXN1 binding motif reduces

FOXN1's ability to bind to DNA[87]. Since the extent of methylation of promoters increases while FOXN1 decreases with age, it is conceivable that FOXN1 mediated target gene recognition and expression is diminished as a result of these sequence related changes. However, this remains to be formally shown. Indeed, it has been shown that FOXN1 target genes are differentially affected by FOXN1 levels at different stages of development[67].

The work presented here identified, to my best of knowledge, a FOXN1 interactome, and I present also for the first time evidence that FOXN1 forms homo-dimers. Under conditions when these complexes are disrupted, e.g. in the presence of the dominant negative *Δ550* FOXN1 mutant, FOXN1's transcriptional competence is severely compromised albeit not completely abolished, as shown in this thesis using RNA-Seq analysis of 4D6 cells transfected with both WT and *Δ550* FOXN1. This brings up the question whether WT-FOXN1 is able to regulate transcription of target genes not only as a dimer but also as a monomer. Interestingly, purified WT-FOXN1 protein was found to bind with a higher affinity to a DNA probe containing a tandem compared to a single FOXN1 binding motif (unpublished data by Dr Joseph Newman). However, in silico analysis revealed the presence of a tandem FOXN1 binding motif in the promoters of only 19% of the high confidence FOXN1 targets described in mouse primary TEC (unpublished data by Dr Adam Handel). Whether one or both FOXN1 molecules in a homo-dimer interact with DNA and whether the formation of FOXN1 homo-dimers occurs independently but is then required for DNA binding or alternatively whether dimerization is a consequence of DNA binding also remain to be explored.

The molecular consistency and the exact role of FOXN1 nuclear bodies needs also to be examined in more detail. Different types of nuclear bodies have been defined, each

with distinct functions[231]. Among them, the so-called nuclear speckles are enriched for mRNA splicing factors and are often in close proximity to actively transcribed genes[231]. Indeed, the list of putative FOXN1 binding partners identified by our proteomics study includes mRNA splicing factors and proteins involved in transcriptional regulation. The assumed physical interactions between FOXN1 and these molecules awaits further verification by reciprocal co-IPs and their colocalization with FOXN1 within nuclear bodies also needs to be shown. Finally, the function of individual binding partners of FOXN1 will also need to be elucidated for example in the EYFP$^{\beta 5t}$FOXN1^{CMV} 4D6 reporter cell line. These cells will allow to interrogate their cooperative function in FOXN1 controlled transcription.

Here we propose that the formation of FOXN1-containing nuclear bodies is essential for FOXN1 mediated transcriptional regulation, since their disruption is associated with impaired FOXN1 functionality. Therefore, it will be informative whether any of these factors plays a role in the formation of these nuclear bodies. Whether the acetylotransferase CBP, shown here to have a functional relationship with FOXN1, has an active role in the formation of the FOXN1 nuclear bodies has not been officially shown. One study proposed that the acetylation by CBP, or other acetyltransferases, of intrinsically disordered protein regions (IDR) can control the formation of nuclear bodies [216]. Whether this mechanism is true for FOXN1 needs to be further explored. Finally, elucidating the molecular networks upstream of FOXN1 could greatly assist in studies that target *FOXN1* with the purpose of thymus regeneration. In this study we showed that transcription of the *Δ550* FOXN1 mutant gene resulted in increased mRNA, but decreased protein levels when compared to WT FOXN1 transcripts and protein respectively. This finding could point to a positive feedback mechanism

whereby an increased degradation of the mutant protein drives *FOXN1* transcription, a concept that already has been suggested for WT FOXN1 in two independent studies [133, 138]. Notably a FOXN1 DNA binding motif can be detected upstream of the *Foxn1* coding sequence (A. Handel personal communication) further supporting the concept of a positive feedback loop that maintains adequate FOXN1 concentration.

In addition to a FOXN1 autoregulatory loop, there is indirect evidence for other factors involved in the regulation of *FOXN1* expression[140], [141, 142], [143-145]. For example, the loss of gene expression for Pax9, Pax1 transcription factors results in athymia or thymic hypoplasia in mice [141, 142]. While loss of *Hoxa2* (homeobox A2), *Eya1* (Eyes Absent Homolog 1) or *Six1* (Sine Oculis Homeobox Homolog 1) disrupt normal TEC development [143-145]. Ectopic *Tbx1* expression in FOXN1 expressing cells of the E11.5 3pharyngyal pouch leads to downregulation of *Foxn1* [147] indicating that TBX1 suppresses TEC differentiation. However, these factors have not been shown to directly bind to *Foxn1* regulatory regions *in vivo* as to control *Foxn1* expression.

CONCLUSION

FOXN1 plays a critical role in thymus biology, acting as a unique transcriptional regulator of the development, function and maintenance of the thymic epithelium. This study provides a deeper understanding into the molecular mechanisms by which FOXN1 functions. The findings described here may furthermore assist in future studies designed to target FOXN1 expression and function for the purposes of thymus regeneration in the context of senescence or impairment secondarily to chemo-radio therapy. Finally, this work may also provide a broader understanding of how master transcriptional regulators control complex gene expression programs during tissue development and for the establishment of specific cell functions.

To my best of knowledge, this is the first study describing a dominant negative *FOXN1* mutant. Although several patients with mutations in the C-terminus of the *FOXN1* gene and various pathologies, have recently been identified it is this study that provides a more detailed mechanism how some of these mutants may impact on thymus organogenesis.

REFERENCES

1. Miller, J.F., *The golden anniversary of the thymus.* Nat Rev Immunol, 2011. **11**(7): p. 489-95.
2. Miller, J.F., *Immunological function of the thymus.* Lancet, 1961. **2**(7205): p. 748-9.
3. Bajoghli, B., et al., *A thymus candidate in lampreys.* Nature, 2011. **470**: p. 90.
4. Boyd, R.L., et al., *The thymic microenvironment.* Immunol Today, 1993. **14**(9): p. 445-59.
5. Boehm, T., et al., *Thymic medullary epithelial cell differentiation, thymocyte emigration, and the control of autoimmunity require lympho-epithelial cross talk via LTbetaR.* The Journal of experimental medicine, 2003. **198**(5): p. 757-769.
6. Brunk, F., et al., *Dissecting and modeling the emergent murine TEC compartment during ontogeny.* European Journal of Immunology, 2017. **47**(7): p. 1153-1159.
7. Takahama, Y., *Journey through the thymus: stromal guides for T-cell development and selection.* Nature Reviews Immunology, 2006. **6**(2): p. 127-135.
8. Anderson, G. and Y. Takahama, *Thymic epithelial cells: working class heroes for T cell development and repertoire selection.* Trends Immunol, 2012. **33**(6): p. 256-63.
9. Nehls, M., et al., *Two genetically separable steps in the differentiation of thymic epithelium.* Science, 1996. **272**(5263): p. 886-9.
10. Lind, E.F., et al., *Mapping precursor movement through the postnatal thymus reveals specific microenvironments supporting defined stages of early lymphoid development.* J Exp Med, 2001. **194**(2): p. 127-34.
11. Plotkin, J., et al., *Critical role for CXCR4 signaling in progenitor localization and T cell differentiation in the postnatal thymus.* J Immunol, 2003. **171**(9): p. 4521-7.
12. Misslitz, A., et al., *Thymic T cell development and progenitor localization depend on CCR7.* J Exp Med, 2004. **200**(4): p. 481-91.
13. Benz, C., K. Heinzel, and C.C. Bleul, *Homing of immature thymocytes to the subcapsular microenvironment within the thymus is not an absolute requirement for T cell development.* Eur J Immunol, 2004. **34**(12): p. 3652-63.
14. Fiorini, E., et al., *Cutting edge: thymic crosstalk regulates delta-like 4 expression on cortical epithelial cells.* J Immunol, 2008. **181**(12): p. 8199-203.
15. Ciofani, M. and J.C. Zuniga-Pflucker, *Notch promotes survival of pre-T cells at the beta-selection checkpoint by regulating cellular metabolism.* Nat Immunol, 2005. **6**(9): p. 881-8.
16. Carpenter, A.C. and R. Bosselut, *Decision checkpoints in the thymus.* Nature immunology, 2010. **11**(8): p. 666-673.
17. Klein, L., et al., *Antigen presentation in the thymus for positive selection and central tolerance induction.* Nature Reviews Immunology, 2009. **9**: p. 833.
18. Witt, C.M., et al., *Directed migration of positively selected thymocytes visualized in real time.* PLoS Biol, 2005. **3**(6): p. e160.

19. Sansom, S.N., et al., *Population and single-cell genomics reveal the Aire dependency, relief from Polycomb silencing, and distribution of self-antigen expression in thymic epithelia.* Genome Res, 2014. **24**(12): p. 1918-31.
20. St-Pierre, C., et al., *Transcriptome sequencing of neonatal thymic epithelial cells.* Scientific Reports, 2013. **3**: p. 1860.
21. Derbinski, J., et al., *Promiscuous gene expression in medullary thymic epithelial cells mirrors the peripheral self.* Nat Immunol, 2001. **2**(11): p. 1032-9.
22. Anderson, M.S., et al., *Projection of an immunological self shadow within the thymus by the aire protein.* Science, 2002. **298**(5597): p. 1395-401.
23. Hasegawa, H. and T. Matsumoto, *Mechanisms of Tolerance Induction by Dendritic Cells In Vivo.* Frontiers in immunology, 2018. **9**: p. 350-350.
24. McCaughtry, T.M., et al., *Clonal deletion of thymocytes can occur in the cortex with no involvement of the medulla.* The Journal of Experimental Medicine, 2008. **205**(11): p. 2575-2584.
25. Liston, A., et al., *Aire regulates negative selection of organ-specific T cells.* Nat Immunol, 2003. **4**(4): p. 350-4.
26. *An autoimmune disease, APECED, caused by mutations in a novel gene featuring two PHD-type zinc-finger domains.* Nat Genet, 1997. **17**(4): p. 399-403.
27. Anderson, G. and E.J. Jenkinson, *Lymphostromal interactions in thymic development and function.* Nat Rev Immunol, 2001. **1**(1): p. 31-40.
28. Cowan, J.E., W.E. Jenkinson, and G. Anderson, *Thymus medulla fosters generation of natural Treg cells, invariant gammadelta T cells, and invariant NKT cells: what we learn from intrathymic migration.* Eur J Immunol, 2015. **45**(3): p. 652-60.
29. Manley, N.R., et al., *Structure and function of the thymic microenvironment.* Front Biosci (Landmark Ed), 2011. **16**: p. 2461-77.
30. Shah, D.K. and J.C. Zuniga-Pflucker, *An overview of the intrathymic intricacies of T cell development.* J Immunol, 2014. **192**(9): p. 4017-23.
31. Brenner, M.B., et al., *Identification of a putative second T-cell receptor.* Nature, 1986. **322**(6075): p. 145-9.
32. Reinherz, E.L., *Revisiting the Discovery of the αβ TCR Complex and Its Co-Receptors.* Frontiers in immunology, 2014. **5**: p. 583-583.
33. Rast, J.P., et al., *alpha, beta, gamma, and delta T cell antigen receptor genes arose early in vertebrate phylogeny.* Immunity, 1997. **6**(1): p. 1-11.
34. Jung, D. and F.W. Alt, *Unraveling V(D)J recombination; insights into gene regulation.* Cell, 2004. **116**(2): p. 299-311.
35. Oettinger, M.A., et al., *RAG-1 and RAG-2, adjacent genes that synergistically activate V(D)J recombination.* Science, 1990. **248**(4962): p. 1517-23.
36. Repasky, J.A., et al., *Mutational analysis of terminal deoxynucleotidyltransferase-mediated N-nucleotide addition in V(D)J recombination.* J Immunol, 2004. **172**(9): p. 5478-88.
37. Meier, J.T. and S.M. Lewis, *P nucleotides in V(D)J recombination: a fine-structure analysis.* Molecular and Cellular Biology, 1993. **13**(2): p. 1078-1092.

38. Borg, N.A., et al., *The CDR3 regions of an immunodominant T cell receptor dictate the 'energetic landscape' of peptide-MHC recognition.* Nature Immunology, 2005. **6**(2): p. 171-180.
39. Fischer, A., et al., *Severe combined immunodeficiencies and related disorders.* Nature Reviews Disease Primers, 2015. **1**: p. 15061.
40. Fischer, A., et al., *Severe combined immunodeficiency. A model disease for molecular immunology and therapy.* Immunol Rev, 2005. **203**: p. 98-109.
41. Buckley, R.H., *Molecular defects in human severe combined immunodeficiency and approaches to immune reconstitution.* Annu Rev Immunol, 2004. **22**: p. 625-55.
42. Cirillo, E., et al., *Severe combined immunodeficiency--an update.* Ann N Y Acad Sci, 2015. **1356**: p. 90-106.
43. Chan, K. and J.M. Puck, *Development of population-based newborn screening for severe combined immunodeficiency.* J Allergy Clin Immunol, 2005. **115**(2): p. 391-8.
44. Vaidya, H.J., A. Briones Leon, and C.C. Blackburn, *FOXN1 in thymus organogenesis and development.* European journal of immunology, 2016. **46**(8): p. 1826-1837.
45. Frank, J., et al., *Exposing the human nude phenotype.* Nature, 1999. **398**(6727): p. 473-4.
46. Rota, I.A. and F. Dhalla, *FOXN1 deficient nude severe combined immunodeficiency.* Orphanet journal of rare diseases, 2017. **12**(1): p. 6-6.
47. Romano, R., et al., *FOXN1: A Master Regulator Gene of Thymic Epithelial Development Program.* Front Immunol, 2013. **4**: p. 187.
48. Nehls, M., et al., *New member of the winged-helix protein family disrupted in mouse and rat nude mutations.* Nature, 1994. **372**(6501): p. 103-7.
49. Kaestner, K.H., W. Knochel, and D.E. Martinez, *Unified nomenclature for the winged helix/forkhead transcription factors.* Genes Dev, 2000. **14**(2): p. 142-6.
50. Brissette, J.L., et al., *The product of the mouse nude locus, Whn, regulates the balance between epithelial cell growth and differentiation.* Genes Dev, 1996. **10**(17): p. 2212-21.
51. Li, J., et al., *Foxn1 promotes keratinocyte differentiation by regulating the activity of protein kinase C.* Differentiation, 2007. **75**(8): p. 694-701.
52. Baxter, R.M. and J.L. Brissette, *Role of the Nude Gene in Epithelial Terminal Differentiation.* Journal of Investigative Dermatology, 2002. **118**(2): p. 303-309.
53. Schlake, T., et al., *The nude gene encodes a sequence-specific DNA binding protein with homologs in organisms that lack an anticipatory immune system.* Proceedings of the National Academy of Sciences of the United States of America, 1997. **94**(8): p. 3842-3847.
54. Su, D.M., et al., *A domain of Foxn1 required for crosstalk-dependent thymic epithelial cell differentiation.* Nat Immunol, 2003. **4**(11): p. 1128-35.
55. Schüddekopf, K., M. Schorpp, and T. Boehm, *The whn transcription factor encoded by the nude locus contains an evolutionarily conserved and functionally indispensable activation domain.* Proceedings of the National

Academy of Sciences of the United States of America, 1996. **93**(18): p. 9661-9664.
56. Coffer, P.J. and B.M.T. Burgering, *Forkhead-box transcription factors and their role in the immune system.* Nat Rev Immunol, 2004. **4**(11): p. 889-899.
57. Pignata, C., et al., *Congenital Alopecia and nail dystrophy associated with severe functional T-cell immunodeficiency in two sibs.* Am J Med Genet, 1996. **65**(2): p. 167-70.
58. Pignata, C., A. Fusco, and S. Amorosi, *Human clinical phenotype associated with FOXN1 mutations.* Adv Exp Med Biol, 2009. **665**: p. 195-206.
59. Chou, J., et al., *A novel mutation in FOXN1 resulting in SCID: a case report and literature review.* Clin Immunol, 2014. **155**(1): p. 30-2.
60. Levy, E., et al., *[Post-thymus transplant vitiligo in a child with Foxn1 deficiency].* Ann Dermatol Venereol, 2012. **139**(6-7): p. 468-71.
61. Firtina, S., et al., *A Novel FOXN1 Variant Is Identified in Two Siblings with Nude Severe Combined Immunodeficiency.* J Clin Immunol, 2019. **39**(2): p. 144-147.
62. Flanagan, S.P., *'Nude', a new hairless gene with pleiotropic effects in the mouse.* Genet Res, 1966. **8**(3): p. 295-309.
63. Pantelouris, E.M., *Absence of thymus in a mouse mutant.* Nature, 1968. **217**(5126): p. 370-1.
64. Wortis, H.H., S. Nehlsen, and J.J. Owen, *Abnormal development of the thymus in "nude" mice.* The Journal of experimental medicine, 1971. **134**(3 Pt 1): p. 681-692.
65. Pignata, C., et al., *Human equivalent of the mouse Nude/SCID phenotype: long-term evaluation of immunologic reconstitution after bone marrow transplantation.* Blood, 2001. **97**(4): p. 880-885.
66. Markert, M.L., et al., *First use of thymus transplantation therapy for FOXN1 deficiency (nude/SCID): a report of 2 cases.* Blood, 2011. **117**(2): p. 688-96.
67. Bosticardo, M., et al., *Heterozygous FOXN1 Variants Cause Low TRECs and Severe T Cell Lymphopenia, Revealing a Crucial Role of FOXN1 in Supporting Early Thymopoiesis.* Am J Hum Genet, 2019. **105**(3): p. 549-561.
68. Abitbol, M., et al., *A Deletion in FOXN1 Is Associated with a Syndrome Characterized by Congenital Hypotrichosis and Short Life Expectancy in Birman Cats.* PLOS ONE, 2015. **10**(3): p. e0120668.
69. Benayoun, B.A., S. Caburet, and R.A. Veitia, *Forkhead transcription factors: key players in health and disease.* Trends Genet, 2011. **27**(6): p. 224-32.
70. Hope, I.A., et al., *The forkhead gene family of Caenorhabditis elegans.* Gene, 2003. **304**: p. 43-55.
71. Jackson, B.C., et al., *Update of human and mouse forkhead box (FOX) gene families.* Hum Genomics, 2010. **4**(5): p. 345-52.
72. Coffer, P.J. and B.M. Burgering, *Forkhead-box transcription factors and their role in the immune system.* Nat Rev Immunol, 2004. **4**(11): p. 889-99.
73. Brunkow, M.E., et al., *Disruption of a new forkhead/winged-helix protein, scurfin, results in the fatal lymphoproliferative disorder of the scurfy mouse.* Nat Genet, 2001. **27**(1): p. 68-73.

74. Hori, S., T. Nomura, and S. Sakaguchi, *Control of regulatory T cell development by the transcription factor Foxp3.* Science, 2003. **299**(5609): p. 1057-61.
75. Castrillon, D.H., et al., *Suppression of ovarian follicle activation in mice by the transcription factor Foxo3a.* Science, 2003. **301**(5630): p. 215-8.
76. Lin, L., J.D. Hron, and S.L. Peng, *Regulation of NF-kappaB, Th activation, and autoinflammation by the forkhead transcription factor Foxo3a.* Immunity, 2004. **21**(2): p. 203-13.
77. Hannenhalli, S. and K.H. Kaestner, *The evolution of Fox genes and their role in development and disease.* Nat Rev Genet, 2009. **10**(4): p. 233-40.
78. Lai, E., et al., *HNF-3A, a hepatocyte-enriched transcription factor of novel structure is regulated transcriptionally.* Genes Dev, 1990. **4**(8): p. 1427-36.
79. Clark, K.L., et al., *Co-crystal structure of the HNF-3/fork head DNA-recognition motif resembles histone H5.* Nature, 1993. **364**(6436): p. 412-20.
80. Weigelt, J., et al., *Solution structure of the DNA binding domain of the human forkhead transcription factor AFX (FOXO4).* Biochemistry, 2001. **40**(20): p. 5861-9.
81. Obsil, T. and V. Obsilova, *Structure/function relationships underlying regulation of FOXO transcription factors.* Oncogene, 2008. **27**(16): p. 2263-75.
82. Seoane, J., et al., *Integration of Smad and forkhead pathways in the control of neuroepithelial and glioblastoma cell proliferation.* Cell, 2004. **117**(2): p. 211-23.
83. Tsai, K.L., et al., *Crystal structure of the human FOXK1a-DNA complex and its implications on the diverse binding specificity of winged helix/forkhead proteins.* J Biol Chem, 2006. **281**(25): p. 17400-9.
84. Greer, E.L., et al., *The energy sensor AMP-activated protein kinase directly regulates the mammalian FOXO3 transcription factor.* J Biol Chem, 2007. **282**(41): p. 30107-19.
85. Li, B., et al., *FOXP3 interactions with histone acetyltransferase and class II histone deacetylases are required for repression.* Proc Natl Acad Sci U S A, 2007. **104**(11): p. 4571-6.
86. van der Horst, A., et al., *FOXO4 transcriptional activity is regulated by monoubiquitination and USP7/HAUSP.* Nat Cell Biol, 2006. **8**(10): p. 1064-73.
87. Newman, J.A., et al., *The structural basis for forkhead box family specificity revealed by the crystal structure of human FOXN1 in complex with DNA.* bioRxiv, 2018: p. 428011.
88. Brent, M.M., R. Anand, and R. Marmorstein, *Structural basis for DNA recognition by FoxO1 and its regulation by posttranslational modification.* Structure, 2008. **16**(9): p. 1407-16.
89. Cirillo, L.A., et al., *Opening of compacted chromatin by early developmental transcription factors HNF3 (FoxA) and GATA-4.* Mol Cell, 2002. **9**(2): p. 279-89.
90. Cirillo, L.A., et al., *Binding of the winged-helix transcription factor HNF3 to a linker histone site on the nucleosome.* Embo j, 1998. **17**(1): p. 244-54.

91. Nowell, C.S., et al., *Foxn1 regulates lineage progression in cortical and medullary thymic epithelial cells but is dispensable for medullary sublineage divergence.* PLoS Genet, 2011. **7**(11): p. e1002348.
92. Swann, J.B., et al., *Conversion of the thymus into a bipotent lymphoid organ by replacement of FOXN1 with its paralog, FOXN4.* Cell Rep, 2014. **8**(4): p. 1184-97.
93. Gordon, J., et al., *Gcm2 and Foxn1 mark early parathyroid- and thymus-specific domains in the developing third pharyngeal pouch.* Mech Dev, 2001. **103**(1-2): p. 141-3.
94. Farley, A.M., et al., *Dynamics of thymus organogenesis and colonization in early human development.* Development, 2013. **140**(9): p. 2015-26.
95. Cordier, A.C. and J.F. Heremans, *Nude mouse embryo: ectodermal nature of the primordial thymic defect.* Scand J Immunol, 1975. **4**(2): p. 193-6.
96. Blackburn, C.C., et al., *The nu gene acts cell-autonomously and is required for differentiation of thymic epithelial progenitors.* Proc Natl Acad Sci U S A, 1996. **93**(12): p. 5742-6.
97. Nowell, C.S., et al., *Foxn1 regulates lineage progression in cortical and medullary thymic epithelial cells but is dispensable for medullary sublineage divergence.* PLoS genetics, 2011. **7**(11): p. e1002348-e1002348.
98. Muñoz, J.J., et al., *Can a Proper T-Cell Development Occur in an Altered Thymic Epithelium? Lessons From EphB-Deficient Thymi.* Frontiers in endocrinology, 2018. **9**: p. 135-135.
99. Itoi, M., et al., *Two distinct steps of immigration of hematopoietic progenitors into the early thymus anlage.* International Immunology, 2001. **13**(9): p. 1203-1211.
100. Mori, K., et al., *Foxn1 is essential for vascularization of the murine thymus anlage.* Cellular Immunology, 2010. **260**(2): p. 66-69.
101. Liu, C., et al., *The role of CCL21 in recruitment of T-precursor cells to fetal thymi.* Blood, 2005. **105**(1): p. 31-9.
102. Bryson, J.L., et al., *Cell-autonomous defects in thymic epithelial cells disrupt endothelial-perivascular cell interactions in the mouse thymus.* PLoS One, 2013. **8**(6): p. e65196.
103. Chen, L., S. Xiao, and N.R. Manley, *Foxn1 is required to maintain the postnatal thymic microenvironment in a dosage-sensitive manner.* Blood, 2009. **113**(3): p. 567-74.
104. Zuklys, S., et al., *Foxn1 regulates key target genes essential for T cell development in postnatal thymic epithelial cells.* Nat Immunol, 2016. **17**(10): p. 1206-1215.
105. Itoi, M., N. Tsukamoto, and T. Amagai, *Expression of Dll4 and CCL25 in Foxn1-negative epithelial cells in the post-natal thymus.* Int Immunol, 2007. **19**(2): p. 127-32.
106. Rode, I., et al., *Foxn1 Protein Expression in the Developing, Aging, and Regenerating Thymus.* J Immunol, 2015. **195**(12): p. 5678-87.
107. Ki, S., et al., *Global transcriptional profiling reveals distinct functions of thymic stromal subsets and age-related changes during thymic involution.* Cell Rep, 2014. **9**(1): p. 402-415.

108. Gray, D., et al., *Proliferative arrest and rapid turnover of thymic epithelial cells expressing Aire.* J Exp Med, 2007. **204**(11): p. 2521-8.
109. Rossi, S.W., et al., *RANK signals from CD4(+)3(-) inducer cells regulate development of Aire-expressing epithelial cells in the thymic medulla.* J Exp Med, 2007. **204**(6): p. 1267-72.
110. Cheng, L., et al., *Postnatal tissue-specific disruption of transcription factor FoxN1 triggers acute thymic atrophy.* The Journal of biological chemistry, 2010. **285**(8): p. 5836-5847.
111. Cheng, L., et al., *Postnatal tissue-specific disruption of transcription factor FoxN1 triggers acute thymic atrophy.* J Biol Chem, 2010. **285**(8): p. 5836-47.
112. Corbeaux, T., et al., *Thymopoiesis in mice depends on a Foxn1-positive thymic epithelial cell lineage.* Proc Natl Acad Sci U S A, 2010. **107**(38): p. 16613-8.
113. Barsanti, M., et al., *A novel Foxn1(eGFP/+) mouse model identifies Bmp4-induced maintenance of Foxn1 expression and thymic epithelial progenitor populations.* Eur J Immunol, 2017. **47**(2): p. 291-304.
114. O'Neill, K.E., et al., *Foxn1 Is Dynamically Regulated in Thymic Epithelial Cells during Embryogenesis and at the Onset of Thymic Involution.* PLOS ONE, 2016. **11**(3): p. e0151666.
115. Vroegindeweij, E., et al., *Thymic cysts originate from Foxn1 positive thymic medullary epithelium.* Mol Immunol, 2010. **47**(5): p. 1106-13.
116. Bennett, A.R., et al., *Identification and characterization of thymic epithelial progenitor cells.* Immunity, 2002. **16**(6): p. 803-14.
117. Gill, J., et al., *Generation of a complete thymic microenvironment by MTS24(+) thymic epithelial cells.* Nat Immunol, 2002. **3**(7): p. 635-42.
118. Rossi, S.W., et al., *Clonal analysis reveals a common progenitor for thymic cortical and medullary epithelium.* Nature, 2006. **441**(7096): p. 988-91.
119. Onder, L., et al., *Alternative NF-kappaB signaling regulates mTEC differentiation from podoplanin-expressing precursors in the cortico-medullary junction.* Eur J Immunol, 2015. **45**(8): p. 2218-31.
120. Ulyanchenko, S., et al., *Identification of a Bipotent Epithelial Progenitor Population in the Adult Thymus.* Cell Rep, 2016. **14**(12): p. 2819-32.
121. Lopes, N., et al., *Thymic Crosstalk Coordinates Medulla Organization and T-Cell Tolerance Induction.* Front Immunol, 2015. **6**: p. 365.
122. Hamazaki, Y., et al., *Medullary thymic epithelial cells expressing Aire represent a unique lineage derived from cells expressing claudin.* Nat Immunol, 2007. **8**(3): p. 304-11.
123. Sekai, M., Y. Hamazaki, and N. Minato, *Medullary thymic epithelial stem cells maintain a functional thymus to ensure lifelong central T cell tolerance.* Immunity, 2014. **41**(5): p. 753-61.
124. Shakib, S., et al., *Checkpoints in the development of thymic cortical epithelial cells.* J Immunol, 2009. **182**(1): p. 130-7.
125. Chaudhry, M.S., et al., *Thymus: the next (re)generation.* Immunol Rev, 2016. **271**(1): p. 56-71.
126. Lynch, H.E., et al., *Thymic involution and immune reconstitution.* Trends Immunol, 2009. **30**(7): p. 366-73.

127. Gui, J., et al., *Thymus Size and Age-related Thymic Involution: Early Programming, Sexual Dimorphism, Progenitors and Stroma.* Aging Dis, 2012. **3**(3): p. 280-90.
128. Aw, D., et al., *Architectural changes in the thymus of aging mice.* Aging Cell, 2008. **7**(2): p. 158-67.
129. Yang, H., Y.H. Youm, and V.D. Dixit, *Inhibition of thymic adipogenesis by caloric restriction is coupled with reduction in age-related thymic involution.* J Immunol, 2009. **183**(5): p. 3040-52.
130. Gray, D.H., et al., *Developmental kinetics, turnover, and stimulatory capacity of thymic epithelial cells.* Blood, 2006. **108**(12): p. 3777-85.
131. Youm, Y.H., et al., *Prolongevity hormone FGF21 protects against immune senescence by delaying age-related thymic involution.* Proc Natl Acad Sci U S A, 2016. **113**(4): p. 1026-31.
132. Ortman, C.L., et al., *Molecular characterization of the mouse involuted thymus: aberrations in expression of transcription regulators in thymocyte and epithelial compartments.* Int Immunol, 2002. **14**(7): p. 813-22.
133. Zook, E.C., et al., *Overexpression of Foxn1 attenuates age-associated thymic involution and prevents the expansion of peripheral CD4 memory T cells.* Blood, 2011. **118**(22): p. 5723-31.
134. Bleul, C.C., et al., *Formation of a functional thymus initiated by a postnatal epithelial progenitor cell.* Nature, 2006. **441**(7096): p. 992-6.
135. Sun, L., et al., *Declining expression of a single epithelial cell-autonomous gene accelerates age-related thymic involution.* Aging Cell, 2010. **9**(3): p. 347-57.
136. Bredenkamp, N., C.S. Nowell, and C.C. Blackburn, *Regeneration of the aged thymus by a single transcription factor.* Development, 2014. **141**(8): p. 1627-37.
137. Griffith, A.V., et al., *Persistent degenerative changes in thymic organ function revealed by an inducible model of organ regrowth.* Aging cell, 2012. **11**(1): p. 169-177.
138. Bredenkamp, N., et al., *An organized and functional thymus generated from FOXN1-reprogrammed fibroblasts.* Nat Cell Biol, 2014. **16**(9): p. 902-8.
139. Uddin, M.M., et al., *Foxn1-β5t transcriptional axis controls CD8+ T-cell production in the thymus.* Nature Communications, 2017. **8**: p. 14419.
140. Abramson, J. and G. Anderson, *Thymic Epithelial Cells.* Annual Review of Immunology, 2017. **35**(1): p. 85-118.
141. Wallin, J., et al., *Pax1 is expressed during development of the thymus epithelium and is required for normal T-cell maturation.* Development, 1996. **122**(1): p. 23-30.
142. Peters, H., et al., *Pax9-deficient mice lack pharyngeal pouch derivatives and teeth and exhibit craniofacial and limb abnormalities.* Genes Dev, 1998. **12**(17): p. 2735-47.
143. Xu, P.X., et al., *Eya1 is required for the morphogenesis of mammalian thymus, parathyroid and thyroid.* Development, 2002. **129**(13): p. 3033-44.
144. Manley, N.R. and M.R. Capecchi, *Hox group 3 paralogs regulate the development and migration of the thymus, thyroid, and parathyroid glands.* Dev Biol, 1998. **195**(1): p. 1-15.

145. Zou, D., et al., *Patterning of the third pharyngeal pouch into thymus/parathyroid by Six and Eya1.* Dev Biol, 2006. **293**(2): p. 499-512.
146. Jerome, L.A. and V.E. Papaioannou, *DiGeorge syndrome phenotype in mice mutant for the T-box gene, Tbx1.* Nat Genet, 2001. **27**(3): p. 286-91.
147. Reeh, K.A.G., et al., *Ectopic TBX1 suppresses thymic epithelial cell differentiation and proliferation during thymus organogenesis.* Development (Cambridge, England), 2014. **141**(15): p. 2950-2958.
148. Garfin, P.M., et al., *Inactivation of the RB family prevents thymus involution and promotes thymic function by direct control of Foxn1 expression.* J Exp Med, 2013. **210**(6): p. 1087-97.
149. Potter, C.S., et al., *The nude mutant gene Foxn1 is a HOXC13 regulatory target during hair follicle and nail differentiation.* J Invest Dermatol, 2011. **131**(4): p. 828-37.
150. Patel, S.R., et al., *Bmp4 and Noggin expression during early thymus and parathyroid organogenesis.* Gene Expr Patterns, 2006. **6**(8): p. 794-9.
151. Bleul, C.C. and T. Boehm, *BMP signaling is required for normal thymus development.* J Immunol, 2005. **175**(8): p. 5213-21.
152. Tsai, P.T., R.A. Lee, and H. Wu, *BMP4 acts upstream of FGF in modulating thymic stroma and regulating thymopoiesis.* Blood, 2003. **102**(12): p. 3947-53.
153. Gordon, J., et al., *Evidence for an early role for BMP4 signaling in thymus and parathyroid morphogenesis.* Dev Biol, 2010. **339**(1): p. 141-54.
154. Neves, H., et al., *Modulation of Bmp4 signalling in the epithelial-mesenchymal interactions that take place in early thymus and parathyroid development in avian embryos.* Dev Biol, 2012. **361**(2): p. 208-19.
155. Balciunaite, G., et al., *Wnt glycoproteins regulate the expression of FoxN1, the gene defective in nude mice.* Nat Immunol, 2002. **3**(11): p. 1102-8.
156. Osada, M., et al., *DKK1 mediated inhibition of Wnt signaling in postnatal mice leads to loss of TEC progenitors and thymic degeneration.* PLoS One, 2010. **5**(2): p. e9062.
157. Osada, M., et al., *The Wnt signaling antagonist Kremen1 is required for development of thymic architecture.* Clin Dev Immunol, 2006. **13**(2-4): p. 299-319.
158. Kurooka, H., et al., *Rescue of the hairless phenotype in nude mice by transgenic insertion of the wild-type Hfh11 genomic locus.* Int Immunol, 1996. **8**(6): p. 961-6.
159. Cunliffe, V.T., A.J. Furley, and D. Keenan, *Complete rescue of the nude mutant phenotype by a wild-type Foxn1 transgene.* Mamm Genome, 2002. **13**(5): p. 245-52.
160. Larsen, B.M., et al., *Identification of an Intronic Regulatory Element Necessary for Tissue-Specific Expression of Foxn1 in Thymic Epithelial Cells.* The Journal of Immunology, 2019: p. ji1801540.
161. Parent, A.V., et al., *Generation of functional thymic epithelium from human embryonic stem cells that supports host T cell development.* Cell Stem Cell, 2013. **13**(2): p. 219-29.

162. Sun, X., et al., *Directed differentiation of human embryonic stem cells into thymic epithelial progenitor-like cells reconstitutes the thymic microenvironment in vivo.* Cell Stem Cell, 2013. **13**(2): p. 230-6.
163. Lai, L. and J. Jin, *Generation of thymic epithelial cell progenitors by mouse embryonic stem cells.* Stem Cells, 2009. **27**(12): p. 3012-20.
164. Gruver, A.L. and G.D. Sempowski, *Cytokines, leptin, and stress-induced thymic atrophy.* J Leukoc Biol, 2008. **84**(4): p. 915-23.
165. Purton, J.F., et al., *Expression of the glucocorticoid receptor from the 1A promoter correlates with T lymphocyte sensitivity to glucocorticoid-induced cell death.* J Immunol, 2004. **173**(6): p. 3816-24.
166. Fletcher, A.L., et al., *Ablation and regeneration of tolerance-inducing medullary thymic epithelial cells after cyclosporine, cyclophosphamide, and dexamethasone treatment.* J Immunol, 2009. **183**(2): p. 823-31.
167. Min, D., et al., *Sustained thymopoiesis and improvement in functional immunity induced by exogenous KGF administration in murine models of aging.* Blood, 2007. **109**(6): p. 2529-37.
168. Dudakov, J.A., et al., *Interleukin-22 drives endogenous thymic regeneration in mice.* Science, 2012. **336**(6077): p. 91-5.
169. Lunter, G. and M. Goodson, *Stampy: a statistical algorithm for sensitive and fast mapping of Illumina sequence reads.* Genome Res, 2011. **21**(6): p. 936-9.
170. Rimmer, A., et al., *Integrating mapping-, assembly- and haplotype-based approaches for calling variants in clinical sequencing applications.* Nat Genet, 2014. **46**(8): p. 912-918.
171. Popitsch, N., *CODOC: efficient access, analysis and compression of depth of coverage signals.* Bioinformatics, 2014. **30**(18): p. 2676-7.
172. Gkazi, A.S., et al., *Clinical T Cell Receptor Repertoire Deep Sequencing and Analysis: An Application to Monitor Immune Reconstitution Following Cord Blood Transplantation.* Front Immunol, 2018. **9**: p. 2547.
173. McCusker, C., J. Upton, and R. Warrington, *Primary immunodeficiency.* Allergy, asthma, and clinical immunology : official journal of the Canadian Society of Allergy and Clinical Immunology, 2018. **14**(Suppl 2): p. 61-61.
174. Davies, E.G., *Immunodeficiency in DiGeorge Syndrome and Options for Treating Cases with Complete Athymia.* Frontiers in immunology, 2013. **4**: p. 322-322.
175. Derpoorter, C., et al., *Genes at the Crossroad of Primary Immunodeficiencies and Cancer.* Frontiers in immunology, 2018. **9**: p. 2544-2544.
176. Bertho, J.M., et al., *Phenotypic and immunohistological analyses of the human adult thymus: evidence for an active thymus during adult life.* Cell Immunol, 1997. **179**(1): p. 30-40.
177. Shearer, W.T., et al., *Lymphocyte subsets in healthy children from birth through 18 years of age: The pediatric AIDS clinical trials group P1009 study.* Journal of Allergy and Clinical Immunology, 2003. **112**(5): p. 973-980.
178. McLean-Tooke, A., et al., *Immunologic defects in 22q11.2 deletion syndrome.* J Allergy Clin Immunol, 2008. **122**(2): p. 362-7, 367.e1-4.
179. Shah, S.S., et al., *Retropharyngeal aberrant thymus.* Pediatrics, 2001. **108**(5): p. E94.

180. Livak, K.J. and T.D. Schmittgen, *Analysis of relative gene expression data using real-time quantitative PCR and the 2(-Delta Delta C(T)) Method.* Methods, 2001. **25**(4): p. 402-8.
181. Hung, M.-C. and W. Link, *Protein localization in disease and therapy.* Journal of Cell Science, 2011. **124**(20): p. 3381-3392.
182. Schüddekopf, K., M. Schorpp, and T. Boehm, *The whn transcription factor encoded by the nude locus contains an evolutionarily conserved and functionally indispensable activation domain.* Proceedings of the National Academy of Sciences, 1996. **93**(18): p. 9661-9664.
183. Schlake, T., et al., *Forkhead/winged-helix transcription factor whn regulates hair keratin gene expression: Molecular analysis of the Nude skin phenotype.* Developmental Dynamics, 2000. **217**(4): p. 368-376.
184. Raj, N. and L.D. Attardi, *The Transactivation Domains of the p53 Protein.* Cold Spring Harb Perspect Med, 2017. **7**(1).
185. Lukoseviciute, M., et al., *From Pioneer to Repressor: Bimodal foxd3 Activity Dynamically Remodels Neural Crest Regulatory Landscape In Vivo.* Developmental Cell, 2018. **47**(5): p. 608-628.e6.
186. Martínez-Martín, N., et al., *Cooperativity Between T Cell Receptor Complexes Revealed by Conformational Mutants of CD3ε.* Science Signaling, 2009. **2**(83): p. ra43-ra43.
187. Koulgi, S., et al., *Investigating DNA Binding and Conformational Variation in Temperature Sensitive p53 Cancer Mutants Using QM-MM Simulations.* PLOS ONE, 2015. **10**(11): p. e0143065.
188. Ishikawa-Ankerhold, H.C., R. Ankerhold, and G.P. Drummen, *Advanced fluorescence microscopy techniques--FRAP, FLIP, FLAP, FRET and FLIM.* Molecules, 2012. **17**(4): p. 4047-132.
189. Krieger, J.W., et al., *Imaging fluorescence (cross-) correlation spectroscopy in live cells and organisms.* Nature Protocols, 2015. **10**: p. 1948.
190. Waithe, D., et al., *FoCuS-point: software for STED fluorescence correlation and time-gated single photon counting.* Bioinformatics, 2016. **32**(6): p. 958-60.
191. Fischer, R. and B.M. Kessler, *Gel-aided sample preparation (GASP)--a simplified method for gel-assisted proteomic sample generation from protein extracts and intact cells.* Proteomics, 2015. **15**(7): p. 1224-1229.
192. Best, D.J. and D.E. Roberts, *The Upper Tail Probabilities of Spearman's RHO.* Journal of the Royal Statistical Society: Series C (Applied Statistics), 1975. **24**(3): p. 377-379.
193. Klaus, B. and K. Strimmer, *Signal identification for rare and weak features: higher criticism or false discovery rates?* Biostatistics, 2013. **14**(1): p. 129-43.
194. Funnell, A.P. and M. Crossley, *Homo- and heterodimerization in transcriptional regulation.* Adv Exp Med Biol, 2012. **747**: p. 105-21.
195. Courchaine, E.M., A. Lu, and K.M. Neugebauer, *Droplet organelles?* The EMBO Journal, 2016. **35**(15): p. 1603-1612.
196. Sawyer, I.A., J. Bartek, and M. Dundr, *Phase separated microenvironments inside the cell nucleus are linked to disease and regulate epigenetic state, transcription and RNA processing.* Seminars in Cell & Developmental Biology, 2019. **90**: p. 94-103.

197. Dundr, M., *Nuclear bodies: multifunctional companions of the genome.* Current Opinion in Cell Biology, 2012. **24**(3): p. 415-422.
198. Gomes, E. and J. Shorter, *The molecular language of membraneless organelles.* Journal of Biological Chemistry, 2019. **294**(18): p. 7115-7127.
199. Li, P., et al., *Phase transitions in the assembly of multivalent signalling proteins.* Nature, 2012. **483**: p. 336.
200. Dundr, M., et al., *In vivo kinetics of Cajal body components.* The Journal of cell biology, 2004. **164**(6): p. 831-842.
201. Woringer, M. and X. Darzacq, *Protein motion in the nucleus: from anomalous diffusion to weak interactions.* Biochemical Society Transactions, 2018: p. BST20170310.
202. Nott, Timothy J., et al., *Phase Transition of a Disordered Nuage Protein Generates Environmentally Responsive Membraneless Organelles.* Molecular Cell, 2015. **57**(5): p. 936-947.
203. Haustein, E. and P. Schwille, *Fluorescence Correlation Spectroscopy: Novel Variations of an Established Technique.* Annual Review of Biophysics and Biomolecular Structure, 2007. **36**(1): p. 151-169.
204. Chevallet, M., S. Luche, and T. Rabilloud, *Silver staining of proteins in polyacrylamide gels.* Nature protocols, 2006. **1**(4): p. 1852-1858.
205. Janknecht, R. and T. Hunter, *Transcriptional control: Versatile molecular glue.* Current Biology, 1996. **6**(8): p. 951-954.
206. Paulson, M., et al., *Stat protein transactivation domains recruit p300/CBP through widely divergent sequences.* J Biol Chem, 1999. **274**(36): p. 25343-9.
207. Pitkänen, J., et al., *The Autoimmune Regulator Protein Has Transcriptional Transactivating Properties and Interacts with the Common Coactivator CREB-binding Protein.* Journal of Biological Chemistry, 2000. **275**(22): p. 16802-16809.
208. Vo, N. and R.H. Goodman, *CREB-binding Protein and p300 in Transcriptional Regulation.* Journal of Biological Chemistry, 2001. **276**(17): p. 13505-13508.
209. Pitkanen, J., et al., *Cooperative activation of transcription by autoimmune regulator AIRE and CBP.* Biochem Biophys Res Commun, 2005. **333**(3): p. 944-53.
210. Song, X., et al., *Structural and Biological Features of FOXP3 Dimerization Relevant to Regulatory T Cell Function.* Cell Reports, 2012. **1**(6): p. 665-675.
211. Inukai, S., K.H. Kock, and M.L. Bulyk, *Transcription factor-DNA binding: beyond binding site motifs.* Current opinion in genetics & development, 2017. **43**: p. 110-119.
212. Jolma, A., et al., *DNA-binding specificities of human transcription factors.* Cell, 2013. **152**(1-2): p. 327-39.
213. Tatomer, D.C., et al., *Concentrating pre-mRNA processing factors in the histone locus body facilitates efficient histone mRNA biogenesis.* The Journal of Cell Biology, 2016. **213**(5): p. 557-570.
214. McManus, K.J. and M.J. Hendzel, *CBP, a transcriptional coactivator and acetyltransferase.* Biochem Cell Biol, 2001. **79**(3): p. 253-66.
215. Chuprin, A., et al., *The deacetylase Sirt1 is an essential regulator of Aire-mediated induction of central immunological tolerance.* Nat Immunol, 2015. **16**(7): p. 737-45.

216. Saito, M., et al., *Acetylation of intrinsically disordered regions regulates phase separation.* Nature Chemical Biology, 2019. **15**(1): p. 51-61.
217. Minezaki, Y., et al., *Human Transcription Factors Contain a High Fraction of Intrinsically Disordered Regions Essential for Transcriptional Regulation.* Journal of Molecular Biology, 2006. **359**(4): p. 1137-1149.
218. Schlake, T., et al., *The nude gene encodes a sequence-specific DNA binding protein with homologs in organisms that lack an anticipatory immune system.* Proc Natl Acad Sci U S A, 1997. **94**(8): p. 3842-7.
219. Machanick, P. and T.L. Bailey, *MEME-ChIP: motif analysis of large DNA datasets.* Bioinformatics, 2011. **27**(12): p. 1696-7.
220. Garner, M.M. and A. Revzin, *The use of gel electrophoresis to detect and study nucleic acid— protein interactions.* Trends in Biochemical Sciences, 1986. **11**(10): p. 395-396.
221. Furey, T.S., *ChIP-seq and beyond: new and improved methodologies to detect and characterize protein-DNA interactions.* Nat Rev Genet, 2012. **13**(12): p. 840-52.
222. Zaret, K.S. and J.S. Carroll, *Pioneer transcription factors: establishing competence for gene expression.* Genes Dev, 2011. **25**(21): p. 2227-41.
223. Han, J., Z. Zhang, and K. Wang, *3C and 3C-based techniques: the powerful tools for spatial genome organization deciphering.* Molecular cytogenetics, 2018. **11**: p. 21-21.
224. Hirakawa, M., et al., *Fundamental parameters of the developing thymic epithelium in the mouse.* Sci Rep, 2018. **8**(1): p. 11095.
225. Dumont-Lagacé, M., C. St-Pierre, and C. Perreault, *Sex hormones have pervasive effects on thymic epithelial cells.* Scientific Reports, 2015. **5**: p. 12895.
226. Rode, I. and T. Boehm, *Regenerative capacity of adult cortical thymic epithelial cells.* Proc Natl Acad Sci U S A, 2012. **109**(9): p. 3463-8.
227. Ritter, M.A. and D.B. Palmer, *The human thymic microenvironment: new approaches to functional analysis.* Seminars in Immunology, 1999. **11**(1): p. 13-21.
228. Berzins, S.P., et al., *Thymic regeneration: teaching an old immune system new tricks.* Trends in Molecular Medicine, 2002. **8**(10): p. 469-476.
229. Nakagawa, Y., et al., *Thymic nurse cells provide microenvironment for secondary T cell receptor α rearrangement in cortical thymocytes.* Proceedings of the National Academy of Sciences, 2012. **109**(50): p. 20572-20577.
230. Yang, Y.A. and J. Yu, *Current perspectives on FOXA1 regulation of androgen receptor signaling and prostate cancer.* Genes & Diseases, 2015. **2**(2): p. 144-151.
231. Fong, K.-W., et al., *Whole-genome screening identifies proteins localized to distinct nuclear bodies.* The Journal of cell biology, 2013. **203**(1): p. 149-164.